DECOFF Probabilities of Failed Operations

Gintautas, Tomas; Sørensen, John Dalsgaard

Publication date:
2015

Document Version
Publisher's PDF, also known as Version of record

Project memo

DECOFF Probabilities of Failed Operations

Description of statistical procedure
Comparison of DECOFF method against standard Alpha-factor method
Effects of weather forecast uncertainty

VERSION	DATE
Version	2015-12-10

AUTHOR(S)
Tomas Gintautas

CLIENT(S)	CLIENTS REF.
NFR	Client's reference

PROJECT NO.	NO. OF PAGES AND APPENDICES:
302000194	91 with appendices

ABSTRACT
A statistical procedure of estimation of Probabilities of Failed Operations is described and exemplified using ECMWF weather forecasts and SIMO output from Rotor Lift test case models. Also safety factor influence is investigated.

DECOFF statistical method is benchmarked against standard *Alpha-factor* method defined by (DNV, 2011) and model performance is evaluated. Also, the effects that weather forecast uncertainty has on the output Probabilities of Failure is analysed and reported.

PREPARED BY	SIGNATURE
Tomas Gintautas	

APPROVED BY	SIGNATURE
John Dalsgaard Sørensen	

Contents

1 Introduction

This report is a product of work conducted at AAU within the frame of activities for the DECOFF project. The main focus is statistical analysis of offshore installation equipment responses in order to estimate the Probability of Failed operation/installation. The report shall cover the following aspects:

- A description of sources of uncertainty and uncertainty handling in DECOFF.
- General notes on Limit states.
- The methodology used to determine the Probabilities of Failure for Hywind Rotor Lift Operation (total operation failure and failure probabilities of individual limit states).
- A brief analysis of deterministic and stochastic Ultimate Limit States.
- SIMO model verification and estimation of operation limiting met-ocean parameters for Hywind Rotor Lift Operation.
- Description of the selected test period, May 01 – August 01 2014.
- Estimation of weather windows for the operation using the standard *Alpha-factor* method.
- Estimation of weather windows for the operation using DECOFF method with ECMWF weather forecasts May 01 – August 01 2014 period.
- Estimation of weather windows for the operation using DECOFF method with met-ocean condition measurements at FINO3 site for May 01 – August 01 2014 period.
- Study of the weather forecast uncertainty in terms of its effect on the uncertainty of individual critical responses and on probabilities of failure of individual limit states.

2 General notes on Uncertainty

2.1 Sources of uncertainty

The parameters subject to uncertainty are assumed to be modelled by stochastic variables and/or stochastic processes / stochastic fields. The uncertainties are divided in the following groups:

Physical uncertainty (aleatory uncertainty) is related to the natural randomness of a quantity, for example the annual maximum mean wind speed or the uncertainty in the yield stress due to production variability.

Measurement uncertainty (epistemic uncertainty) is related to imperfect measurements of for example a geometrical quantity.

Statistical uncertainty (epistemic uncertainty) is due to limited sample sizes of observed quantities. Data of observations are in many cases scarce and limited. Therefore, the parameters of the considered random variables cannot be determined exactly. They are uncertain themselves and may therefore also be modelled as random variables. Are additional observations provided then the statistical uncertainty may be reduced.

Model uncertainty (epistemic uncertainty) is the uncertainty related to imperfect knowledge or idealizations of the mathematical models used or uncertainty related to the choice of probability distribution types for the stochastic variables. Some of the most important model uncertainties for structural reliability assessment of wind turbine components are related to site assessment and the aerodynamic models.

The above types of uncertainty can be handled by structural reliability methods. Another 'type' of uncertainty which is not mentioned above and not covered by these methods is gross / human errors. These types of errors can be defined as deviation of an event or process from acceptable engineering practice and is generally handled by quality control measures.

It is noted that some aleatory uncertainties 'change' to epistemic uncertainties when the system is realized.

The reference period for the use of the stochastic model is also important when modelling stochastic variables and processes. It is often assumed that ergodic stochastic processes may be used. However, the influence of long-term effects (e.g. climate change) may also need to be considered. Some uncertainties may for short reference periods appear reasonable but when predictive models are extrapolated for long reference periods then uncertainties can easily propagate and increase to unrealistic levels.

2.2 Sources modelling uncertainty

The physical and model uncertainties are among others related to the wind and wave parameters such as long-term and extreme mean wind speeds, turbulence and long-term and extreme significant wave heights. The long-term uncertain parameters are e.g. related to serviceability and fatigue limit states whereas the extreme uncertain parameters are e.g. related to ultimate limit states implying total or partial collapse / failure of structural components.

Each of the uncertain parameters modelled by stochastic variables $X_i, i = 1,2,...,n$ is assumed to be modelled by a distribution function $F_{X_i}(x_i;\boldsymbol{\alpha}_i)$ where $\boldsymbol{\alpha}_i$ denotes the statistical parameters. Dependency between the stochastic variables can be modelled by joint distribution functions or correlation coefficients. A number of methods can be used to estimate the statistical parameters $\boldsymbol{\alpha}_i$ in distribution functions, e.g. the Maximum Likelihood method or Bayesian statistics. It is noted that using the Maximum Likelihood method also gives a consistent estimate of the *statistical uncertainties* if the number of data is larger than 25-30, see e.g. (Lindley, 1976):

Model uncertainty, see (EN 1990, 2002) and (ISO, 1998) can be assessed if a mathematical model h is introduced to describe / approximate a physical phenomenon (e.g. the load bearing capacity of a wind turbine component). The mathematical model is assumed to be a function of a number of physical uncertainties (e.g. strength parameters) modelled by stochastic variables $\mathbf{X}$ with realizations denoted $\mathbf{x}$. Further, the model is assumed to be a function of a number of regression parameters denoted $R_1,..., R_m$. The regression parameters are determined by statistical methods, and are therefore

subject to statistical uncertainty. The model is not perfect; therefore model uncertainty has in general also to be introduced. This is often done by a multiplicative stochastic variable Δ. The model can thus be written:

$$f(x) \cong \Delta \cdot h(\boldsymbol{X}, \boldsymbol{R_1}, \dots, \boldsymbol{R_m}) \quad (2.1)$$

It is assumed that N data sets are available from measurements or tests. The model uncertainty Δ is assumed to be modelled by a Log-Normal distributed stochastic variable with mean (bias) b and standard deviation σ_Δ and can be determined following the procedures in e.g. (EN 1990, 2002) and (ISO, 1998).

2.3 Uncertainty handling in DECOFF

The following sources of uncertainty will be considered:

1) Wind and wave characteristics as input for SIMO: the physical and model uncertainties related to this input will be assumed covered by an appropriate number of ensemble time series.

2) Other input parameters for SIMO: this could be damping and stiffness parameters used in the modelling of the dynamic properties of the structural models used e.g. for cranes. These uncertainties can be modelled as stochastic variables using information from e.g. (JCSS, 2002).

3) The output from SIMO consists in time series of various response parameters, incl. (see (Vatne, 2013) and (Vatne, 2015)):

- Nacelle acceleration
- Crane loads
- Lift wire tension
- Airgap between rotor and vessel
- Airgap between blades and waves
- Acceleration rotor
- Sway motion
- Surge motion
- Relative motion between rotor and special tool
- Relative velocity

For each of these response parameters the following should be considered:

- Estimation of mean and standard deviation (or alternatively fit of a distribution function to data for the response parameters considered). The stochastic models should be selected according the type of limit state associated with the response:
    - If extreme response is critical then an extreme type stochastic model for an appropriate reference time should be used.

    - If the response is used in a serviceability limit state then a stochastic model for the long-term response should be used.
- Stochastic model for the model uncertainty associated with the structural modelling in SIMO, i.e. bias and COV for model uncertainty.

4) Limit states functions should be formulated for each of the critical limit states / events:

$$g = X_R \cdot R(\boldsymbol{X}) - X_e \cdot E(\boldsymbol{X}) \tag{2.2}$$

Where

$E(\mathbf{X})$ models the load effect (e.g. acceleration or stresses)

X_E models the model uncertainty connected to estimation of the load effect by SIMO

$R(\mathbf{X})$ models the 'resistance' (e.g. maximum, critical acceleration or yield stress), which for some limit states can be considered as a stochastic variable

X_R model uncertainty related to 'resistance' model

5) Using the limit state in the stochastic models for the uncertain parameters the probability that the critical limit state / event occurs is estimated and used as input for the risk assessment, see below.

3 General notes on Critical limit states

This section describes how to model different critical limit states / events. Generally the events are divided in two groups a) serviceability limit states and b) ultimate limit states:

a) Serviceability limit states: model events that mainly influences the function of the system (vessel, cranes, wind turbine) without resulting in permanent excessive deformations and / or rupture. Examples are too large accelerations and velocities of components.
b) Ultimate limit states: model events resulting in rupture or failure of components or the whole system. An example is failure of a steel component where the load effect exceeds the yielding (or rupture) strength.

In order to model the limit states the following aspects are to be considered:

- Consequences of exceedance of critical limits of the response
- Critical limits for response

3.1 Serviceability limit states, SLS

The limit states have to take into account:

- The critical level of the response
- How long time is the critical level exceeded

Therefore, for serviceability limit states various critical events can be formulated for each response parameter (e.g. acceleration) involving combinations of how much and how long time a critical level is exceeded.

For each of the critical events the consequences have to be assessed (and if possible quantified in terms of economic loss).

For each critical event the probability of exceedance per phase is estimated considering the uncertainties described in section 2. Also, the consequence in terms of costs is estimated

3.2 Ultimate limit states, ULS

The limit states have to take into account:

- The critical level of the response, e.g. yield stress
- The maximum load effect during the duration of the phase considered

For each of the critical events the consequences have to be assessed (and if possible quantified in terms of economic loss). For each critical event the probability of exceedance per phase and the consequence in terms of costs is estimated.

4 DECOFF system description

This section briefly describes the DECOFF forecasting system topology. Figure 4.1 shows the general structure of the DECOFF system. This report will focus on the part highlighted in green square.

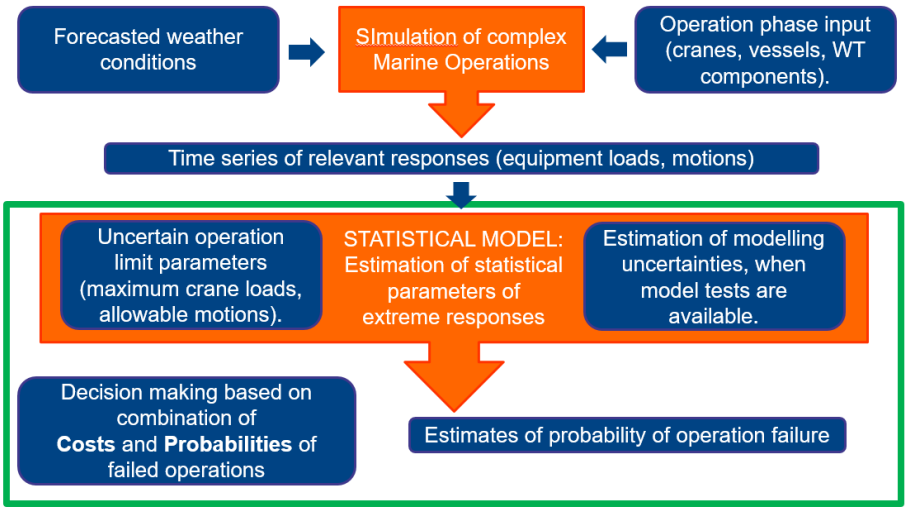

Figure 4.1. DECOFF forecasting system. Graphical representation.

5 Failure probability estimation procedure and initial testing

This section describes the procedure to estimate the probability of failure for Hywind Rotor Lift operation. The focus is mainly establishing the procedure and validating it throughout a simple short term analysis. Failure probabilities are estimated using a simple Monte Carlo simulation technique. SIMO is used to simulate motions of involved floating vessel system.

5.1 Input to SIMO

The multi-parametric ECMWF weather forecasts are used as input for SIMO. In the following example the weather forecast for the period from 2013-08-06 00:00:00 to 2013-08-09 24:00:00 (forecasted at 2013-08-01 for 3 days in advance) will be used. The following figures show the 51 ensembles of forecasted weather conditions:

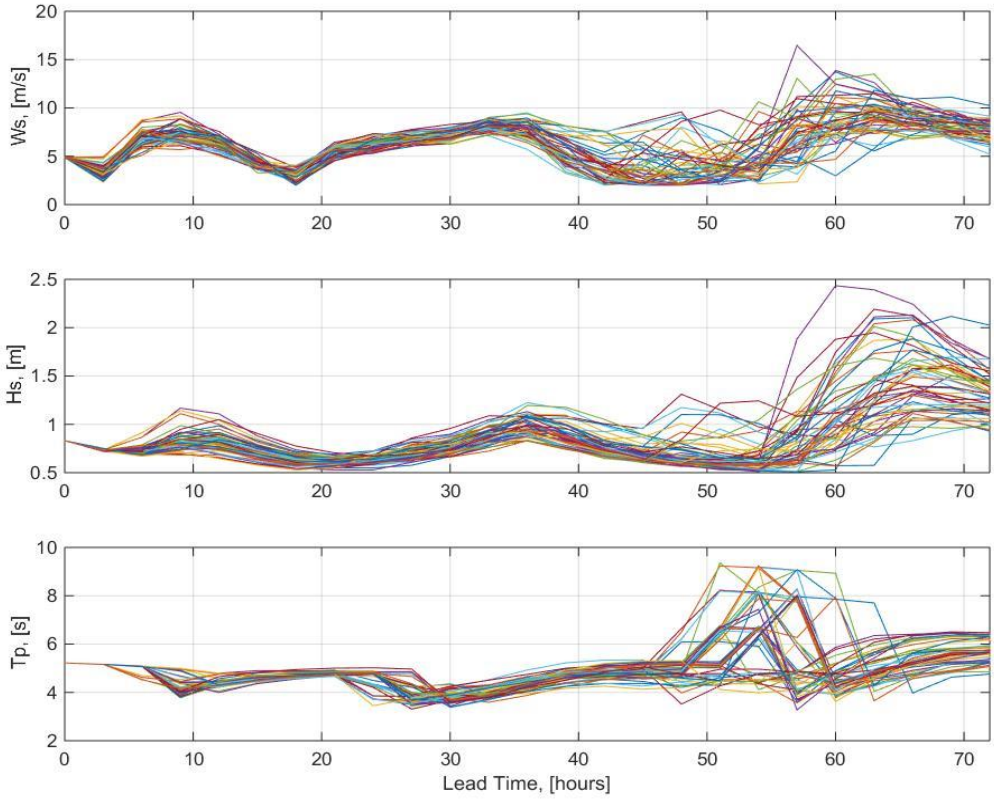

Figure 5.1. ECMWF weather forecast for 2013-08-01 - 2013-08-03.

Input parameters from ECMWF forecasts used as SIMO input:

- **Wind speed and direction** (Ws, WsDir).
- **Significant wave height and peak period** (Hs, Tp, JONSWAP 1D spectrum), wave direction the same as wind direction (WsDir, wind generated waves).

- **Swell significant wave height and mean period** (HsSwell, TmSwell, Pierson-Moscowitz spectrum) and direction (SwellDir).

5.2 SIMO model and simulation

Phases 3-6 are simulated using model files according to (Vatne & Helian, 2014) and (Vatne, 2013), see Table 5.1. During these phases wind turbine rotor is lifted up from the barge and fitted to the nacelle on top of floating Wind Turbine tower (Figure 5.2). The Phase 3-6 sequence has to be simulated in sequence and has to be analysed as a continuous operation because it is not possible to stop and restart the sequence (non-reversible operation).

Table 5.1. Rotor lift phases.

Phase no	Phase	Total hours	Hours after start-up												
			8	9	10	11	12								13
1	Transit to field	8	8												
2	Preparation for lift	3		3											
3	Lift up rotor from vessel	0.2					0.2								
4	Rotate rotor	0.2						0.2							
5	Lift rotor to close to nacelle	0.4								0.4					
6	Connect the rotor to special tool	0.2											0.2		
7	Connect the rotor flanges	0.1													0.1

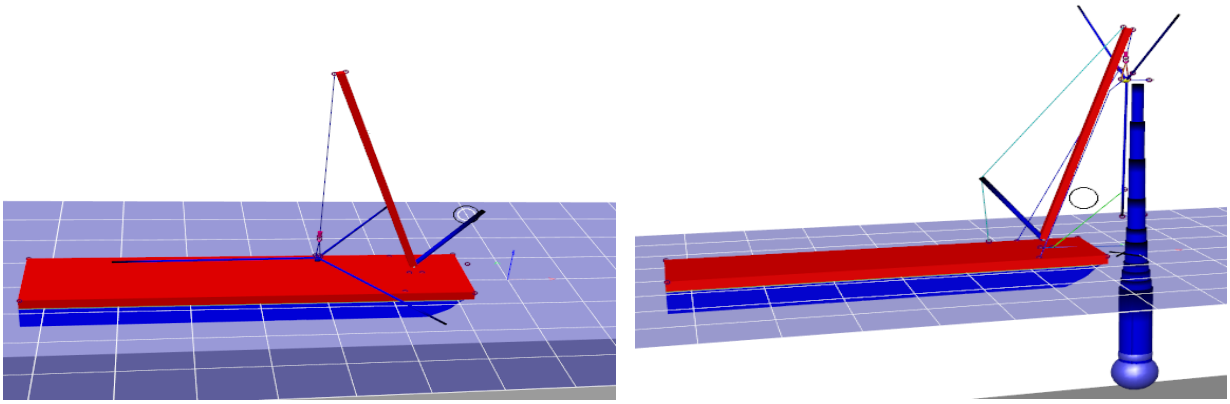

Figure 5.2. Phases 3-6 of rotor lift operation. Lift up (Phase 3) and fitting to the nacelle (Phase 6).

Every simulation is performed with additional 120s in the beginning to eliminate any initialization effects present in SIMO software. Later when the response is analysed the first 120s will be removed

from every simulation in order to conform to the required operation phase lengths, given in (Vatne & Helian, 2014). Convergence of the final results is achieved by performing a minimum number of 16 simulations (with different seeds) for each weather forecast ensemble, the requirement is based on (IEC, 2014) Annex G.

5.3 Aggregation of response time series

Response time series of multiple operation phases and simulation seeds are aggregated based on active limit states in the following manner:

- Selecting one limit state from Table 5.2 and combining relevant SIMO output time series according to excel spreadsheet (Vatne, 2015).
- Joining the response time series end to end for each phase, where the limit state is active. The weather input should be kept the same. Example: Crane Load limit (green in Table 5.2) is active in Phases 3-5, therefore the crane load response time series should be combined together (see Figure 5.3). Total duration of the time series should constitute the duration of the 3 involved phases (720+720+1440=2880s).

Since every forecasted weather ensemble has to be simulated using at least 16 different seeds, the resulting time series also have to be aggregated and analyzed together. The resulting time series should be similar to Figure 5.4. Total duration of resulting time series – 2880*(number of seeds).

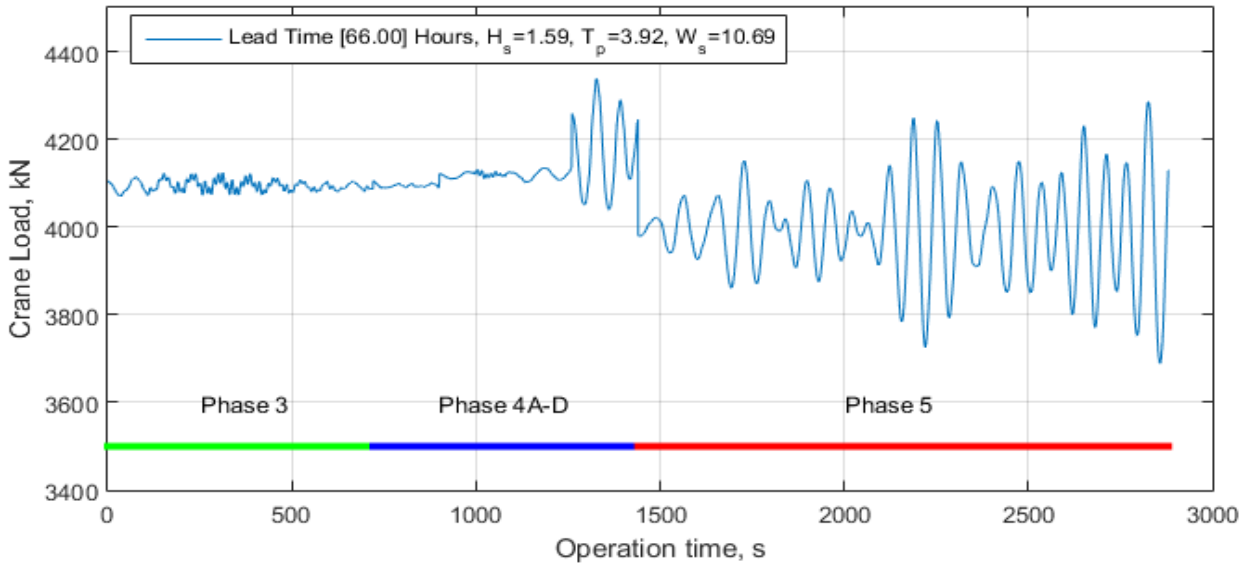

Figure 5.3. Aggregating response from different phases.

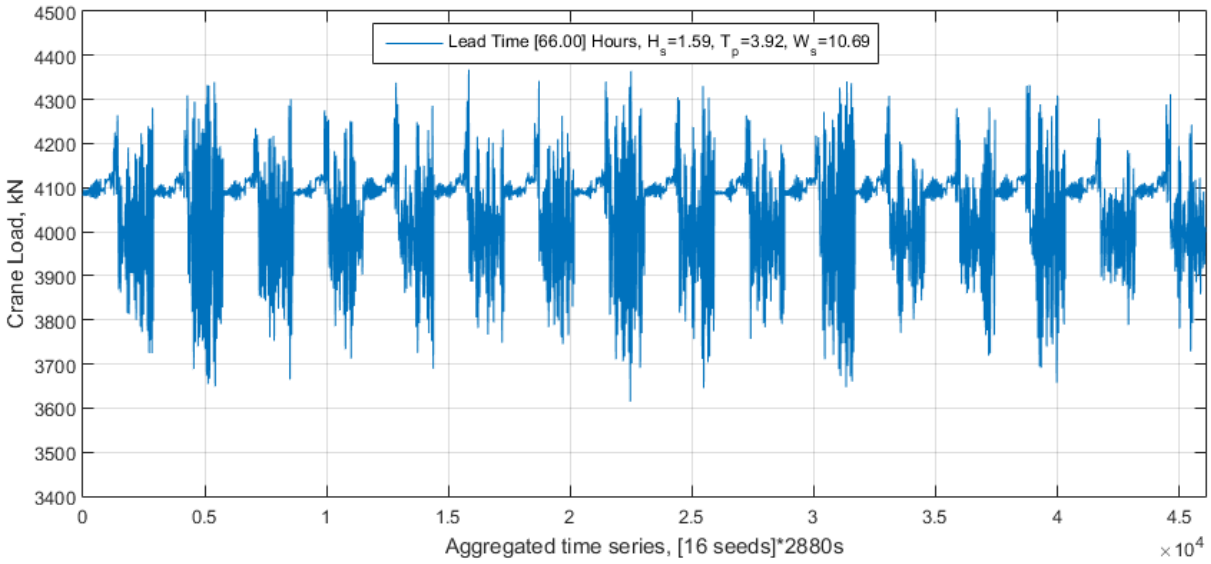

Figure 5.4. Multiple simulations aggregated. Same weather conditions, different SIMO input seed.

Table 5.2. Limits for rotor lift operation.

Phase nr	Phase	Critical response parameters	Acceptance limit
1	Transit to field	Airgap between blade 1 and waves	> 3 m
		Airgap between blade 2 and waves	> 3m
2	Preparation for lift	Airgap between blade 1 and waves	> 3 m
		Airgap between blade 2 and waves	> 3 m
3	Lift up rotor from vessel	Crane loads	< 4250kN
		Lift wire tension	> 0
		Tug wire tension	> 0
		Airgap between blade 1 and waves	> 3 m
		Airgap between blade 2 and waves	> 3 m
		Acceleration rotor	< 4 m/s^2
		Rotational acceleration rotor	< 5 rad/s^2
		Rotor sway motion	< 1 m
		Rotor surge motion	< 1 m
4	Rotate rotor	Crane loads	< 4250kN
		Lift wire tension	> 0
		Tug wire tension	> 0
		Acceleration rotor	< 4 m/s^2
		Rotational acceleration rotor	< 5 rad/s^2
		Rotor sway motion	< 1 m
		Rotor surge motion	< 1 m
5	Lift rotor up to close to nacelle	Crane loads	< 4250kN
		lift wire tension	>0
		tug wire tension	>0

		Airgap blade 3 and tower	>0 m
		Acceleration rotor	< 4 m/s^2
		Rotational acceleration rotor	< 5 rad/s^2
		Yaw and tilt angle	< 5 degrees
		Rotor sway motion	< 1 m
		Rotor surge motion	< 1 m
6	Connect the rotor to the special tool/crib	Relative yaw angle between rotor and special tool	< 5 degrees
		Relative tilt angle between rotor and special tool	< 5 degrees
		Relative radial velocity	<0.4 m/s
		Relative axial velocity	<0.1 m/s
		Airgap blade 3 and tower	>0 m

5.4 Response analysis

The required responses according to Table 5.2 extracted from SIMO output file and then post-processed in the following way (example figures are for "Crane Load" limit state, 16 seeds were used):

1. The maximum responses are extracted from the aggregated time series of 16 seeds per weather forecast ensemble using a Peak Over Threshold method.

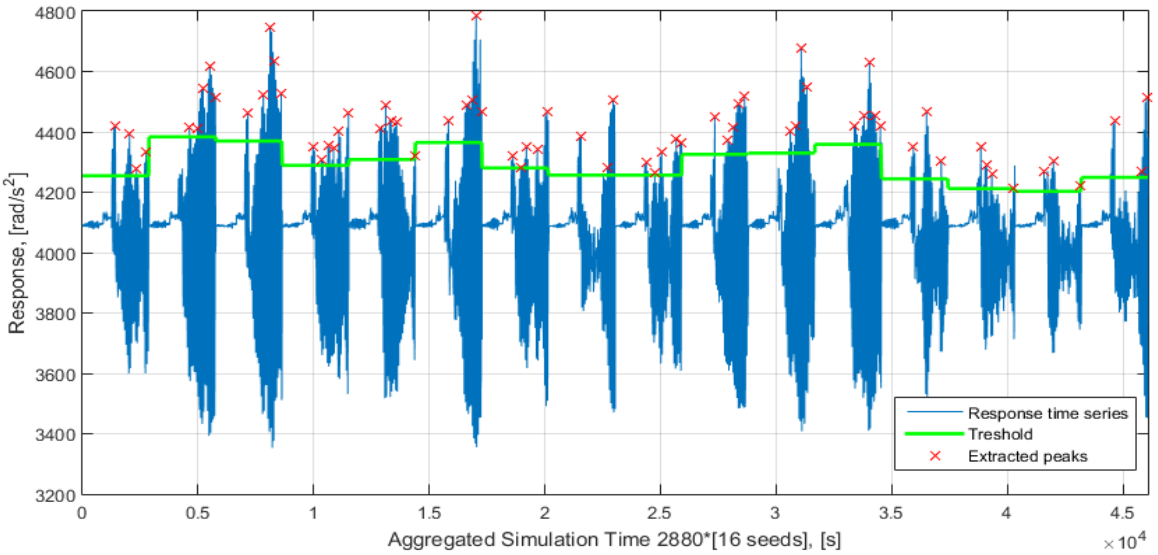

Figure 5.5. Example time series of crane load time series and extracted peaks.

In order to ensure statistical independence of the extracted peaks, a time separation of 3 response cycles is used, based on (IEC, 2014) Annex G. Adaptive threshold is used to extract

peaks, each simulated seed should have a threshold calculated using the following equation (the threshold jump indicates different seeds in Figure 5.5):

$$Th = mean(Response) + 1.4 \cdot \sqrt{var(Response)} \quad (5.1)$$

2. A Weibull distribution is fitted to the extracted peaks using Maximum Likelihood method to estimate distribution parameters. Since 16 seeds of the same weather situation are simulated, the fitted distribution function has to be adjusted using the following equation (example in Figure 5.6):

$$F_{non-exceedace}(r < R_{max}) = F_{local}(r < R_{max})^{E(n_p)} \quad (5.2)$$

$$E(n_p) = \frac{n_{peaks}}{N_{seeds}} \quad (5.3)$$

where:

$F_{short\ term}(r < R_{max})$ – Adjusted distribution function of maximum response;

$F_{local}(r < R_{max})$ – Local distribution function of maximum response, defined by all peaks from 16 simulations.

n_{peaks} – Total number of peaks, extracted from aggregated time series of 16seeds*2880s.

N_{seeds} – Number of simulated seeds per weather situation (16 in this case).

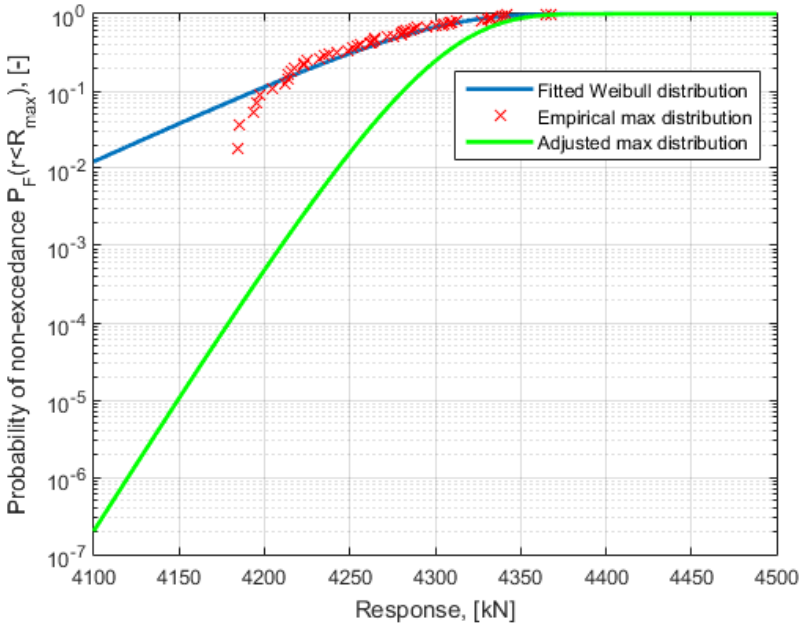

Figure 5.6. Fitted Weibull distribution.

Weibull distribution is fitted for every weather forecast ensemble individually resulting in 51 distributions per forecasted weather situation. Exceedance function for every ensemble is

calculated as follows (example in Figure 5.7), and later used in calculation of probability of operation failure:

$$P_{exceedance,ensemble}(r > R_{max}) = 1 - F_{non-exceedance,ensemble}(r < R_{max}) \quad (5.4)$$

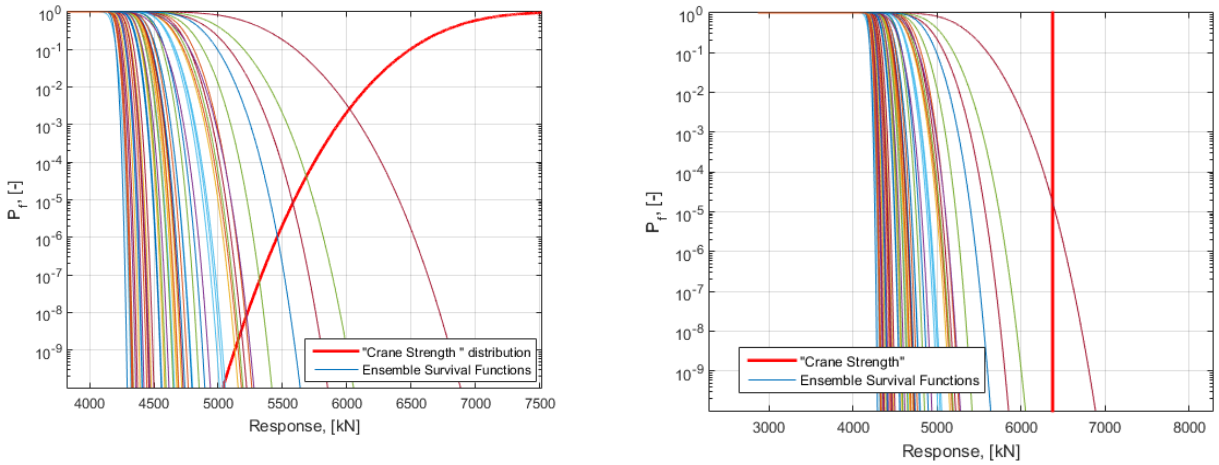

Figure 5.7. Exceedance functions for all 51 ensembles of one weather forecast, deterministic (right figure) and stochastic (left figure) failure limits.

Depending on the acceptance limit, the calculation of probability of operation failure can be different as follows:

a. When the acceptance limit is considered non-deterministic and a distribution function is used, example - Crane load limit . In this case, a log-normally distributed crane hook/lifting cable strength with the following parameters is used:

Table 5.3. Parameters of acceptance limit distributions.

Limit state	SWL, [kN]	Assumed safety factor, [-]	5% Characteristic value, [kN]	Expected value of LogNormal Distribution, [kN]	COV, %	Dist
Crane Load	4250	1.5	6375	6930	5	LN
Rotor Acc	4	1.2	4.8	5.225	5	LN
Rotor Acc Ang	5	1.2	6	6.25	5	LN

Then the probability of failed operation (for the phases considered) can be calculated as an integral, or numerically by discretizing (Figure 5.7 to the left):

$$P_{F,ensemble} = \int P_{exceedance,ensemble}(R) \cdot f(R|\mu_{ln}, \sigma_{ln})\, dR = \sum P_{exceedance,ensemble}(R) \cdot f(R|\mu_{ln}, \sigma_{ln})\, \Delta R \quad (5.5)$$

where:

$P_{exceedance,ensemble}(R)$ – Exceedance function evaluated at crane load R;

$f(R|\mu_{ln}, \sigma_{ln})$ – Probability density function of crane lifting cable strength, evaluated at crane load R;

ΔR – bin (discretization) width of crane load R.

b. When the acceptance limit (R_{max}) is considered deterministic, a single value is used as a failure limit. In this case, probability of a failed operation is calculated simply, as the exceedance function evaluated at the acceptance limit (Figure 5.7 to the right):

$$P_{F,ensemble} = P_{exceedance,ensemble}(R_{max}) \quad (5.6)$$

c. When the acceptance limit is defined as "response cannot be negative", example – no slack in Lift wires – Lift wire tension > 0 (Table 5.2. blue) it implies that non-exceedance probability is to be considered as failure probability, therefore the probability of failure is calculated as Cumulative Distribution Function (CDF) evaluated at the acceptance limit (R_{max}):

$$P_{F,ensemble} = F_{non-exceedance,ensemble}(R_{max}) \quad (5.7)$$

Furthermore, since Weibull distribution is not defined for negative or 0 values, a normal distribution is fitted to the extracted minima. The same procedure is used as described in (1-2) but a low threshold is applied and minima are extracted, see Figure 5.8 and Figure 5.9.

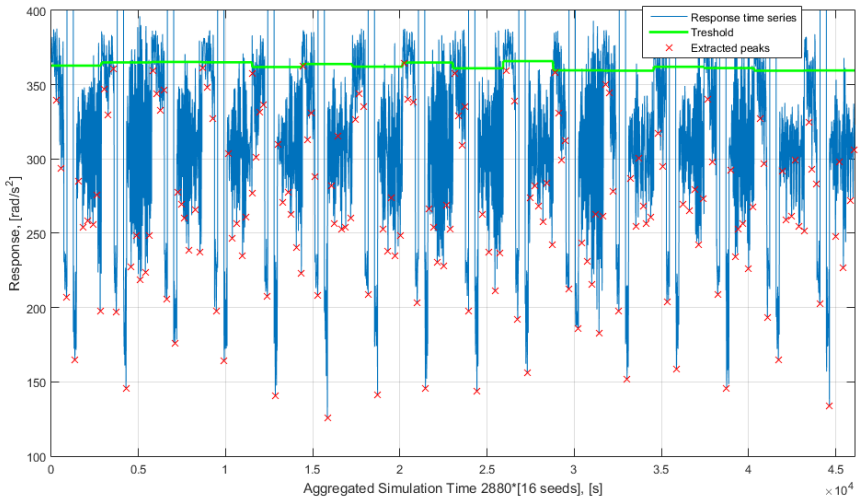

Figure 5.8. Lower threshold and extracted minimal Lift Wire load limit state.

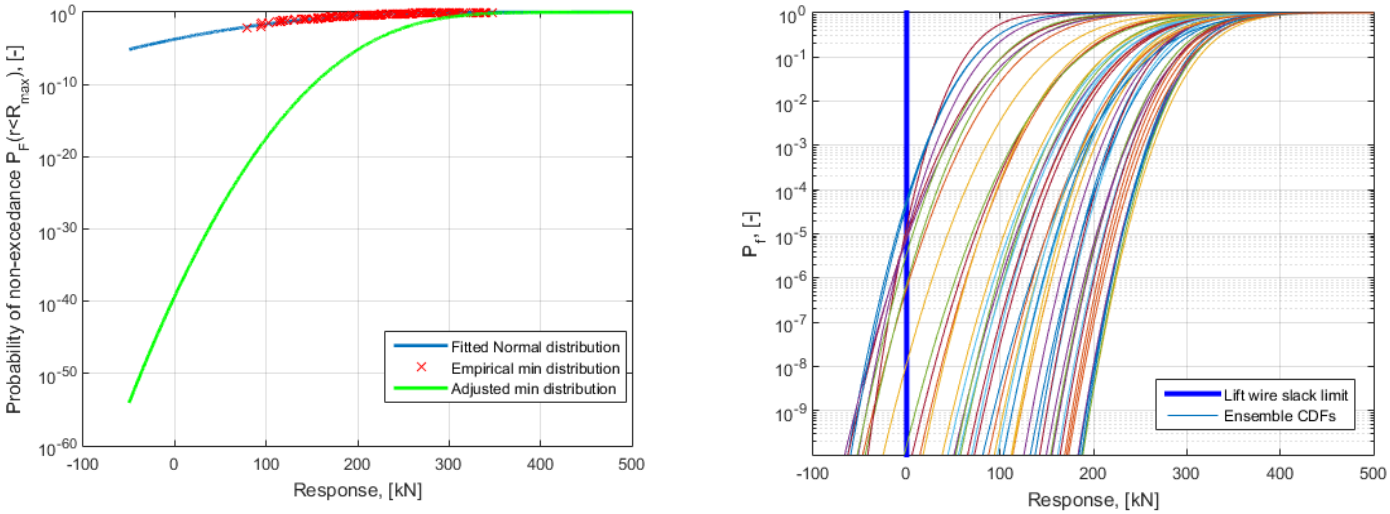

Figure 5.9. Fitted Normal distribution and CDFs for all 51 ensembles of one weather forecast.

3. Probabilities of failed operations are calculated for each ensemble using the appropriate distributions and acceptance limit and further, the expected probability of failure can be estimated for each limit state as follows:

$$P_{F,Limit\ State} = \frac{\sum_{i=1}^{N} P_{F,Ensemble}}{number\ of\ ensembles\ N} \tag{5.8}$$

The following figure shows a couple of examples out of the 13 limit states that are relevant to the Rotor lift operation.

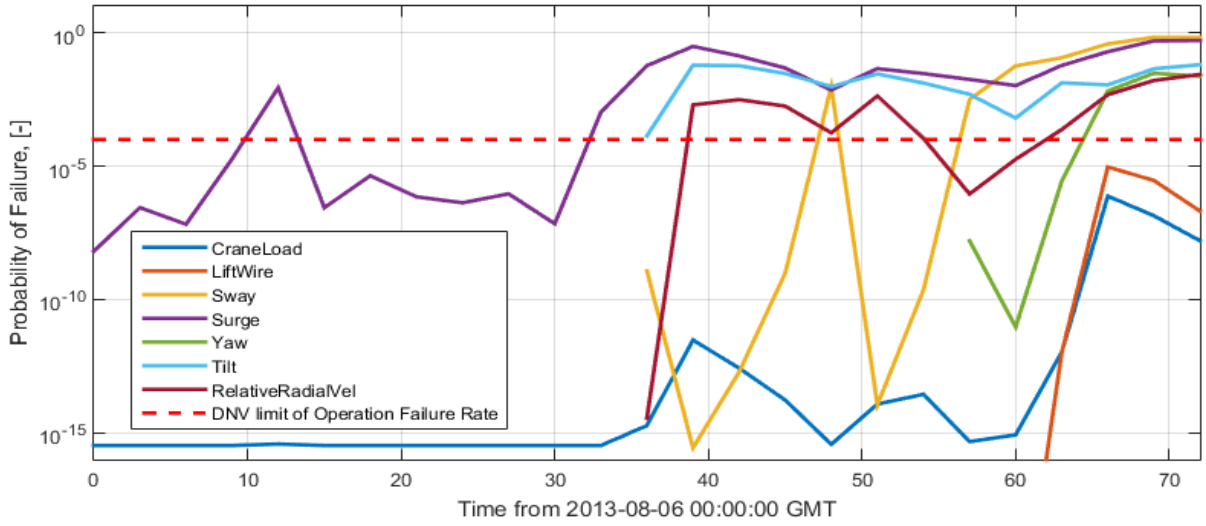

Figure 5.10. Expected values of some Limit States for Rotor Lift operation.

It is clearly visible, that some limit states exceed the acceptance limit of 1/10000 (10^{-4}) suggested by (DNV, 2011).

4. Final failure rate of a given operation is calculated as a series system of Limit State probabilities of failure, therefore product of success probabilities is used:

$$P_{F,Operation} = 1 - \prod_{i=1}^{N_{Lim\ States}} (1 - P_{F,\mathrm{Lim}\,State,\ i}) \tag{5.9}$$

Alternatively, if the Limit States could be considered as a parallel system, total probability of operation failure would be a product of individual Limit State Probabilities of failure:

$$P_{F,Operation} = \prod_{i=1}^{N_{Lim\ States}} P_{F,\mathrm{Lim}\,State,\ i} \tag{5.10}$$

The following Figure 5.11 summarizes the analysis, giving the overall Failure Rate of the Rotor Lift Operation (Limit States are considered as series system), involving 13 different limit states. Based on the results it can be concluded, that if the DNV limit for Operation Failure is used, a weather windows suitable for installation can be found between 16 and 30 hours lead time.

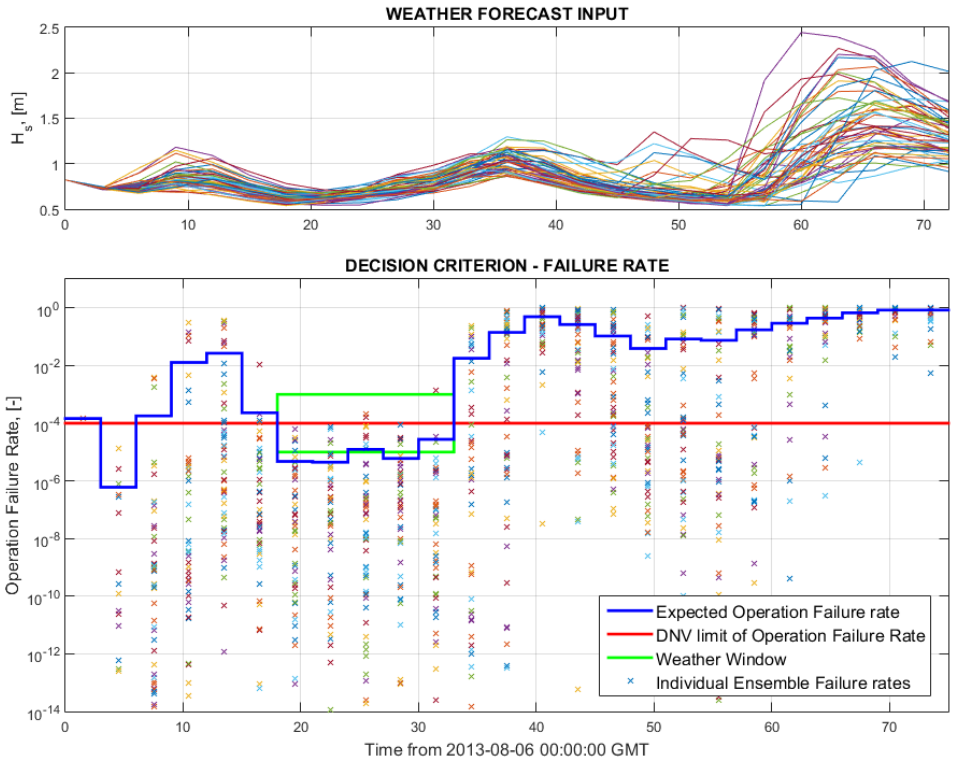

Figure 5.11. Total Expected Failure Rate of Rotor Lift Operation.

5.5 Alternative decision criteria for decision making

For decision making a number of alternatives should be considered, including different routes, different vessel types, etc. For each alternative, the total expected costs can be determined by the following equation:

$$C_{total} = C_{waiting} + C_{equipment} + \sum_{i=1}^{N_{Phases}} \left(\sum_{j=1}^{N_{LimStates}} P_{LS,i,j} C_{LS,i,j} \right) \tag{5.11}$$

where

N_{phases} number of phases

N_{ULS} number of ULS events

$P_{ULS,i,j}$ probability that ULS critical event no *j* in phase *i* occurs

$C_{ULS,i,j}$ cost if ULS critical event no *j* in phase *i* occurs

$C_{waiting}$ cost of waiting time (due to bad weather conditions), incl. the cost of 'doing nothing' due to lost production benefits

$C_{equipment}$ cost of equipment, incl. vessel type, …

The optimal decision is generally the decision with the lowest expected costs, C_{total}. This type of analysis in only applicable when it is possible to define monetary consequences to each type of failure. *Note: restrictions and costs due to risk of safety for people 'operations' are not included in the present cost model for decision making.*

6 Effect of stochastic critical response limits

An investigation was performed in order to give some insight on the effects of safety factors and non-deterministic acceptance limits on the Probabilities of Failed Operations. A more detailed analysis was conducted for Crane Load limit state (also as a direct result, a non-deterministic limit for "Crane Strength" was used in previous estimation of total Failure Rate of the Rotor Lift Operation).

A sensitivity analysis was performed on the Crane Load limit state using the following parameters defining the distribution of "Crane Strength" in Table 6.1. Figure 6.1 shows a graphical representation of safety factors and characteristic values of strength. The values in the table below are considered to be reflective of actual uncertainty related to strength of wire ropes. It has to be noted, that the partial safety factor found in the table below only accounts for the variation of strength of lifting equipment (wire rope) and does not include any other uncertainties that might be related to lifting operations (skew loads, wear, sling terminations and other unexpected events or manufacturing tolerances etc.).

Table 6.1. Parameters for Crane Load sensitivity analysis.

Safety factor, [-]	Coefficient of Varation COV, [%]	Expected value of Strength, [kN]	Standard deviation of strength, [kN]	LogNormal Parameters		Characteristic strength, 5% quantile, [kN]
				μ_{LN}	σ_{LN}	
1.2	5	5544	277,2	8.619	0.05	5100
1.2	7	5736	401.5	8.653	0.07	5100
1.5	5	6930	346.5	8.842	0.05	6375
1.5	7	7170	501,9	8.875	0.07	6375

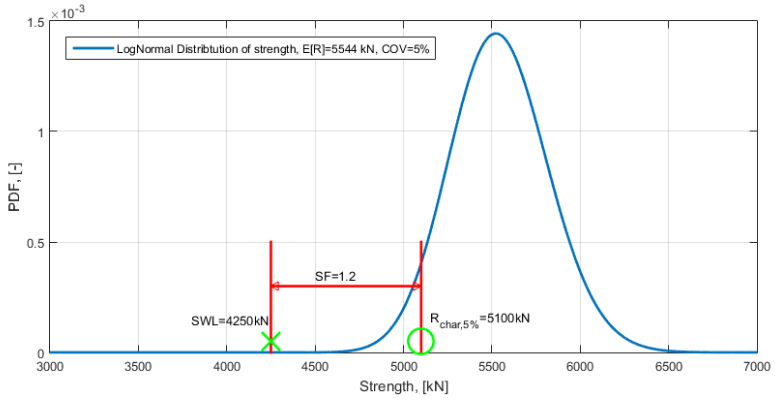

Figure 6.1. Strength distribution and relevant parameters.

The following figure shows the resulting distributions of non-deterministic strength from Table 6.1 that will be used in the sensitivity analysis.

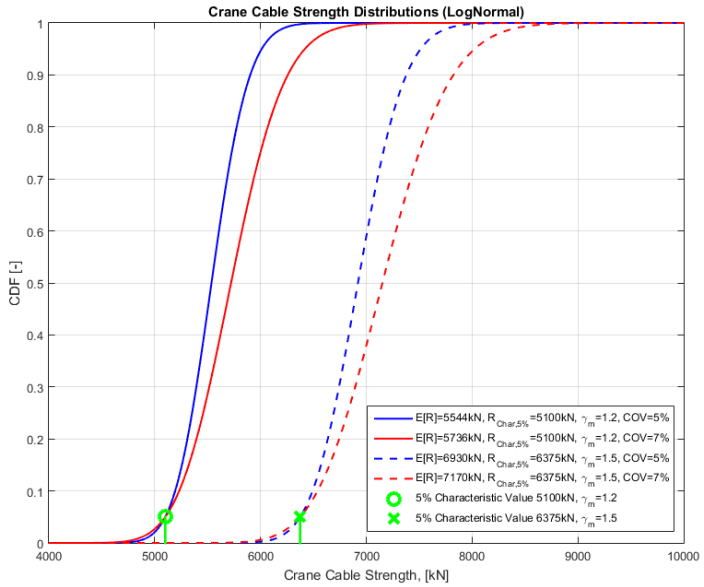

Figure 6.2. Distributions of Strength associated with Table 6.1.

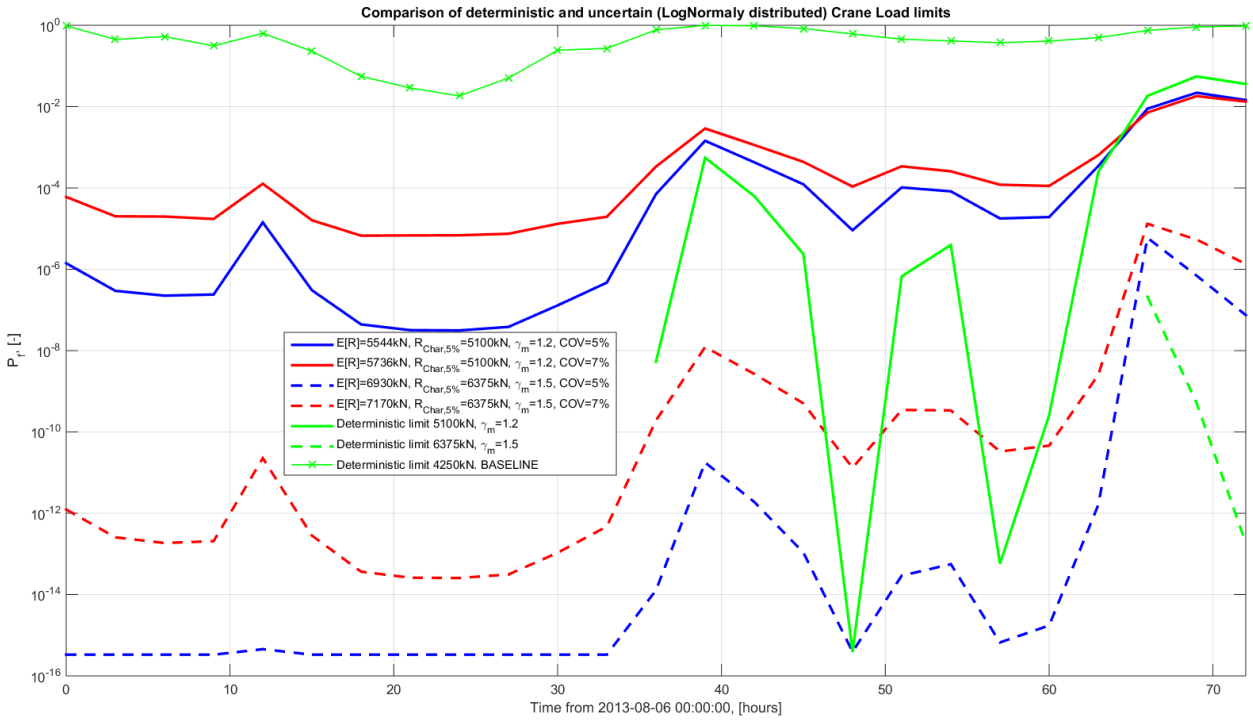

Figure 6.3. Results of sensitivity analysis.

It is clearly visible, that by using only baseline deterministic acceptance limit of SWL=4250kN the Probability of Failure of only Crane Load limit state indicates failure of the whole operation, therefore it is advisable to use a stochastic acceptance limit. It should be noted that with increasing uncertainty of the Strength variable (increasing COV) the Probability of Operation Failure increases significantly. There is also a clearly visible increase of PF when safety factors are reduced.

Based on this analysis, the calculations of PF for the whole Rotor Lift Operation were performed with a stochastic Crane Load limit, also stochastic limits were applied to Rotor Linear and Angular accelerations.

7 SIMO model verification

This section describes how well the SIMO model of the Hywind Rotor Lift operation is performing and what weather conditions could be suitable for the installation to be commenced. This analysis is based purely on whether the SIMO model can simulate a given weather situation without encountering numerical errors and crashing. The information from this section serves as a first insight on what weather situations should be analyzed in more detail using statistical analysis.

7.1 Initial analysis. SIMO model performance

It is assumed that if the SIMO model of the operation cannot compute the responses of the installation equipment, the operation should not be attempted under certain weather conditions. Typically a failed SIMO simulation would look similar to the one in Figure 7.1. A percentage of the time series that is not computed is used as an indicator of the model performance.

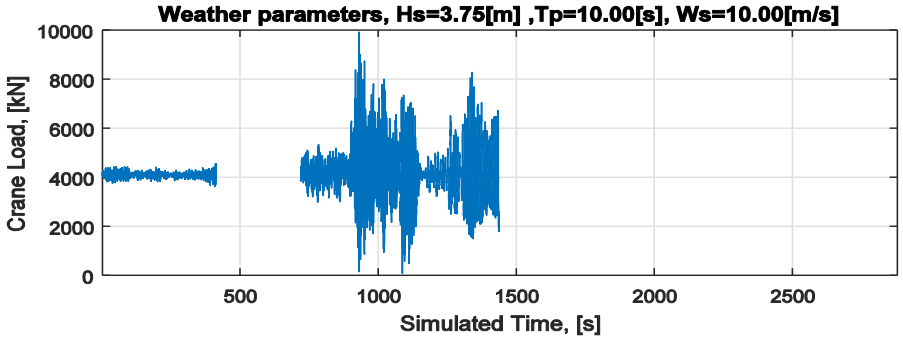

Figure 7.1. Example of (partially) failed simulation, Phases 3-6.

When SIMO fails it outputs '0' for every time step after the numerical computation failure in every response variable. Determining whether SIMO failed to compute the simulation fully is done by selecting a typically non-zero response (e.g. crane load) as an indicator of simulation failure. '0' values are found in the time series and the percentage of non-simulated time series is calculated. The following figures show the SIMO model performance under different weather conditions.

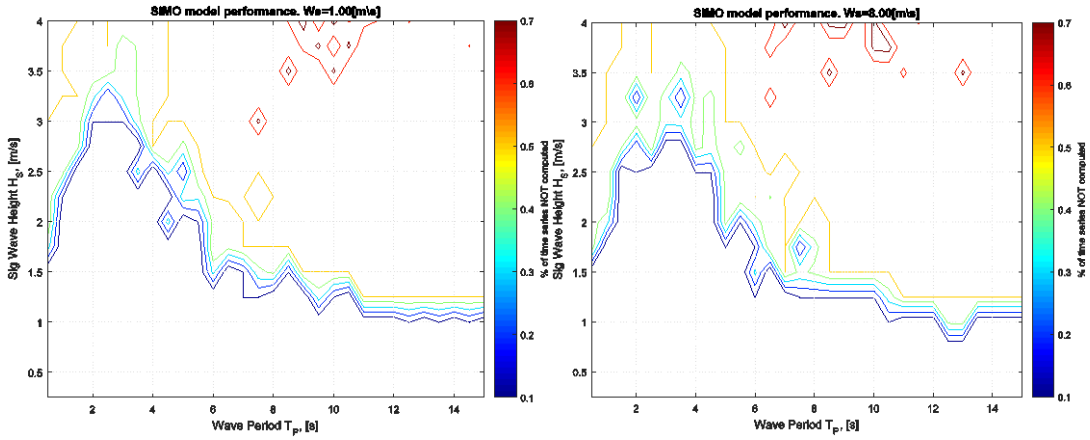

Figure 7.2. Phases 3-6 SIMO model performance, Wind Speed 1 and 8 m/s.

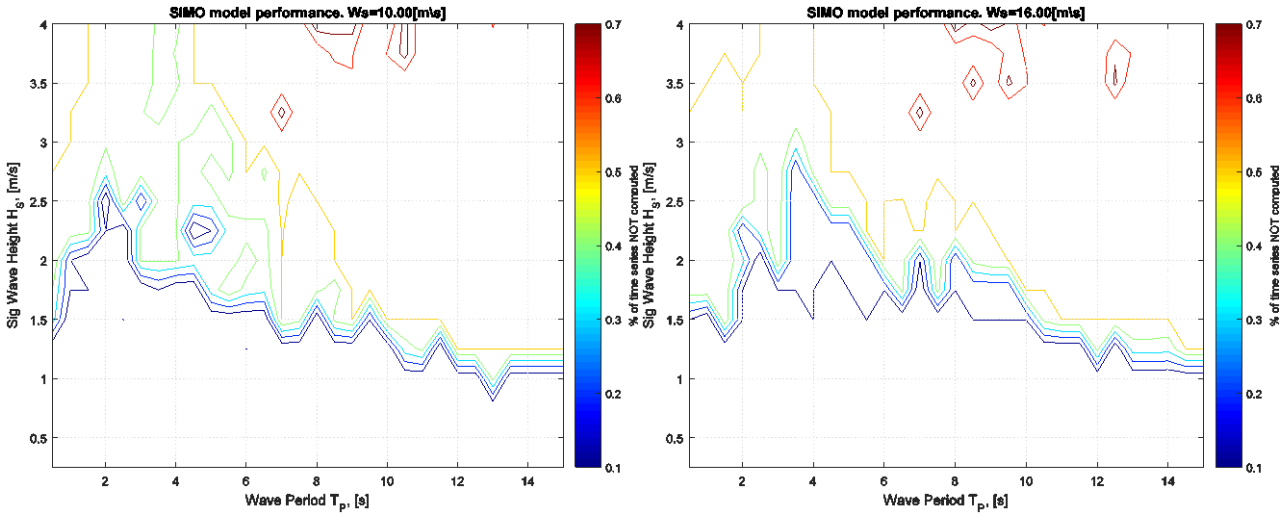

Figure 7.3. Phases 3-6 SIMO model performance, Wind Speed 10 and 16 m/s.

It is assumed that if >10% of the total time series is not computed the results are not reliable and the operation should not be attempted in those weather conditions. It is clearly visible that there is a safe region up to ~2.5m (H_s) significant wave height and ~5s (T_p) peak period when the wind speed is below ~8m/s. The safe region reduces to (H_s) ~1.25-1.5m significant wave height at peak periods from 1-15s when wind speed is increased to 10-16 m/s.

Based on this simple analysis, it could be concluded that in order to obtain reliable results from SIMO, weather situations for simulation should be limited to maximum **2.5m (H_s)** significant wave height, **5s peak period (T_p)** when the wind speeds **(Ws) are below 8m/s**. Up to 16 m/s W_s the maximum **significant wave height (H_s) should not be more than 1.25-1.5m**, the peak period (T_p) has less of an influence in these cases.

7.2 Further analysis. Weather limits for Alpha-Factor method

Further analysis focuses on selected few operation critical response parameters in order to determine when the operation can be completed. The results of this analysis will be later used as basis to set weather limits for Alpha-Factor method (standard method to determine weather windows for weather critical operations).

Figures from section 7.1 are overlaid on top of the figures with critical response parameter values in order to see if the SIMO model can be trusted. The ***greyed area*** in all the following plots indicates that simulations under those conditions were completed with numerical errors and the results are not reliable (>10% of time series is zero-padded).

Crane Load. The limit for maximum crane load is set to 6375kN (assuming the 4250kN limit from (Vatne, 2015) is defined with a safety factor of 1.5 therefore 4250kN x 1.5=6375kN). The following Figure 7.4 shows the crane load under different weather conditions. The areas coloured in *"white"*

are where the response exceeds the assumed limit (Response ≥ 6375kN), the combination of weather conditions in *"white"* are not acceptable and operation should not be attempted.

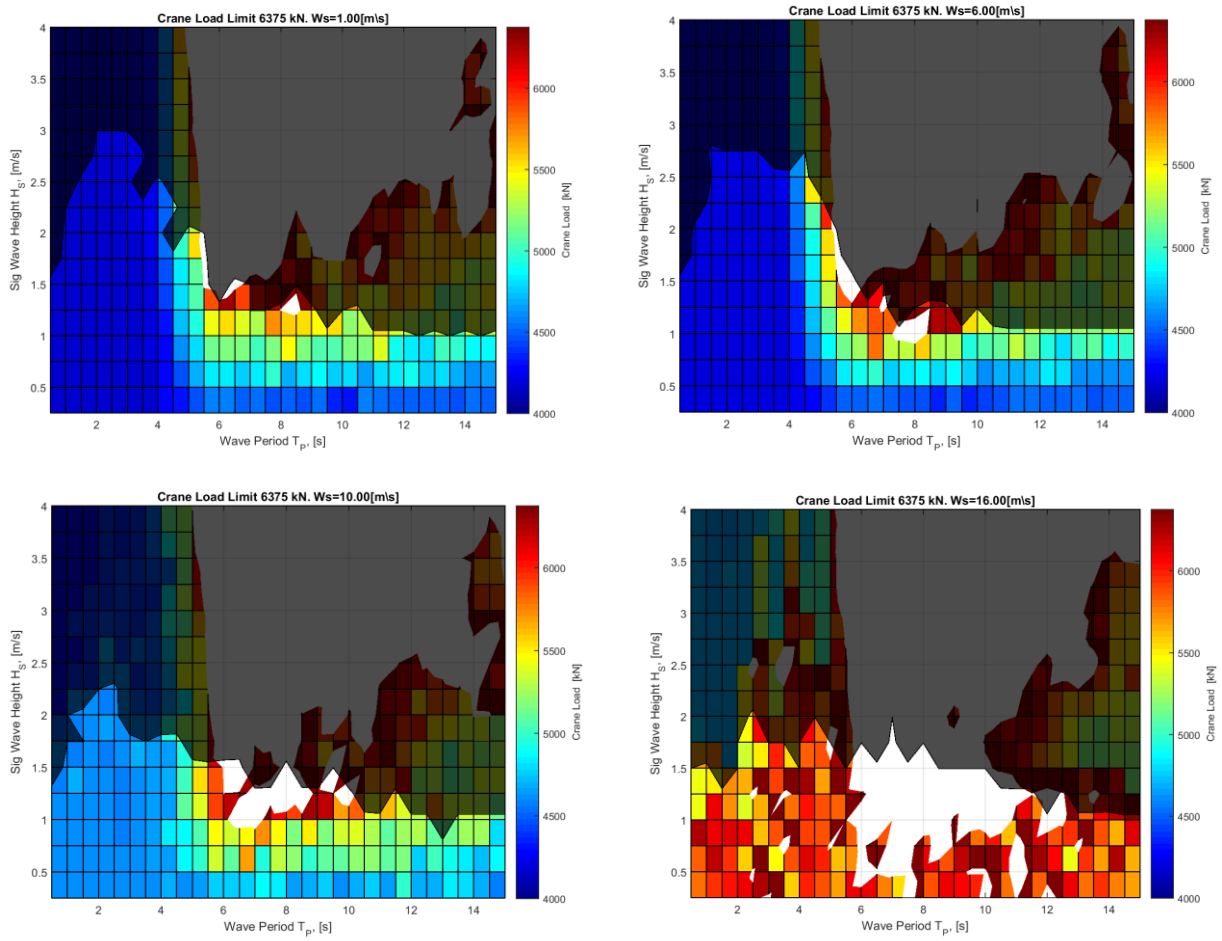

Figure 7.4. Crane Load critical response under different weather conditions.

It seems reasonable to conclude that below 5s (T_p) the operation could be completed under any (H_s≤4m) significant wave height and (W_s≤16m/s) wind speed. It has to be kept in mind that SIMO results are not reliable under certain weather conditions, therefore the limit for operation should be set at:

$$H_{s,lim} = \begin{cases} 1.75m, & Tp \leq 6s, Ws \leq 10m/s \\ 1.5m, Tp \geq 6s, Ws \leq 10\, m/s \\ 0 \;\; otherwise \end{cases}$$

There is also a clear indication that the natural frequency of the system is somewhere in the range of T_p=[5:8] because the response increases significantly when T_p≥5s. Although it is not possible to estimate the natural frequency accurately due to the fact that numerical simulation errors start to arise when input T_p≥5-8s and SIMO tends to crash and produce unreliable results. Therefore weather conditions where T_p> 5-8s should be analysed with care and, if possible, avoided alltogether.

Rotor Acceleration. The limit for maximum rotor acceleration is set to 4m/s^2. The following Figure 7.5 show the rotor acceleration under different weather conditions. The areas coloured in *"white"* are where the response exceeds the assumed limit, the combination of weather conditions in *"white"* are not acceptable and operation should not be attempted.

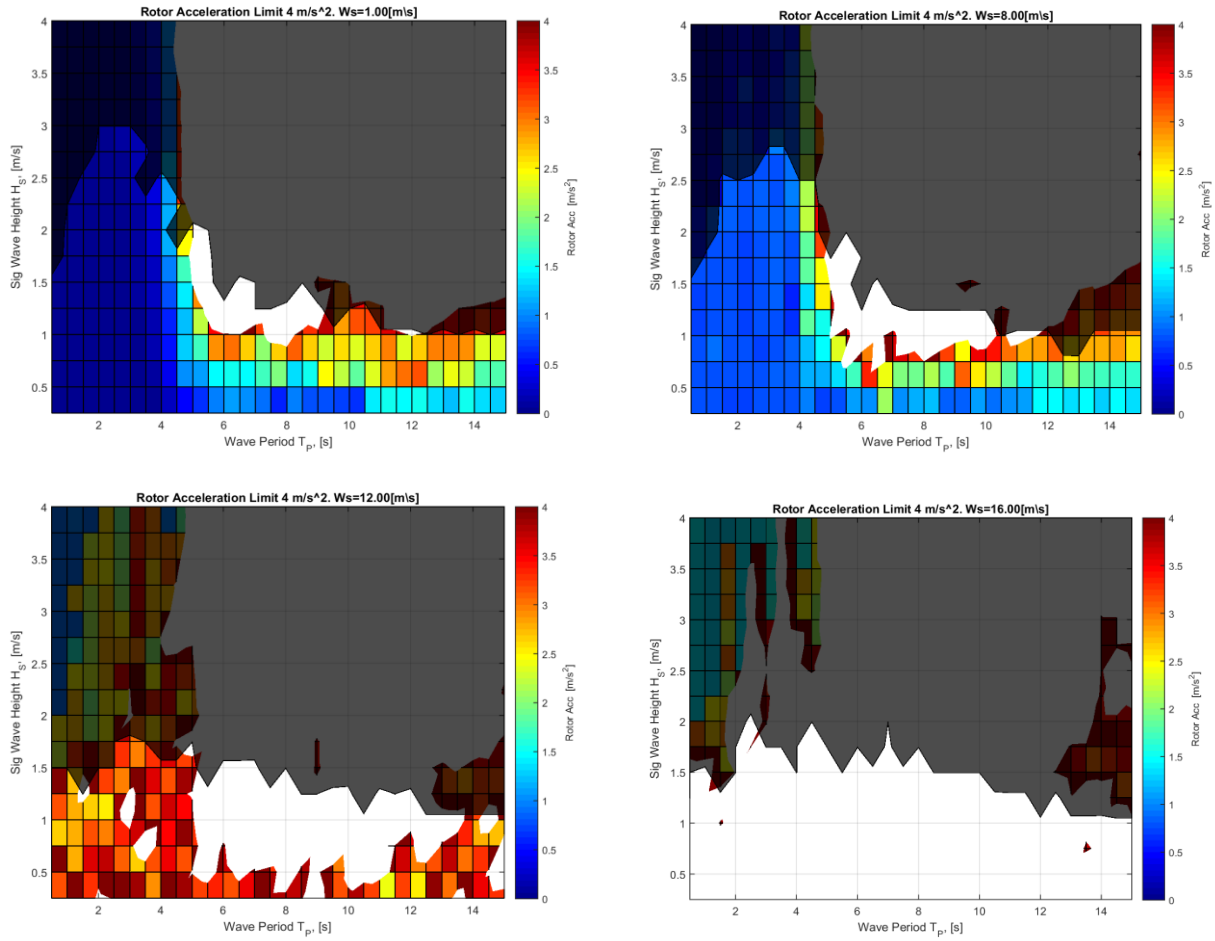

Figure 7.5. Rotor Acceleration critical response under different weather conditions.

From the figures above it can be concluded that wind speeds $W_s \geq 12$m/s are generally not acceptable under rotor acceleration limit state. The limits should be set at 1.5m H_s @[$T_p \leq 5$s;$W_s \leq 12$m/s], and 0.5m H_s @[$T_p \geq 5$s;$W_s \leq 12$m/s].

$$H_{s,lim} = \begin{cases} 1.5m, & Tp \leq 5s, Ws \leq 12m/s \\ 0.5m, Tp \geq 5s, Ws \leq 12\,m/s \\ 0 \;\; otherwise \end{cases}$$

The same logic can be used for all the limit states mentioned in (Vatne, 2015) (see figures in Appendix A and limits for all the limit states in Table 5.2. Limits for rotor lift operation.) and then a

combination of weather limits for different critical response parameters can be reduced to general requirements for limiting met-ocean conditions for the whole operation.

As a general trend throughout all the limit states, there is a value for $T_{p,low}$ (wave peak period) after which the critical response increases significantly. This implies that in each limit state (critical response parameter) the weather limits for H_s can be split in limit for sea states with $T_p < T_{p,low}$ and $T_p > T_{p,low}$. The limit on wind speed (W_s) is set to represent the situation where the critical response is exceeding the limit without taking T_p into account. The results are presented in the table below.

Table 7.1. Weather limits for selected limit states.

Limit State (critical response parameter)	**H_s, [m]**		**T_p, [s]**	**W_s, [m/s]**
	$< T_{p,low}$	**$> T_{p,low}$**	**$T_{p,low}$**	
Crane Load	1,75	1,5	6	16
Rotor Acceleration	1,5	0,5	5	12
Rotor Angular Acceleration	2,5	0	4	7
Rotor Sway Motion	1,5	1,5	5	12
Rotor Yaw angle	1,5	1,25	5	11
Rotor Tilt angle	2,5	0	4	8
Relative Yaw angle	2,5	1	6	8
Relative Tilt Angle	1,5	0,5	5	13
Radial Velocity	2,5	0,5	4	9
Axial Velocity	2	0,5	5	10
Minimums	**1,5**	**0**	**~5**	**7**
Adjusted for Maximum Values	**2,7 (H_{max})**	**0**	**~3.9 (T_z)**	**~10 ($W_{s,max}$)**

To summarize the table above, it should be noted that different limit states have different weather limitations. Furthermore, some of the limit states are violated or very close to critical limits if the wave peak period (T_p) is above 4-6s regardless of what wave height and wind speed is used (e.g. Rotor Angular Acceleration or Rotor Velocities). Therefore for *Alpha-Factor* method analysis, met-ocean conditions with T_p > 6s should regarded as unfeasible for the operation. On the other hand, since the statistical *DECOFF* method uses the actual critical response time series as indication of operation failure, any met-ocean situation can be analysed by the *DECOFF* method provided that SIMO can simulate given situation with minimal numerical errors.

Since all limit states are active in parallel and all critical responses have to be below certain values, the limit for maximum allowable met-ocean parameters are set to the minimum values form the table. Namely, in order to successfully complete the Rotor Lift Operation (Phases 3-6) the met-ocean conditions should not exceed **1.5 meters** significant wave height (H_s) at maximum peak period (T_p) of **5-6 seconds** and maximum wind speed (W_s) of **7m/s**.

Furthermore, since the parameters above are by definition parameters of a met-ocean state (statistical parameters of x-hour sea state), the actual limits for **maximum wave height (H_{max}), wave period (T_z)** and **maximum wind speed ($W_{s,max}$)** can be estimated. This is only done for the sake of completeness and these values are not directly used in the further analysis, but are useful as an indication of what extreme met–ocean conditions the model can withstand. In theory, there are equations relating the statistical parameters of a certain met-ocean state and values for maximum wave height, wind speed and wave period. One can use the following equations:

$$H_{max} = SF \cdot H_s \tag{7.1}$$

$$\frac{T_z}{T_p} \approx 0{,}78 \text{ for JONSWAP spectrum with } \gamma = 3.3; \tag{7.2}$$

where:
H_{max} – Maximum wave height;
SF – Storm Factor, 1.8-2 for operations of 30min-3h operations, (DNV, 2004);
H_s – Significant wave height;
T_z ,T_p– wave mean zero up-crossing and peak periods.

Although it is possible to estimate the maximum values using the equations, it is necessary to know the actual values that caused responses that exceeded the operational thresholds. These maximum values can be estimated directly from simulations by finding the exact point in time where the response becomes higher that the operational limit. Also a general analysis of the simulation output wave and wind time series can be performed in order to see how the sea state parameters are relate to the maximum values of interest. The following figures show the relation between the wave parameters:

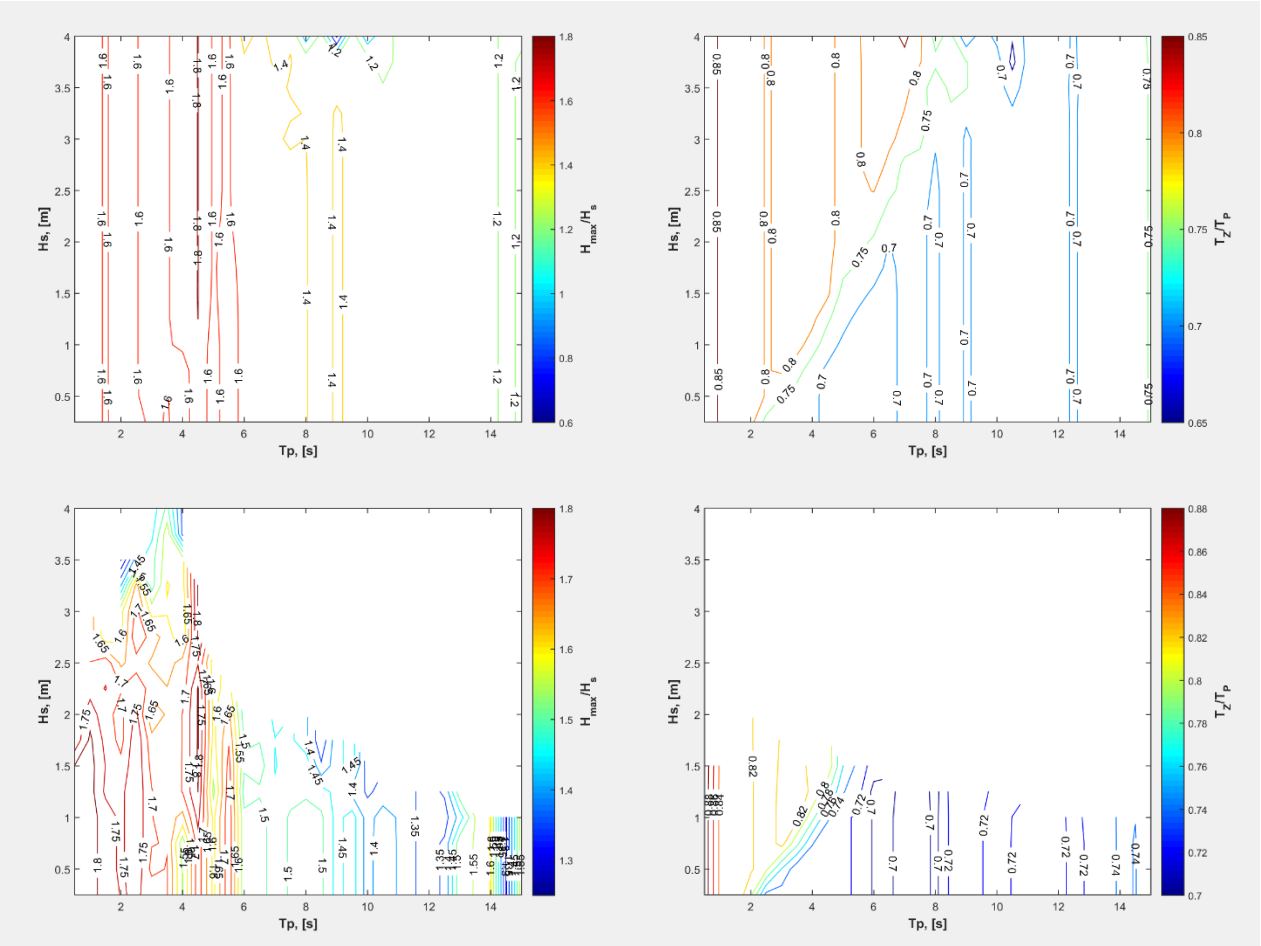

Figure 7.6. Sea state parameter relations (Phase3 – up, Phase5 – down).

It is visible from the figures above, that the theoretical values match closely to what is obtained through simulation (Storm Factor for maximum wave height – 1.6-1.8 and ratio between wave periods of ~0.75-0.85). Therefore, the factors for maximum wave height and wave period will be taken as follows: 1.8 for maximum wave and 0.78 for mean wave up-crossing period.

The same logic is applied to wind speed, since input to SIMO is 10 min average wind speed. The following figure shows the relation between 10 min mean wind speed and the expected (simulated) maximum.

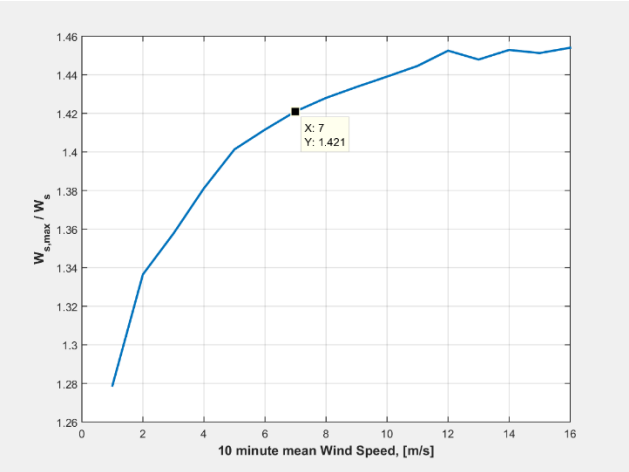

Figure 7.7. Maximum and mean Wind speed relation.

According to Figure 7.7, the maximum wind speed at which the equipment response exceeds the operational limits (at 7m/s 10 min mean) is 1.42 times higher than the input 10min mean wind speed. The factors found from the figures are used to determine the maximum values for operation limits in Table 5.2. Limits for rotor lift operation.

Here it has to be noted that the extreme values are not directly used in further analysis and is only an indication of what extreme met-ocean conditions the model can withstand. The *alpha-factor method* focuses on significant wave height rather than maximum wave height rather than maximum values. Furthermore, the forecasted met-ocean conditions are also described by significant wave height, peak wave period and 10min average wind speed at reference height (10m).

8 Test period May-July 2014

In this section a brief description of weather conditions and the location for the virtual installation case assessment is given. The virtual test case is set to be a Hywind Rotor installation at FINO3 measurement mast location. This location is chosen because measurements of met-ocean conditions are available from the FINO3 met-mast.

The weather forecasts are ECMWF supplied every 24 hours, a total of 92 files for the whole May 01 – Aug 01 period. The weather forecasts are aggregated in such a way that the forecast provided at 00:00 hours is used until a new forecast is supplied the next day at 00:00 hours. This reduces the uncertainty in the forecast and also represents a close-to-reality situation, when the least uncertain weather forecasts would be used as soon as they are available. The ECMWF weather forecasts have a 3 hour temporal resolution and thus all the forecasted parameters are regarded as 3-hour sea state parameters.

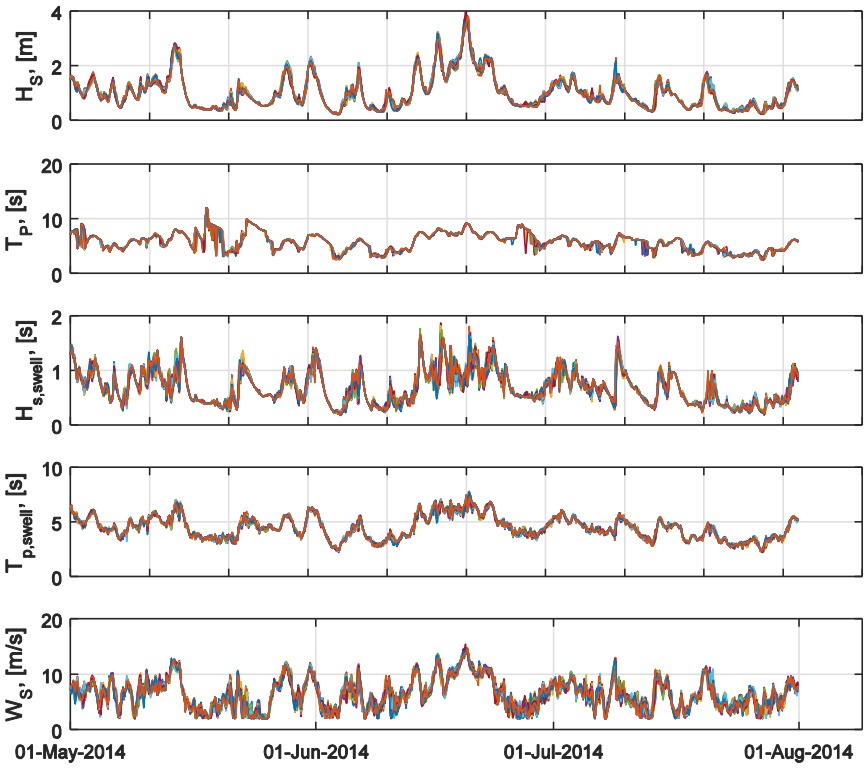

Figure 8.1. Weather conditions during the test period.

9 Weather window estimation using Alpha-Factor method

This section describes how a standard Alpha-Factor method can be applied to estimate the weather windows for Hywind rotor lift operation. The test period considered is *late spring-summer of 2014 (May 01 to August 01)*.The analysis is based on (DNV, 2011) section 4. The procedure for weather window estimation is clearly defined for weather forecasts that do not include multiple ensemble members. According to the guidance note in (DNV, 2011) sec. 4 B 701, ensemble forecasts can be used as an alternative to the standard Alpha-Factor method.

There are multiple ways to use the *alpha-factor* methodology described in (DNV, 2011), the simplest and most straight-forward one is to use predefined tabulated *alpha-factors* which are valid for the whole North Sea. This will be presented in the following section. Also it is possible to derive the *alpha-factors* based on measurement data at the installation site, this will also be investigated in section 9.2.

9.1 Tabulated *Alpha-Factors* based on (DNV, 2011) standard

State of the art in determining weather windows today is using the tabulated *alpha-factors* defined by (DNV, 2011) . The standard provides *alpha-factors* for significant wave height for different

weather forecast qualities and operation durations (for reference see Tables 4-1 to 4-5 in (DNV, 2011)).

Based on the findings in section 7.2 and Table 7.1 the limiting wave height for Hywind Rotor Lift Operation is H_s=1.5m, this value is used to determine the *alpha-factors* from the Tables 4-1 to 4-5 in (DNV, 2011). Based on Table 4-6 in (DNV, 2011) *alpha-factor* for wind speed W_s=7m/s is selected to be equal to $\boldsymbol{\alpha_{Ws}}$ **=0.8.**

Since the Hywind Rotor system seems to be highly sensitive to the incoming wave period when being installed, based on the fact that the SIMO model becomes unstable or critical responses exceed the limits when Tp≥5~6s, *alpha-factor* has to be defined for wave period. There is no clear standardized way to define the *alpha-factor* for wave period, therefore for the initial analysis the *alpha-factor* is taken either $\boldsymbol{\alpha_{Tp}=1}$ **or** $\boldsymbol{\alpha_{Tp}=\infty}$**,** which represents either no reduction (=1) in the limiting wave peak period or disregarding (=∞**)** the limitations on wave period entirely. The middle value $\boldsymbol{\alpha_{Tp}=0.}$78 is estimated based on FINO3 measurement data (see section 9.2).The following table summarizes selection of tabulated alpha factors for different weather forecast levels.

Table 9.1. Tabulated *alpha-factors*.

	α_{Hs} for H_s = 1.5m	α_{Tp} for T_p = 5s			α_{Ws} for W_s = 7m/s	Quantile
T 4-1. WFQ = C	0.705	inf	0.78	1	0.8	mean
T 4-2. WFQ = B	0.740	inf	0.78	1	0.8	maximum
T 4-3. WFQ = A+M	0.780	inf	0.78	1	0.8	maximum
T 4-4. WFQ = A+C	0.925	inf	0.78	1	0.8	maximum
T 4-5. WFQ = A+M+C	0.925	inf	0.78	1	0.8	maximum
FINO3 measurements	0.810	inf	0.78	1	0.8	maximum

T x-y – table indicator for reference in (DNV, 2011);
WFQ – weather forecast quality class **A, B** or **C**.
+M – meteorologist on site, +**C** – calibrated based on measurement data.

The following figures show an example of estimated weather windows based on **T 4-3. WFQ=A+M** case with $\boldsymbol{\alpha_{Tp}=0.79.}$ Individual met-ocean condition limits (Figure 9.2) are summarized into combined weather windows taking all the limits into account (Figure 9.1).

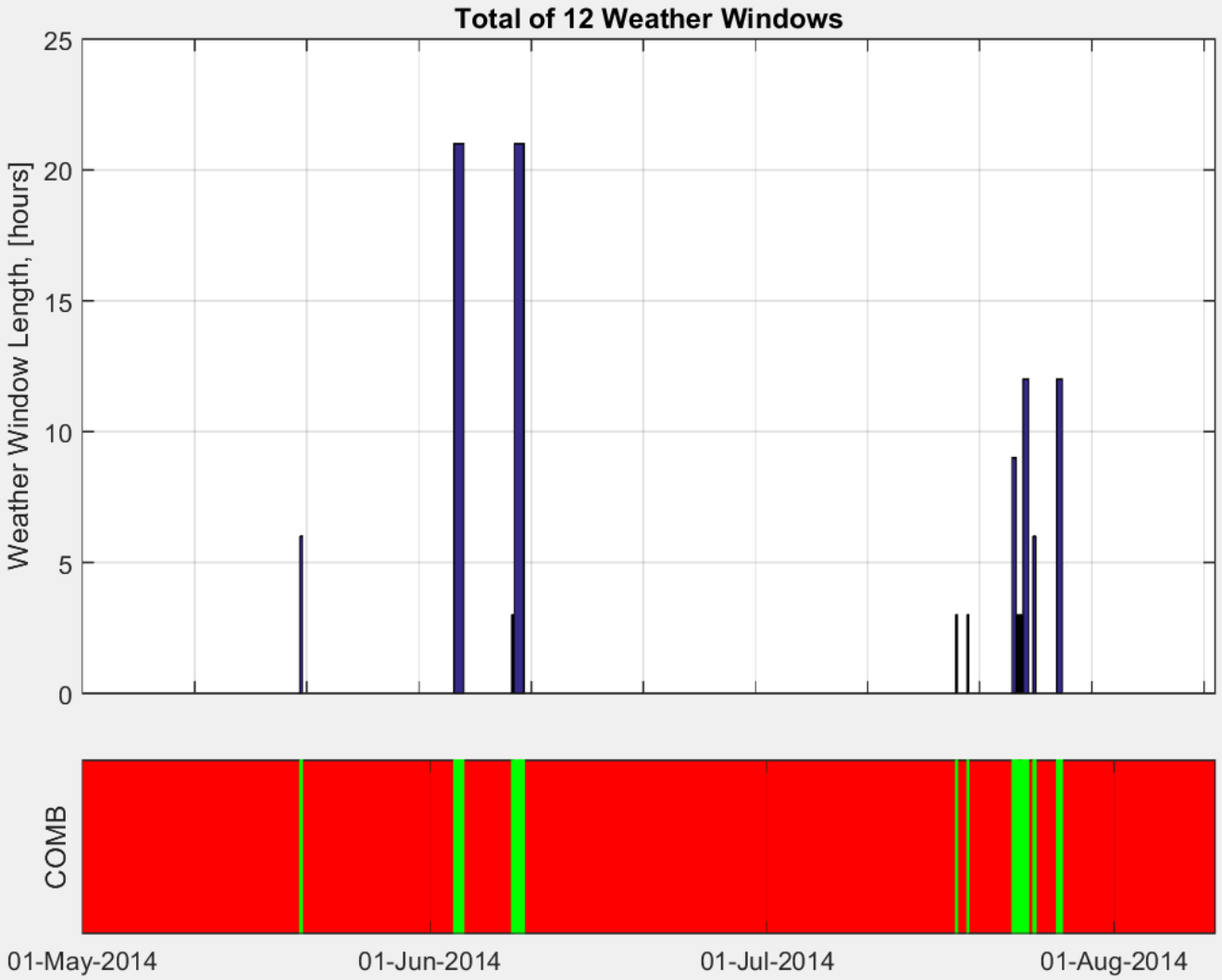

Figure 9.1. Weather windows for Combined Weather Limits, *alpha-factor* method using ECMWF forecasts as input.

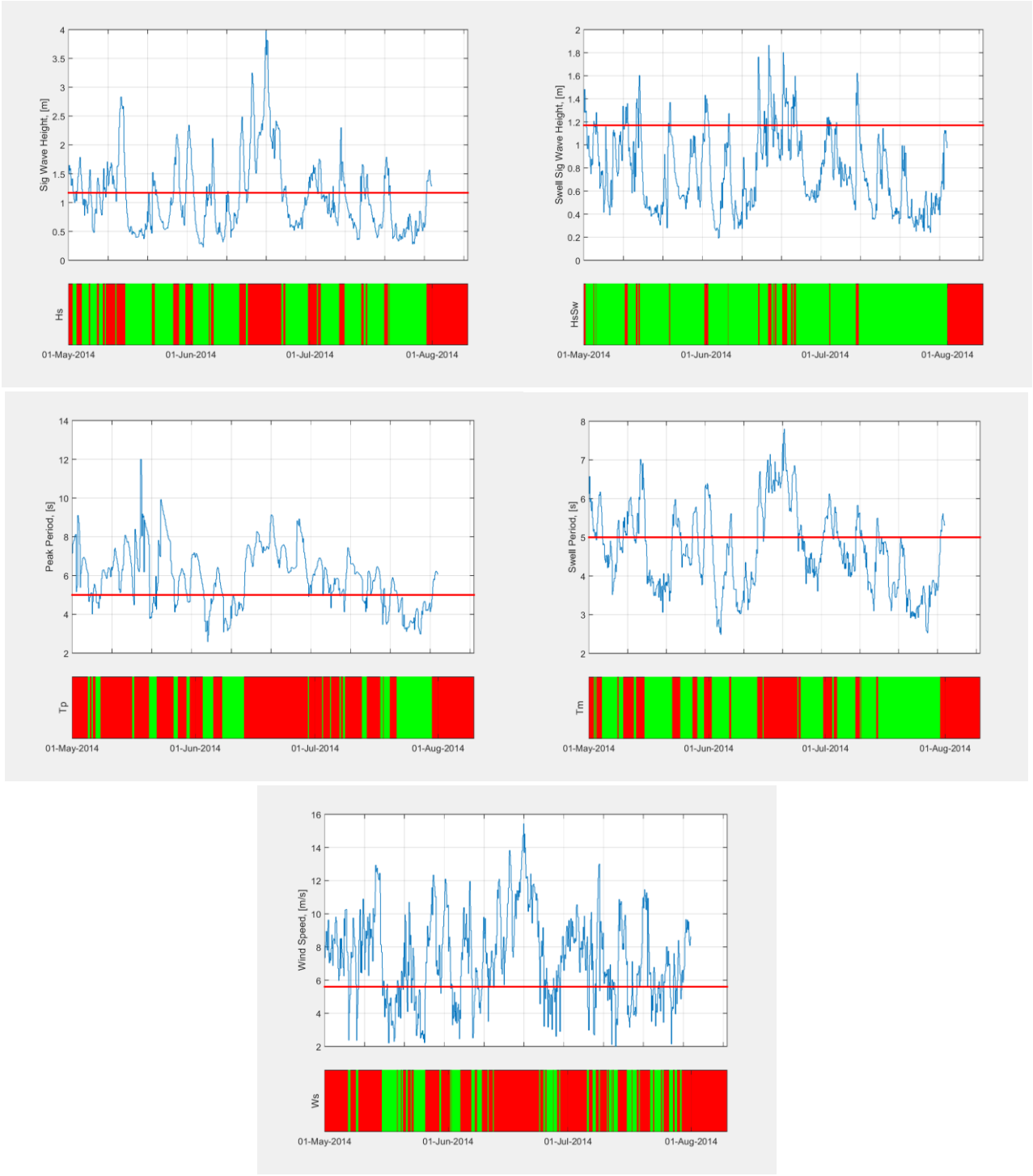

Figure 9.2. Weather windows for individual Weather Limits.

It is clearly evident from the figures above that for this particular installation process (floating crane installing on floating wind turbine tower) weather conditions are not very favourable even during the summer months of 2014 with only 12 available weather windows. The same analysis was performed using different weather forecast qualities and the following Figure 9.3 summarizes the results. The

measure on Y axis is selected to be a multiplication of number and length of estimated weather windows due to the fact that both of these criteria are equally important.

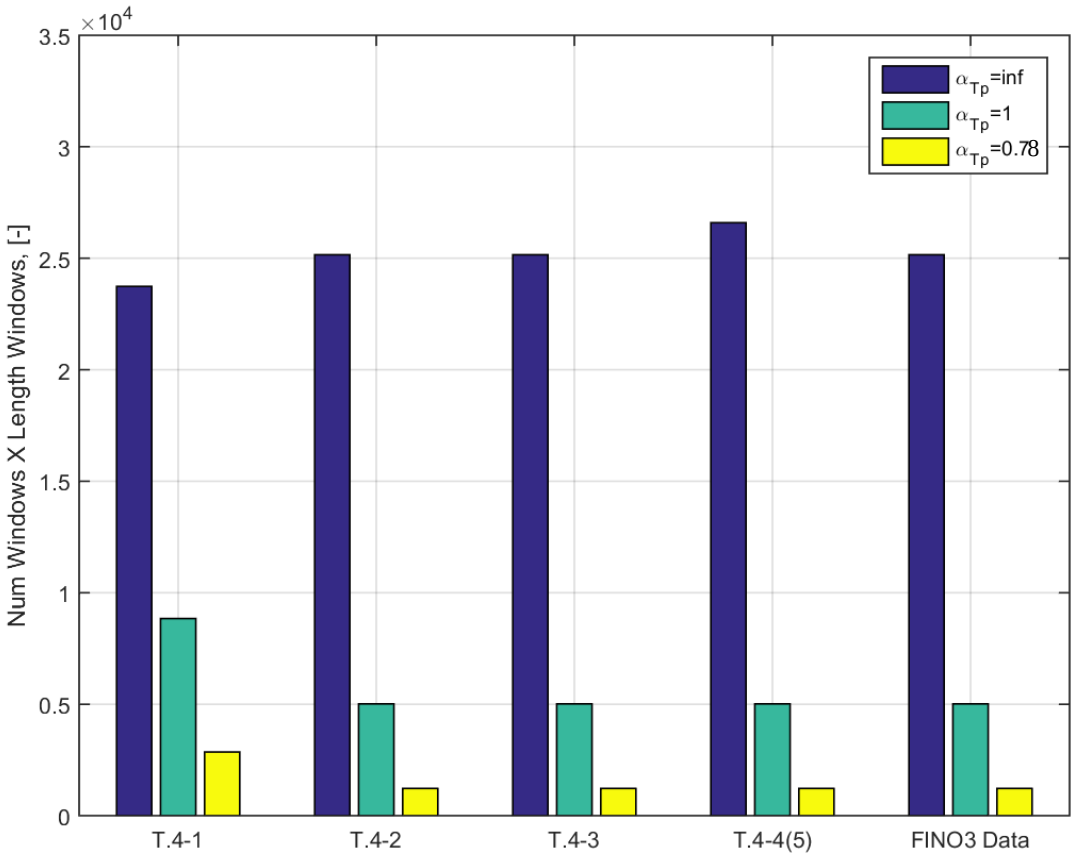

Figure 9.3. Summary of weather windows estimation.

It has to be noted that some benefits of increased weather forecasts quality (having meteorologists or calibration equipment on board) can be observed, although the differences are not very big. Furthermore, it is clear that *alpha-factor* applied to wave peak period reduces the number and duration of weather windows significantly and thus needs a more detailed analysis (see section 9.2). Also, it is visible that when *alpha-factor* is applied to wave peak period (green and yellow bars) the amount and duration of weather windows stays relatively stable even if *alpha-factor* for wave height is increased with increasing weather forecast quality. It indicates that for the selected Hywind Rotor Lift test case, the most influential met-ocean parameter in determining the weather windows is wave period. This can be easily explained by the natural frequency of the whole installation system being in the range of dominant North Sea wave periods (4-8s during summer 2014 based on measurements at FINO3 site).

9.2 *Alpha-factors* based on FINO3 measurements

This section describes the methodology of determining the *alpha-factors* when measurement data is available. The analysis is based on (Wilcken, 2012), which in turn was based on theoretical background presented in (DNV JIP, 2007) later on to be used to update the *alpha-factors* (DNV, 2011).

The typical procedure of using tabulated *alpha-factors* can be substituted by statistical analysis of weather forecasts and measurements at the location of interest (installation). In general *alpha-factor* is a measure of uncertainty related to weather forecasts, therefore, if properly analysed, measurement and weather forecast data can be used to define specific *alpha-factors* for a given location. The following equation is used to define *alpha-factors:*

$$\alpha = \frac{H_{max}}{H_{max,Wf}} \tag{9.1}$$

Where:
H_{max} – maximum wave height with a probability of exceedance of 10^{-4} during a certain period;
$H_{max,Wf}$ - maximum wave height with a probability of exceedance of 10^{-4} during a certain period taking into account the bias and variance of the weather forecast.

Bias and variance of the forecast are calculated in terms of mean and standard deviation of the error term:

$$H_{error} = H_{forecasted} - H_{measured} \tag{9.2}$$

$$E[H_{error}] = \frac{1}{n}\sum_{i=1}^{n} H_{error,i} \tag{9.3}$$

$$\sigma_{error} = \sqrt{\frac{\sum(H_{error} - E[H_{error}])^2}{n-1}} \tag{9.4}$$

The measured and forecasted weave heights are grouped into bins of 1m in order to conform to the format used in (DNV, 2011) for tabulated *alpha-factors.* The following figure shows the measured and forecasted significant wave height at FINO3 site. Figure 9.4 shows the maximum spread of a ECMWF weather forecast, but only up to +72 hours forecast time (green scatter in the figure) will be used in this analysis. Although it is not necessary to define the alpha factors beyond the expected 1-2 hours of operation duration, a more detailed analysis of up to +72 hours forecast time will provide insight on whether the calculations are correct (by comparison to tabulated alpha factors in (DNV, 2011)).

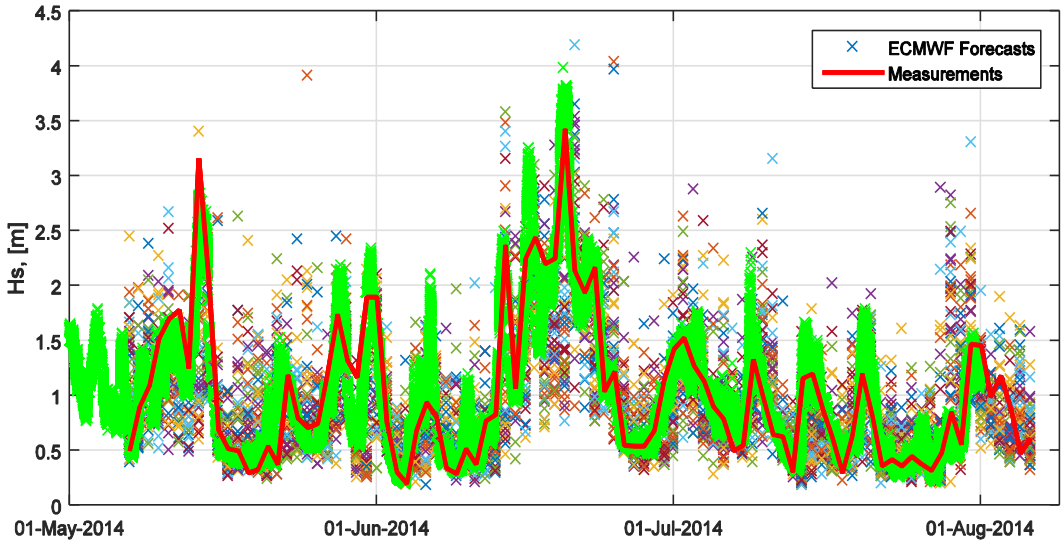

Figure 9.4. Measurements and forecasts of Hs at FINO3.

The following two figures show the bias and the variance of the weather forecasts. It has to be noted that the figures conform to what was initially obtained in (DNV JIP, 2007), therefore the results are considered to be correct.

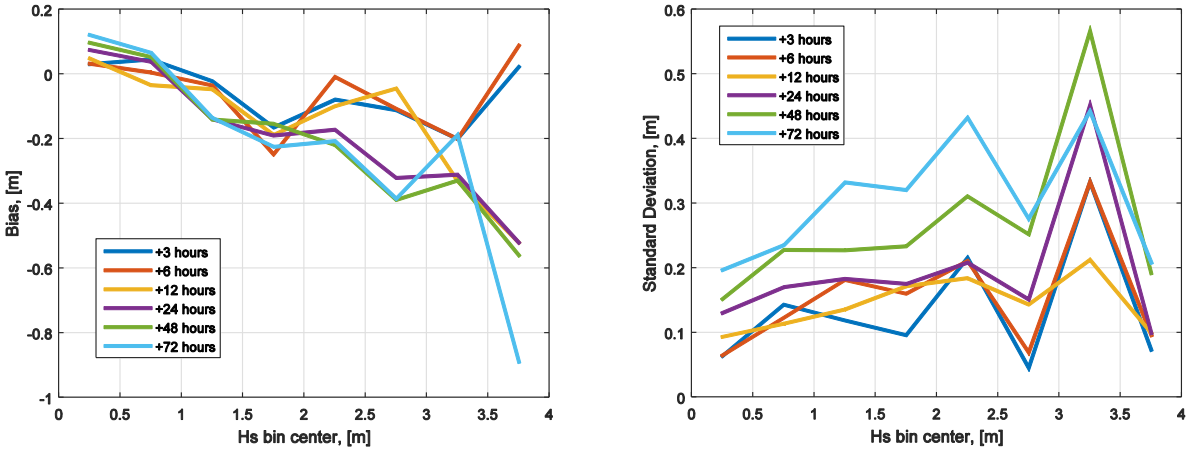

Figure 9.5. Forecast bias and standard deviation for Hs, FINO3 site.

The bias and standard deviation of the forecast will be later on used in order to properly define the weather forecast uncertainty. The maximum wave height for a 3 hour forecast period can be obtained using the following equation (Rayleigh CDF for for wave height conditioned of H_s):

$$P(H_{max} \leq H) = \left[1 - e^{\left(-2\frac{H^2}{H_s^2}\right)}\right]^{n=\frac{t_f}{T_p}} \tag{9.5}$$

Where:
H_{max} - maximum wave height;
n – expected number of waves during a certain period;
t_f – forecast duration, 3 hours=3600s;
T_p – forecasted wave peak period;
H_s - forecasted significant wave height;

The forecasted values are adjusted for bias based on Figure 9.5 and the maximum wave height is calculated from the Rayleigh CDF at 10^{-4} probability of exceedance:

$$1 - P(H_{max} \leq H) = 10^{-4} \tag{9.6}$$

$$1 - P\left(H_{max,WF} \leq H\right) = 10^{-4} \tag{9.7}$$

Also $H_{max,Wf}$ is calculated at the same probability exceedance, but due to the fact that full weather forecast uncertainty has to be taken into account, the joint probability density of H and H_s is used:

$$p(H, H_s) = p(H|H_s)p(H_s) \tag{9.8}$$

Where:
$p(H, H_s)$ – joint probability density function of wave height H and significant wave height H_s;
$p(H|H_s)$ – conditional probability density function of wave height H, Rayleigh distribution;
$p(H_s)$ – probability density function of significant wave height H_s, assumed to be normal distributed with mean value of H_s adjusted for bias and standard deviation taken as the standard deviation of the error terms: $N(\mu_{Hs,f} + bias, \sigma_{error})$.

The cumulative density function used to determine $H_{max,WF}$ then becomes:

$$P\left(H_{max,WF} \leq H\right) = \int_0^{H_{max}} \int_0^{\infty} p(H|H_s)p(H_s)\, dH_s\, dH \tag{9.9}$$

$$P\left(H_{max,WF} \leq H\right) = \int_0^{H_{max}} \int_0^{\infty} \frac{43200 \cdot H \cdot e^{\left(-2\frac{H^2}{H_s^2}\right)} \cdot \left(1 - e^{\left(-2\frac{H^2}{H_s^2}\right)}\right)^{\frac{10800}{T_p}-1}}{T_p \cdot H_s^2} N(\mu_{Hs,f} + b, \sigma_{error}) dH_s\, dH \tag{9.10}$$

By integrating, H_{max} is determined as the upper limit of the integral that gives the exceedance probability of 10^{-4}. The following figure shows the calculated alpha factors for up to +72 hours forecast time and up to 4 meters wave height.

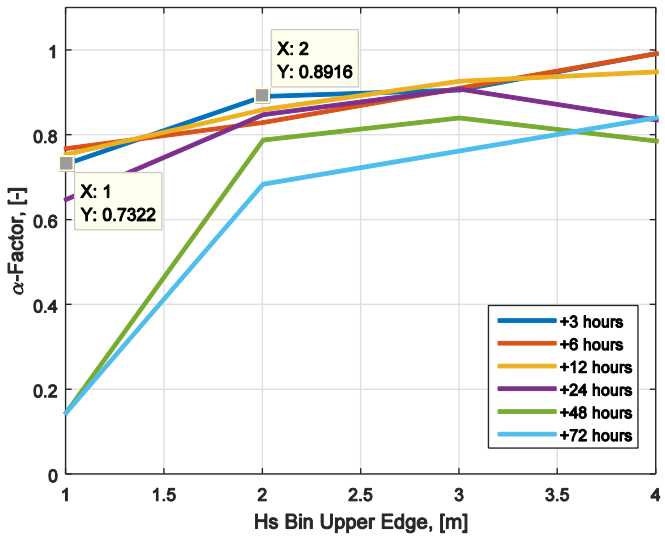

Figure 9.6. *Alpha-factor* for Hs, at FINO3.

When compared to the values of *alpha-factors* in (DNV, 2011), the results from Figure 9.6 seem to be following the same trends and close to the actual tabulated values. The *alpha-factor* of interest for the Hywind Rotor Lift operation is for < 3 hours of operation period and at 1.5m significant wave height. By linear interpolation, alpha factor is $\boldsymbol{\alpha_{Hs}=0.81}$.

As previously mentioned in section 7.2, there is no standard way to define *alpha-factors* for wave periods, therefore the same methodology as for wave heights will be used to determine site specific *alpha-factor* for wave peak period. The following figures show the dataset used to define the *alpha-factor* and the forecast uncertainty in terms of bias and standard deviation of error term. The same procedure is used as for significant wave height.

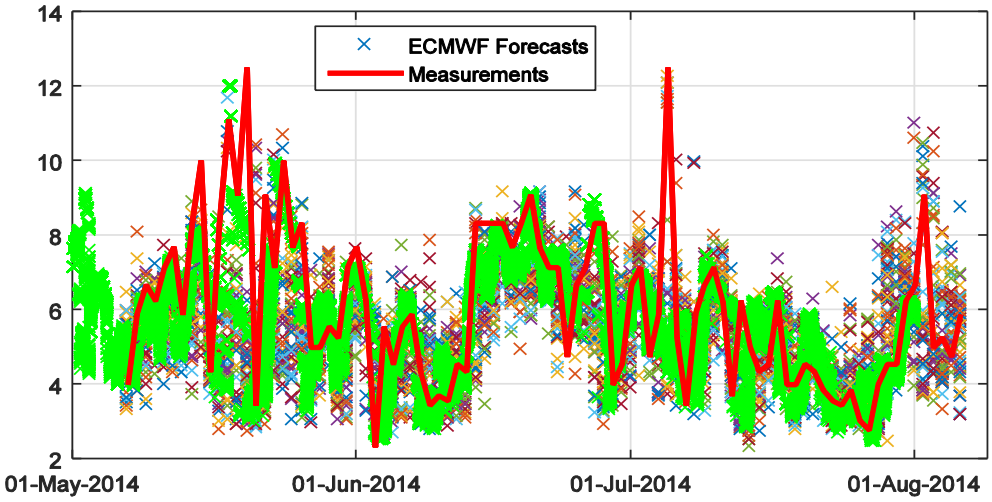

Figure 9.7. Measurements and forecasts of T_p at FINO3.

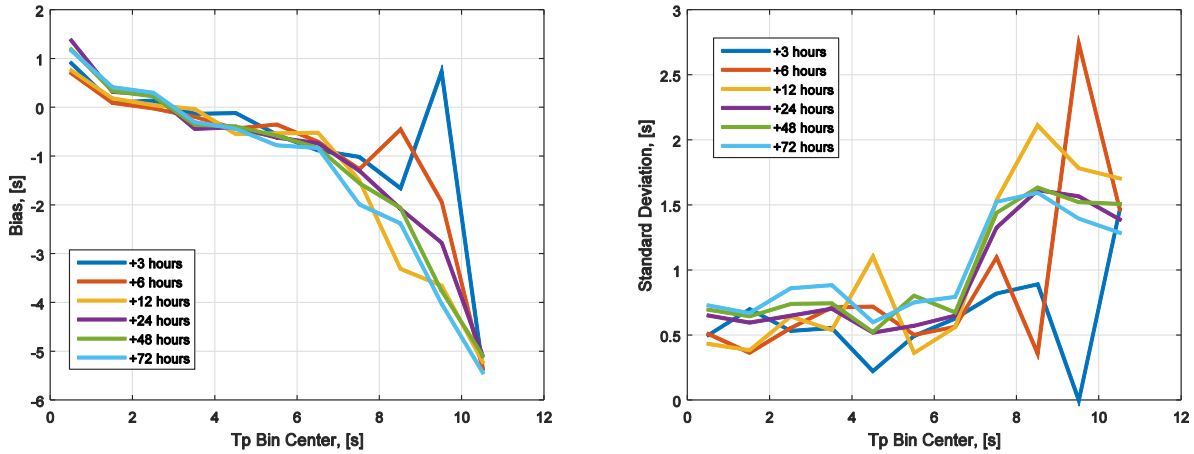

Figure 9.8. Forecast bias and standard deviation for Tp, FINO3 site.

In order to properly define the *alpha-factor* for wave peak period, a distribution of wave periods is necessary. For this analysis Bretschneider distribution wave periods will be used (based on (Wist, 2003) and (Clauss, et al., 1994)):

$$P(T_{max} \leq \tau) = \left[1 - e^{\left(-0.675\frac{\tau^4}{T_{m01}^4}\right)}\right]^{n=\frac{t_f}{T_p}} \tag{9.11}$$

Where:
T_{max} - maximum wave period;
n – expected number of waves during a certain period;
t_f – forecast duration, 3 hours=3600s;
T_p – forecasted wave peak period;
T_{m01} - mean wave period, related to wave peak period $T_{m01} = T_p/1.2$;

Again, forecasted values are adjusted for bias based on Figure 9.8 and the maximum wave period is calculated from the Rayleight CDF at 10^{-4} probability of exceedance:

$$1 - P(T_{max} \leq T) = 10^{-4} \tag{9.12}$$

$$1 - P\left(T_{max,WF} \leq T\right) = 10^{-4} \tag{9.13}$$

The joint density for wave periods is obtained the same way as it was for the wave heights, but by using the Bretschneider distribution as basis. The cumulative density function used to determine $T_{max,WF}$ then becomes:

$$P\left(T_{max,WF} \leq T\right) = \int_0^{H_{max}} \int_0^{\infty} p(T|T_{m01})p(T_{m01})\, dT_{m01}\, dT \tag{9.14}$$

$$P\left(T_{max,WF} \le T\right) =$$

$$= \int_0^{T_{max}} \int_0^{\infty} \frac{29160 \cdot \tau^3 \cdot e^{\left(-0.675\frac{\tau^4}{T_{m01}^4}\right)} \cdot \left(1 - e^{\left(-0.675\frac{\tau^4}{T_{m01}^4}\right)}\right)^{\frac{10800}{T_p}-1}}{T_p \cdot T_{m01}^4} N\left(\mu_{Tm01,f} + b, \sigma_{error}\right) dT_{m01}\, dT \tag{9.15}$$

By integrating, T_{max} is determined as the upper limit of the integral that gives the exceedance probability of 10^{-4}. The following figure shows the calculated alpha factors for up to +72 hours forecast time and up to 15s wave period.

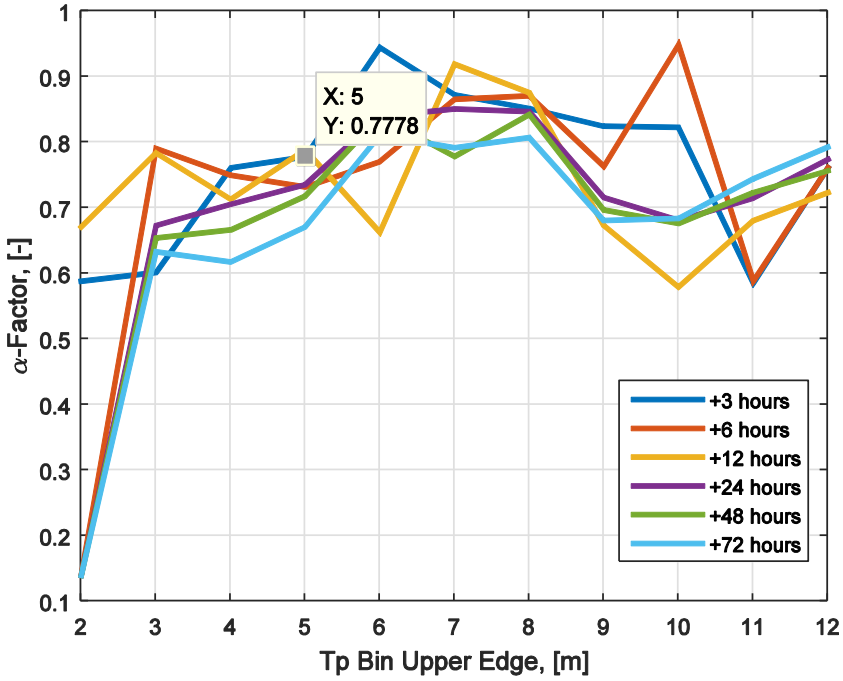

Figure 9.9. *Alpha-factor* for Tp, at FINO3.

Alpha-factor for 5s wave peak period is obtained $\boldsymbol{\alpha_{Tp}=0.78}$.

Looking back at the figure Figure 9.3 it is now clear that the most reasonable results are the ones represented in yellow, since the *alpha-factor* there is determined from actual FINO3 data. Although unlimited wave period would give a lot more and longer weather windows during the test period of summer 2014 it is clearly an unrealistic scenario, therefore it will be disregarded in further analysis. Furthermore, even the situation where $\boldsymbol{\alpha_{Tp}=1}$ is very unrealistic, because it would represent a situation where the weave periods are forecasted with 100% accuracy which is impossible. $\boldsymbol{\alpha_{Tp}=1}$ scenario will be kept only for comparison.

10 Weather window estimation using DECOFF method

In this section, statistical DECOFF method is used to determine weather windows for Hywind Rotor Lift Operation. The procedure proposed in section 4 is used throughout this section. The test period is *May 01 – August 01 2014.* Main focus will be directed to the part of the Hywind Rotor Lift Operation when the barge is already positioned at the installation location and the rotor is lifted up and bolted to the nacelle (the same part of operation that was analyzed in section 4).

It has to be noted that (partially) failed SIMO simulations are considered unusable if >10% of output time series is corrupted (usually 0-padded). Whenever a failed simulation is detected the probability of failure for that particular combination of met-ocean conditions is considered to be 1 (complete failure). Two cases are analyzed – using either ECMWF forecasts or measurements at FINO3 site as input to SIMO and DECOFF statistical method.

10.1 Weather windows using DECOFF method with ECMWF forecasts

This section describes the results of DECOFF method for weather window estimation when multi-ensemble weather forecasts. The simulations are performed for every day within the test period with temporal resolution of 3 hours using all 51 ensembles contained in ECMWF forecast. Although it has to be noted that due to limited amount of time and computation power, only one seed is used to simulate the responses in contrast to 16 seeds that were used in section 4. This implies a higher uncertainty in the results, but significantly reduces the amount of time necessary to perform all the simulations.

The limit states under consideration remain the same as in section 4 (see Table 5.2). Only phases 3-6 are simulated and analyzed because they are the most important and also the most sensitive to changing met-ocean conditions. Furthermore, phases 3-6 have to be analyzes together because the operation is non-reversible after phase 3 has started.

Input parameters from ECMWF forecasts used as SIMO input:

- **Wind speed and direction** (Ws, WsDir). Wind direction is taken as zero under the assumption that the vessel aligns itself with the dominant direction of the wind/wind waves in order to avoid waves coming from the sides of the vessel. ISO 19901-1 NPD wind spectrum used, defined by:

  1. reference height (10m);
  2. mean wind velocity at reference height;
  3. wind profile exponent (0.11).

- **Significant wave height and peak period** (Hs, Tp, JONSWAP 3 parameter spectrum) and wave direction the same as wind direction (WsDir, wind generated waves, equal to zero, see previous bullet). Spectrum is defined by:

1. significant wave height Hs;
2. peak period Tp;
3. peakedness parameter γ, calculated using the following equations:

$$\gamma = 5 \; for \; T_p/H_s \leq 3.6$$
$$\gamma = \exp\left(5.75 - 1.15\, T_p/H_s\right) \; for \; 3.6 \leq T_p/H_s < 5 \quad (10.1)$$
$$\gamma = 1 \; for \; 5 \leq T_p/H_s$$

- **Swell significant wave height and mean period** (HsSwell, TmSwell, JONSWAP 3 parameter spectrum) and direction (SwellDir). The actual swell direction is calculated as the misalignment between wind waves and swell waves, also since the coordinate systems of SIMO and ECMWF do not match, the direction has to be taken negative and thus becomes:

$$SwellDir = 0 - (SwellDir - WsDir) \quad (10.2)$$

Since there is only one seed simulated per ensemble member, aggregation of the time series is done in two steps, skipping the last one from section 5.3. The response is analysed as described in section 5.4. The limit state probabilities ($P_{F,Limit\ State}$) are calculated as an average over the number of ensembles and weather windows are estimated for each limit state separately. Later, the limit state probabilities of failure are combined together in a simplified way, rather than using rules for parallel or series systems. This is done in order to avoid over estimating the probability of total operation failure when taking all the limit states as a series system ($P_{F,Op} = 1 - \prod(1 - P_{F,Limit\ State})$) or underestimating the probability of failure when taking all the limit states as a parallel system ($P_{F,Op} = \prod(P_{F,Limit\ State})$). Clearly the real system is somewhere in between the two extremes, because in general it behaves as a series system with some unknown correlation. The correlation between limit states is beyond the scope of this report, therefore a simplified approach is used. The following figures show a few examples of weather windows for individual limit states (more in Appendix B).

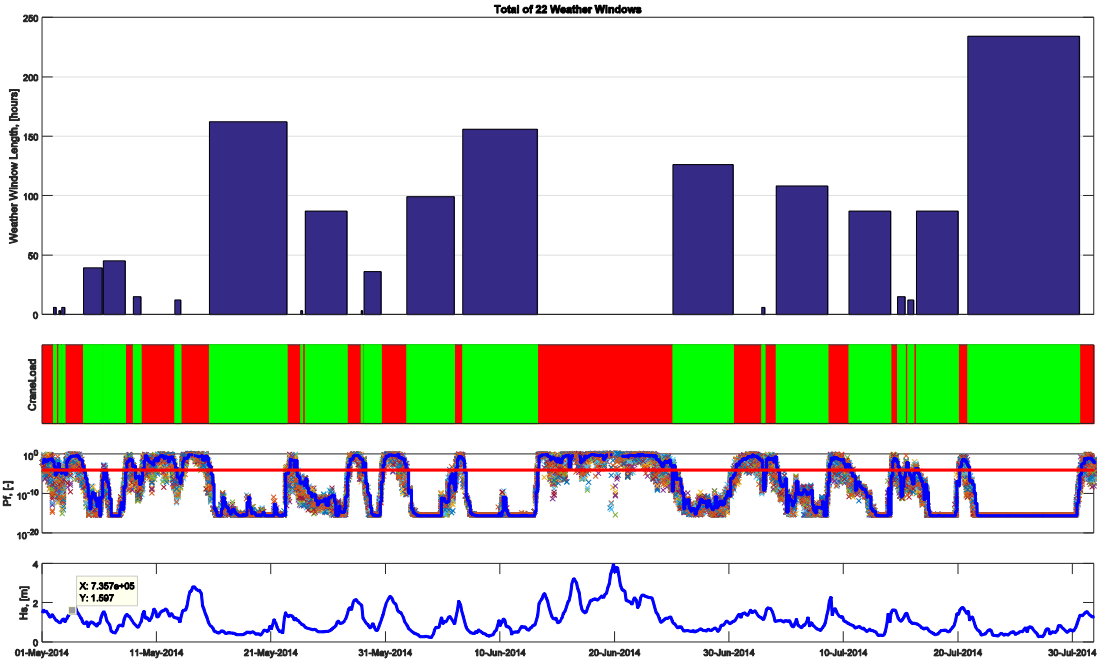

Figure 10.1. Weather windows for CraneLoad limit state.

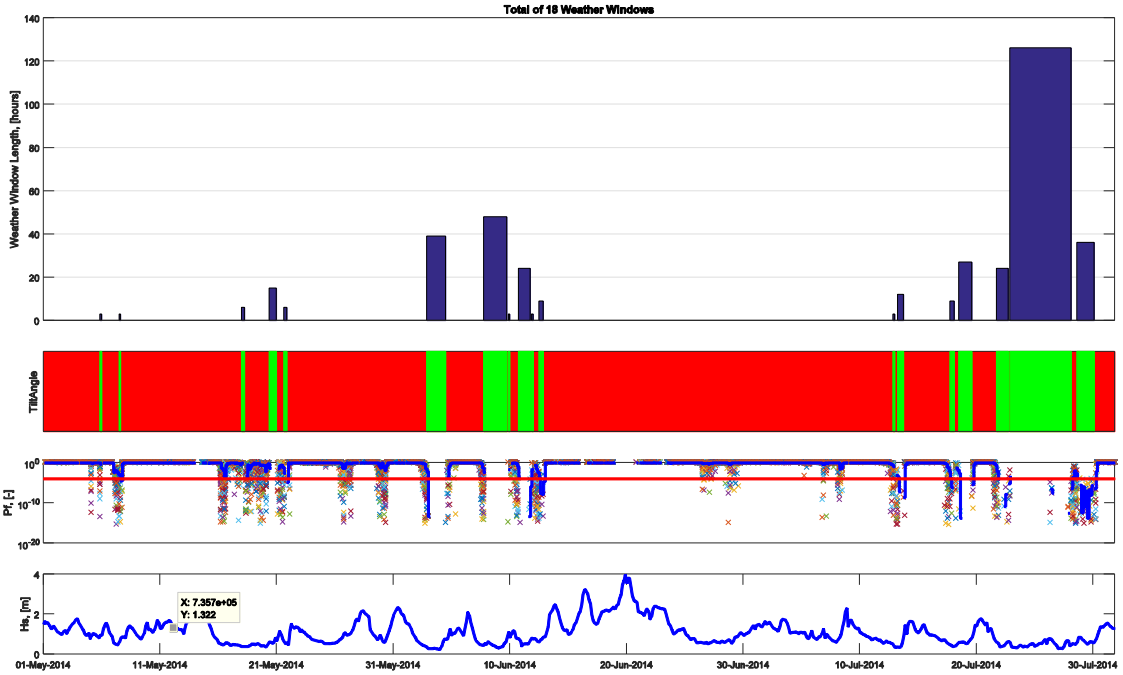

Figure 10.2. Weather windows for RotorTiltAngle limit state.

The weather windows for all limit states can be combined by extracting a Go-NoGo vector of "ones" and "zeros" (**1- operation possible**, response is below critical limit of 10^{-4} exceedance probability, **0 – operation not possible**, response is above critical limit of 10^{-4} exceedance probability) for each limit state and then multiplying the vectors together to produce one vector that shows the resulting weather window for all limit sates being above or below their respective critical limits with 10^{-4} exceedance probability. The resulting weather windows for the whole operation (considered phases 3-6) are shown in Figure 10.3.

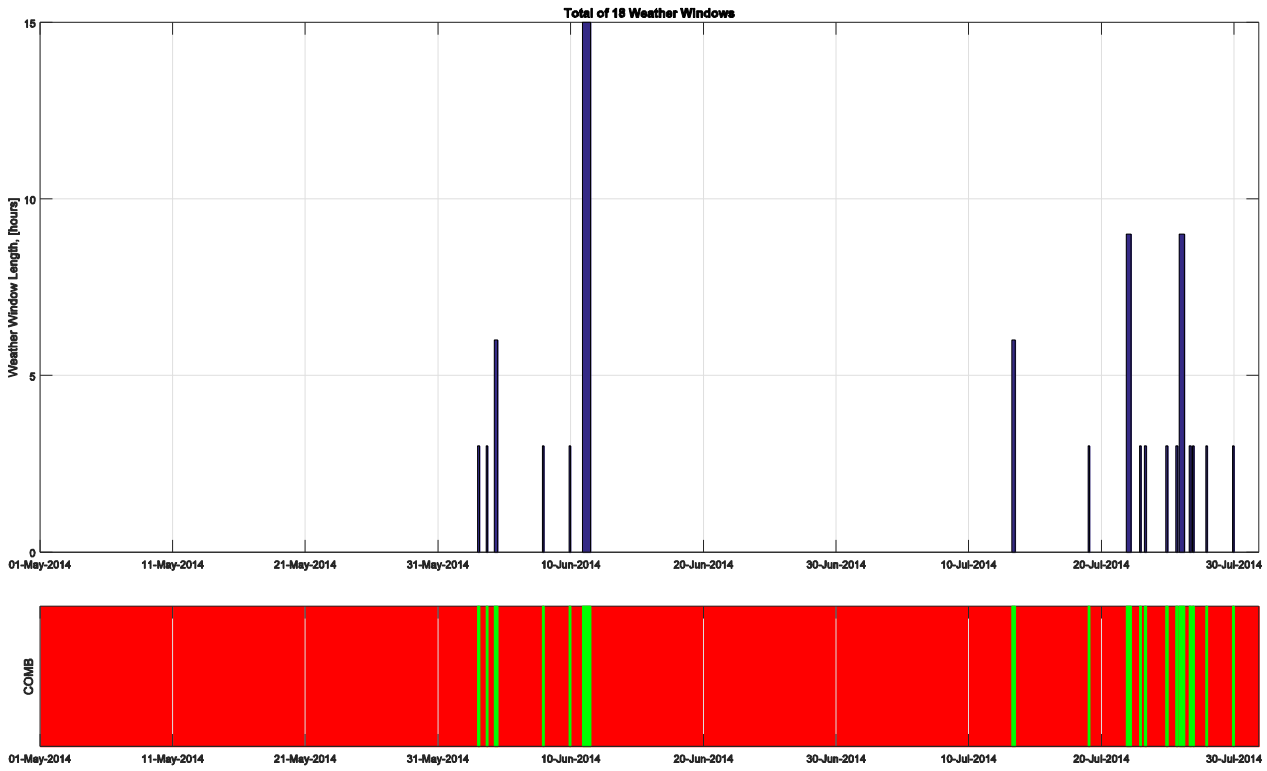

Figure 10.3. Weather windows for the whole operation (considered phases 3-6), DECOFF method using ECMWF multi-ensemble forecasts as input.

It is clearly visible, that although some of the limit sates allow the operation for long periods of time, others can limit the installation possibilities significantly. When compared to the number of weather windows, obtained by *alpha-factor* method, the DECOFF method performs better in terms of number of weather windows suitable for installation (12 to 18). A full comparison will be presented in section 11 where *alpha-factor* based analysis will be compared to DECOFF analysis with forecasts and measurements at FINO3 site.

10.2 Weather windows using DECOFF method with measurements at FINO3

This section will describe the weather windows obtained by DECOFF method by using measurements at FINO3 site instead of ECMWF forecasts. This will give insight on the impact that weather forecast uncertainty has on the number and length of weather windows.

The simulations are performed for the same period of *May 01- August 01 2014*. Measurements from FINO3 site are used as input, ocean parameters are based on Buoy measurements and meteorological parameters are based on met-mast measurements (anemometers). Some limitations of available measurements at FINO3 has to be mentioned, namely that the buoy measures the water surface elevation and no explicit distinction between wind generated and swell waves is possible. Therefore in this case, a general sea state (defined by Torstenhagen spectrum, as suggested by MARINTEK) is used as input to SIMO in contrast to ECMWF case, where separate inputs for wind generated and swell waves was used (JONSWAP 3 parameter spectrum for each). The following Figure 10.4 shows the measurements and forecasts together.

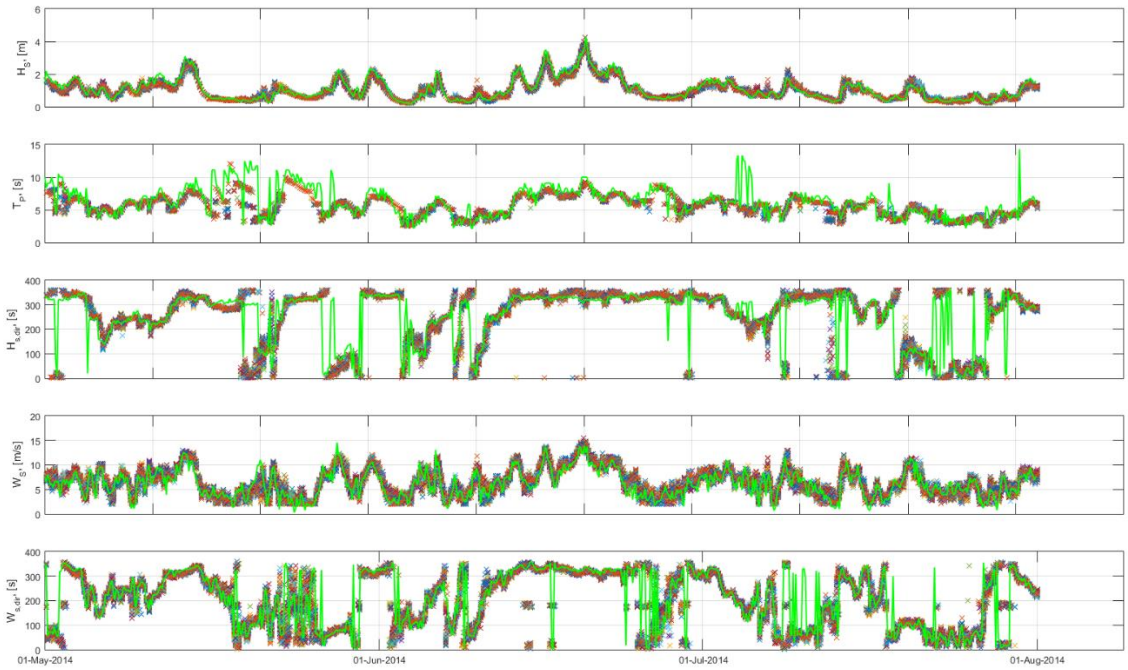

Figure 10.4. Weather Forecasts (scatter) and measurements (green line).

The forecasts are scattered around the measurements but predicts the actual met-ocean conditions reasonably well.

The following Figure 10.5-Figure 10.6 show two examples of weather windows for selected limit states (more in appendix C). For comparison purposes the limit states are identical to those in Figure 10.1 Figure 10.2.

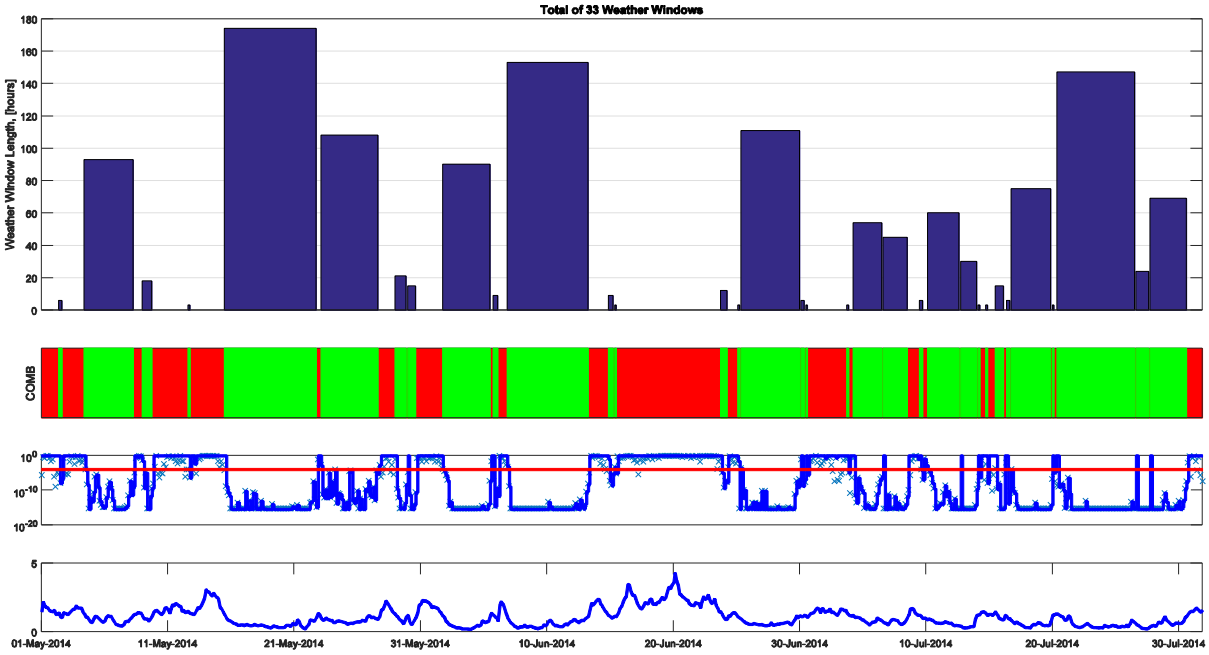

Figure 10.5.Weather Windows for Crane Load limit state.

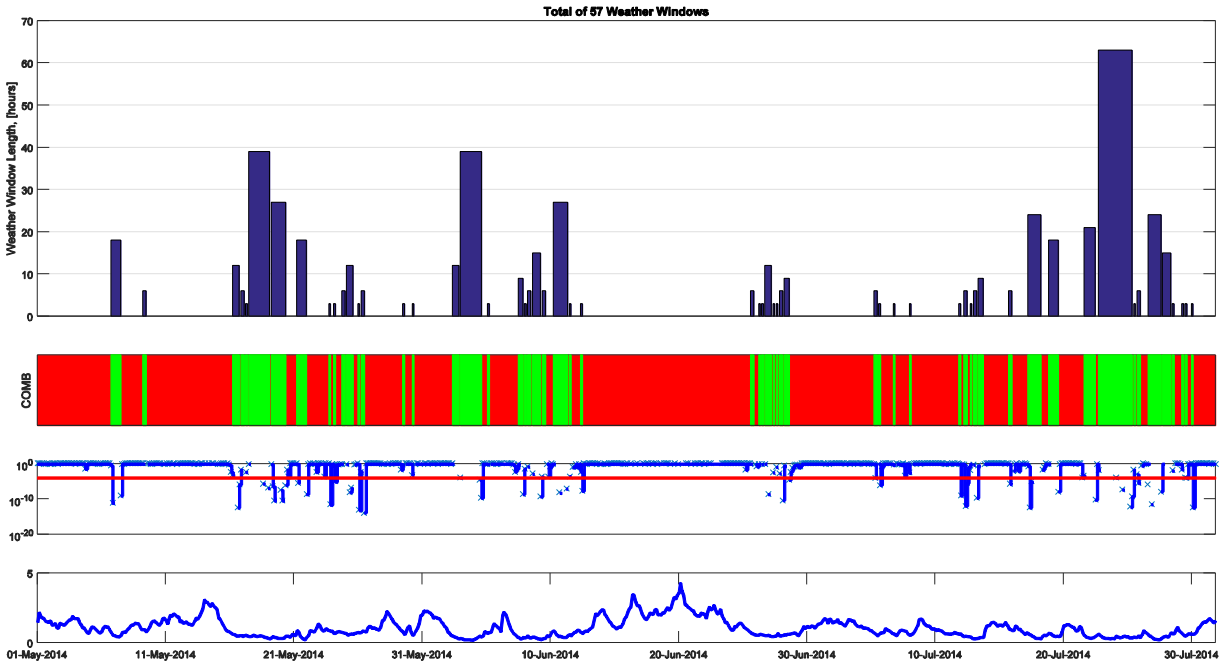

Figure 10.6.Weather Windows for Rotor Tilt Angle limit state.

By visual comparison it can be concluded that in both cases (forecasts and measurements) the predicted weather windows are relatively at the same locations in time, although when forecasts are used weather windows are shorter and fewer in number. This is a proof of DECOFF statistical model robustness – with increasing uncertainty of the input the locations of weather windows stay the same, only their duration changes.

The following Figure 10.7 shows the weather windows when all the limit states are combined together. The combination is done the same way as it was in section 10.1.

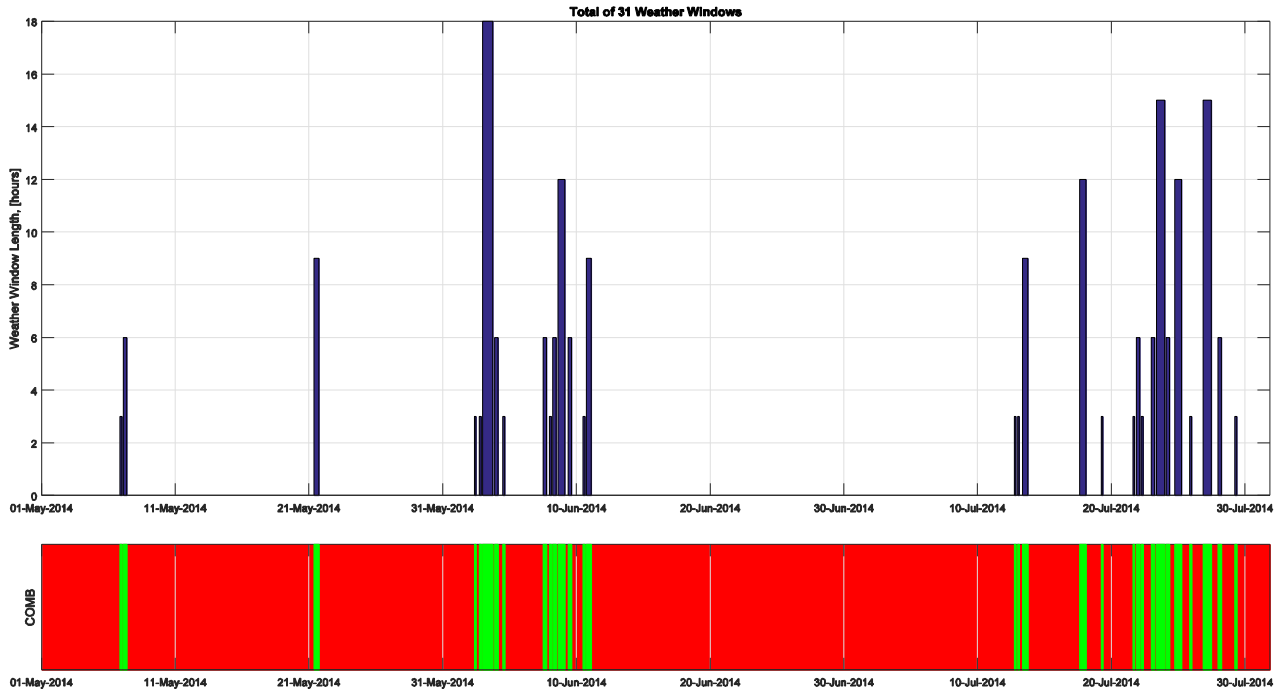

Figure 10.7. Weather windows for the whole operation (considered phases 3-6), DECOFF method using measurements at FINO3 as input.

As it was for the individual limit states, when using measurements as input to DECOFF model there are more weather windows predicted than for the case with DECOFF model run with ECMWF forecasts (31 windows for Measurements, 18 windows for Forecasts). More detailed analysis is presented in the next section.

11 Summary of different methods for weather window estimation

This section focuses on overall comparison of different methods of predicting operational weather windows for Hywind Rotor Lift Operation. The comparison is made among all the investigated cases of tabulated *alpha-factors,* custom site specific alpha factors for FINO3 and DECOFF method with either FINO3 measurements or ECMWF forecasts. The unrealistic cases of unlimited wave peak period in *alpha-factor* cases are removed from analysis as was discussed in 9.2. The following Figure 11.2 shows the difference in total number of predicted weather windows.

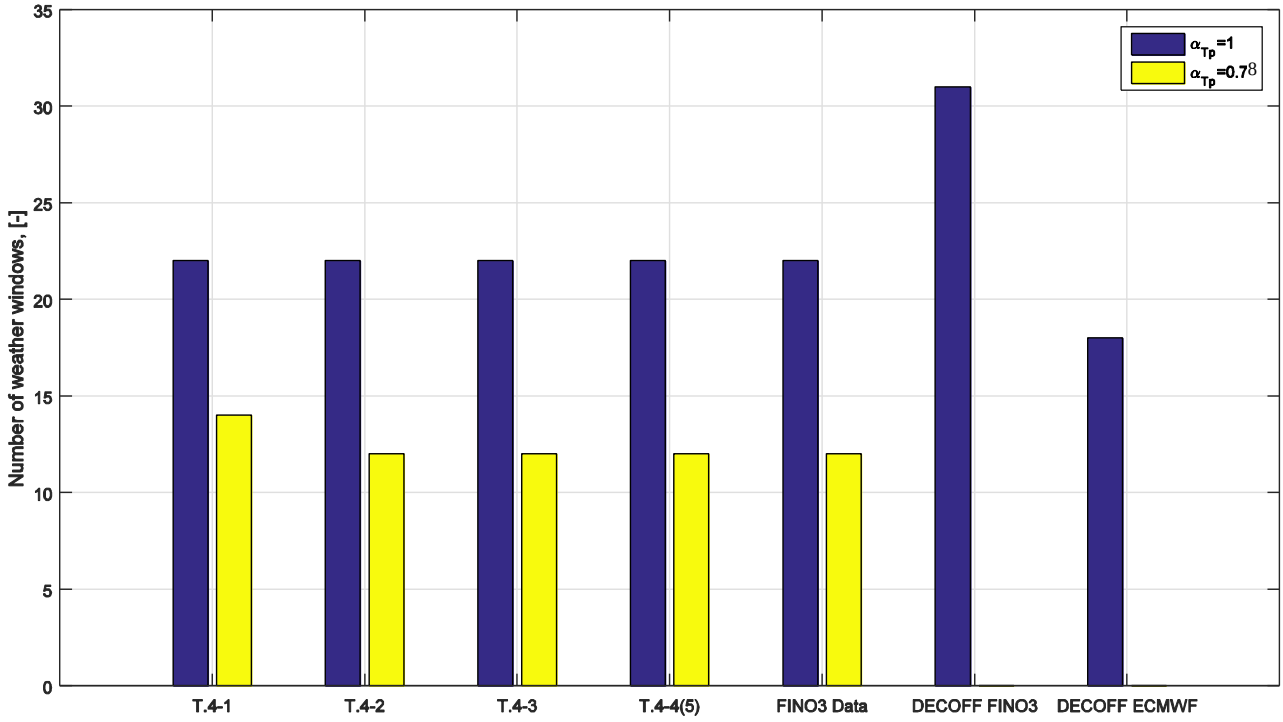

Figure 11.1. Comparison of number of weather windows.

It has to be noted that when looking at standard method from (DNV, 2011) (cases T.X-X) **the yellow bars are representative** and the blue bars are only to show that DECOFF method in some cases outperforms even standard *alpha-factor* method with less limitations. That being said, it is visible that in terms of number of windows DECOFF method is outperforming the *alpha- factor* method even when the highest weather forecast quality or measurement data from installation locations is used (T.4-4(5) and FINO3 data cases). The DECOFF ECMWF bar represents the DECOFF model run with ECMWF forecasts and as expected the number of predicted weather windows is lower than that of the case when measurements at FINO3 is used as input to DECOFF method. This is mainly because increased input uncertainty has a significant effect on the output Probabilities of Failure and thus the weather windows (for more details on weather forecast uncertainty effects see section 12).

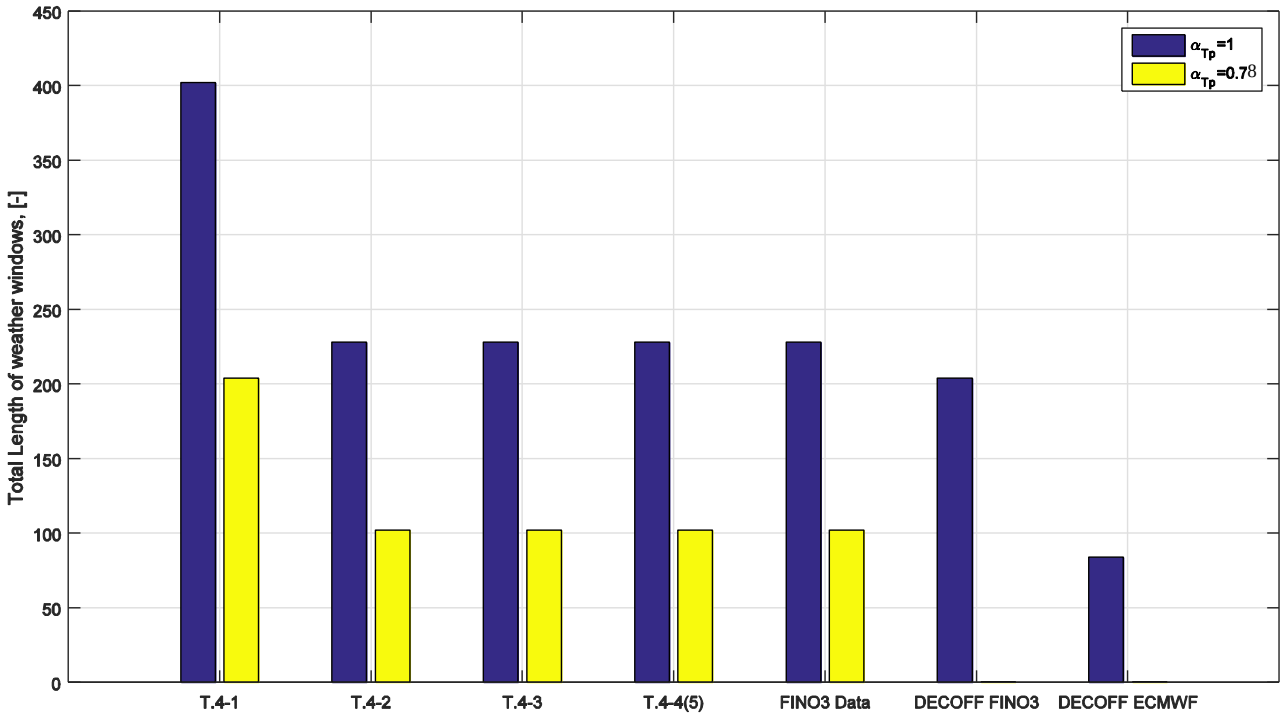

Figure 11.2. Comparison of number total length.

When the results are analysed in terms of total length of weather windows, it is again visible that DECOFF method with FINO3 measurement data outperforms all cases of standard method. DECOFF method with ECMWF forecasts as input here is performing slightly worse than the standard cases but it should be noted that the total length of weather windows ~17% lower. This difference could easily be reduced by having more accurate weather forecasts. For this analysis weather forecasts were provided daily (at 00:00) every day, in real case it would be possible to get weather forecasts every 12 or even 6 hours. This would reduce the input uncertainty and thus increase the number/duration of predicted weather windows.

Total duration and number of weather windows are both equally important parameters therefore a new measure of model performance is introduced to see the overall performance of the standard and DECOFF methods. The new measure is a multiplication of predicted number of weather windows and the total length of weather windows. The next Figure 11.3 shows the comparison.

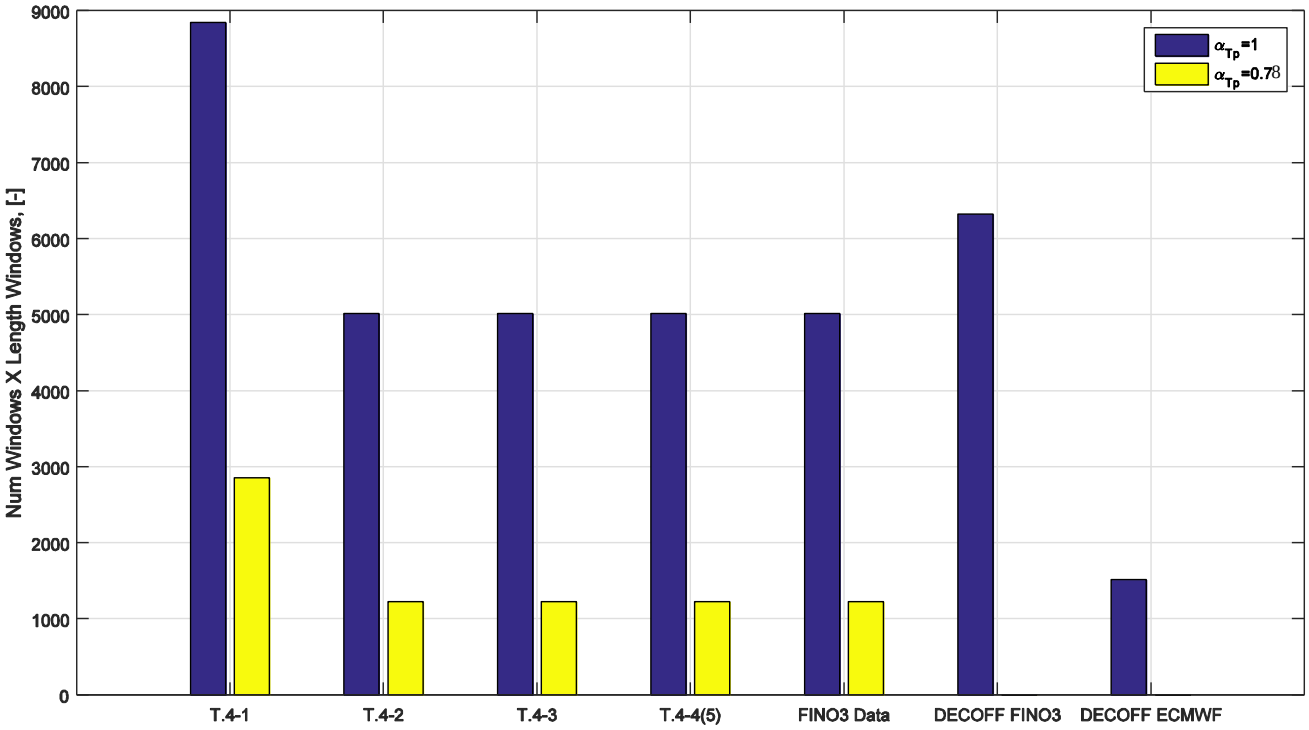

Figure 11.3. Comparison of weather windows.

It is clearly visible that DECOFF model with ECMWF forecasts as input outperforms most of the standard cases, with the exception of T.4-1. It has to be noted that case T.4-1 would rarely be used in real case for a complex installation as Hywind Rotor Lift because it is usually used for simple barge towing operations in sheltered waters and on-shore/near shore lifting. This being said it is safe to conclude that DECOFF method outperforms all standard cases. It should also be noted that when measurements are used as input to DECOFF method (this would represent a hypothetical case of a perfect weather forecast) DECOFF method out-performs even the standard cases where no *alpha-factor* for peak period is used. This shows good promise of increasing DECOFF model performance with decreasing input (weather forecast) uncertainty.

12 Effects of Weather forecast uncertainty

This section focusses on the effect that weather forecasts uncertainty has on the final output of the analysis – the probability of failure with a given limit state. Also, the effect of weather forecast uncertainty on critical response parameters are studied.

The input for SIMO is multi-parametric (wind speed and direction, swell and wind wave height and direction, swell and sea wave periods) therefore it is necessary to define one measure of uncertainty that would represent the combined uncertainty of a multi-parametric met ocean condition forecast. A multivariate Coefficient of Varation (COV_m) is chosen as such measure. The definition of COV_m is based on the following equation (Albert & Zhang, 2010):

$$COV_m = \left[\frac{\left(\overline{\boldsymbol{x}}^T \boldsymbol{S} \overline{\boldsymbol{x}}\right)}{\left(\overline{\boldsymbol{x}}^T \overline{\boldsymbol{x}}\right)^2}\right]^{1/2} \tag{12.1}$$

Where:
$\overline{\boldsymbol{x}}$ – vector of sample means of multiple input parameters;
$\boldsymbol{S}$ – dispersion matrix (covariance matrix).

The following Figure 12.1 shows the combined Coefficient Of Variation (COV) of the input.

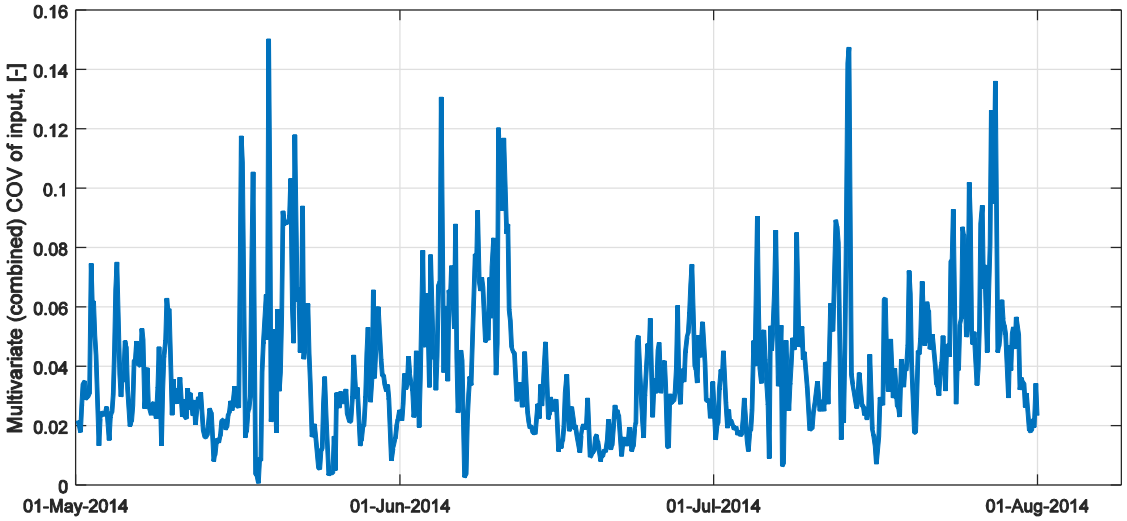

Figure 12.1. COV of input variables.

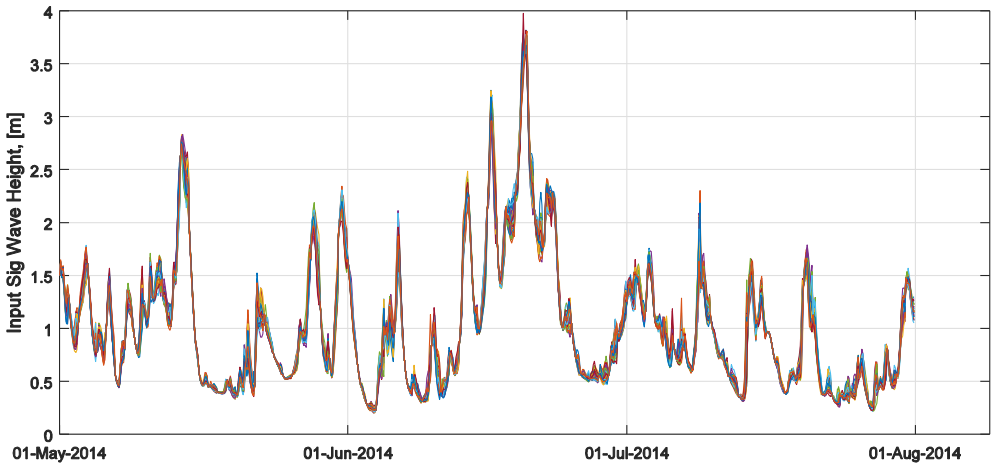

Figure 12.2. Input significant wave height.

It is obviously correct to assume that as the met-ocean conditions become more unstable (during or after a storm) the uncertainty (COV) in the forecast should increase. This can be seen when looking at Figure 12.1-Figure 12.2. Although it has to be noted that this is not true for every case, eg. Mid July storm with a high peak in Hs but no significant peak in COV.

Because of the fact that COV of the met-ocean forecasts depends not only on the forecast lead time (the further in time forecast predicts – the higher the uncertainty (COV)) but also on the stability of the weather itself, the analysis of the effects of uncertainty becomes more difficult. This implies that a simple look at the output data just based on weather forecast lead time is not enough to clearly see the effects of forecast uncertainty on the output probabilities of failure. Therefore the further analysis is based on the magnitude of COV rather than forecast lead time. This approach will allow to clearly see the effect of increasing variance in weather forecast.

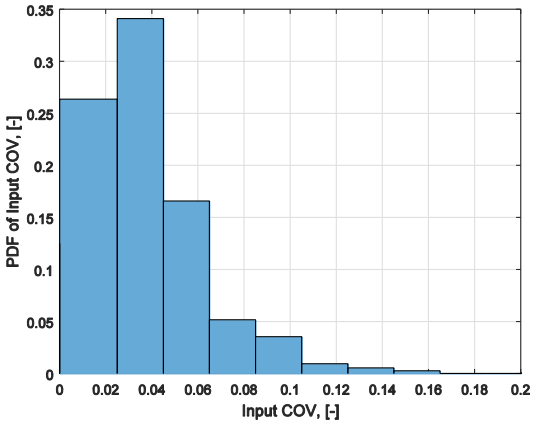

Figure 12.3. Distribution of input COV.

Also, weather forecast uncertainty can be described by miss-prediction. Miss-prediction can be analysed in terms of prediction error (Forecast - Measurement) or in terms of Bias. Effects of both – forecast bias and forecast error will be also investigated. Since it is difficult to define a combined bias and error for the multivariate input, significant wave height is chosen as representative variable and thus bias and error in significant wave height forecast will be used as basis. And again, since bias and error of the forecast depends on more than just forecast lead time, the analysis will be performed using the magnitude of forecast bias and/or error. The following figures show the time series and distributions of forecast bias and error.

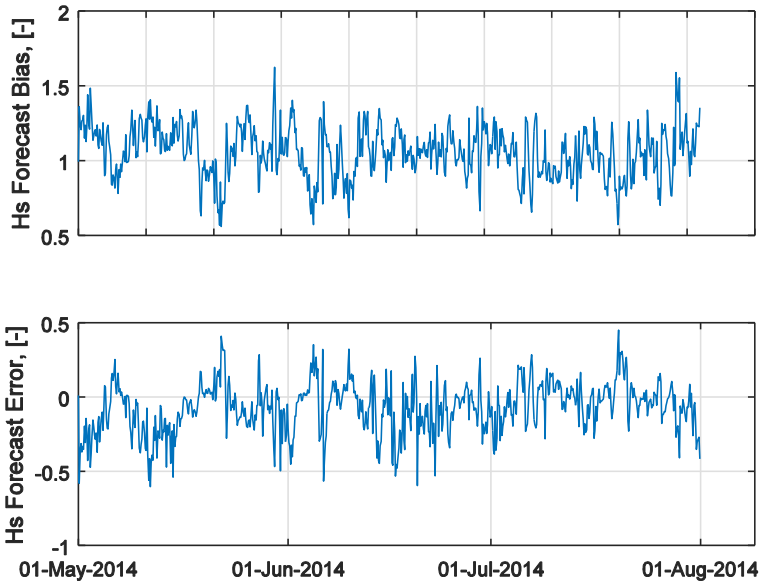

Figure 12.4. Bias and Error of the forecasted Hs.

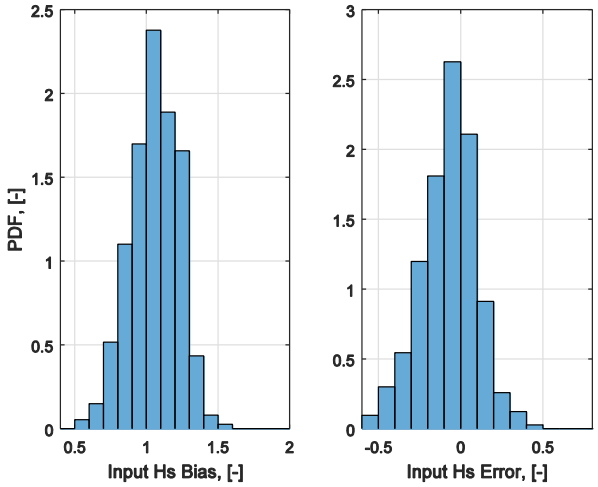

Figure 12.5.Distributins of Bias and Error of the forecasted Hs.

All analyzed outputs (critical responses and Probabilities of Failure) are arranged in bins based on the distribution of the COV of the input (Figure 12.3) or distributions of weather forecast Error or Bias. Also, Probabilities of Failure are also analyzed in connection with input weather forecast bias and error and therefore also arranged in bins based on forecasted Hs bias and error.

12.1 Weather forecast uncertainty and its effects on Probabilities of Failure

This section focuses on the effects that weather forecast uncertainty has on Probabilities of Failure. The output Probabilities of Failure (PFs) are analyzed in terms of COV also. This is done because the range of predicted PFs is in a range of 10^{-15} to 1 and it is a lot easier to interpret the results when normalized. The COV_{PF} is obtained using the following equation:

$$COV_{PF|COV_{input}} = \frac{\mu_{PF|COV_{input}}}{\sigma_{PF|COV_{input}}} \tag{12.2}$$

Where:

$\mu_{\mu_{PF|COV_{input}}}$ – mean value of Probability of Failure, evaluated at a given level of COV_{input};

$\sigma_{PF|COV_{input}}$ - Standard deviation of Probability of Failure, evaluated at a given level of COV_{input}.

PFs for all limit states are not combined together in any way to give a representative total operational PF for particular point in time. Individual limit state PFs are treated as separate outcomes of simulation. The following figure shows the effect that input uncertainty (COV) has on the COV_{PF} after the response of the Hywind Rotor Lift Operation is simulated with SIMO and the vessel responses are analyzed using the DECOFF statistical method.

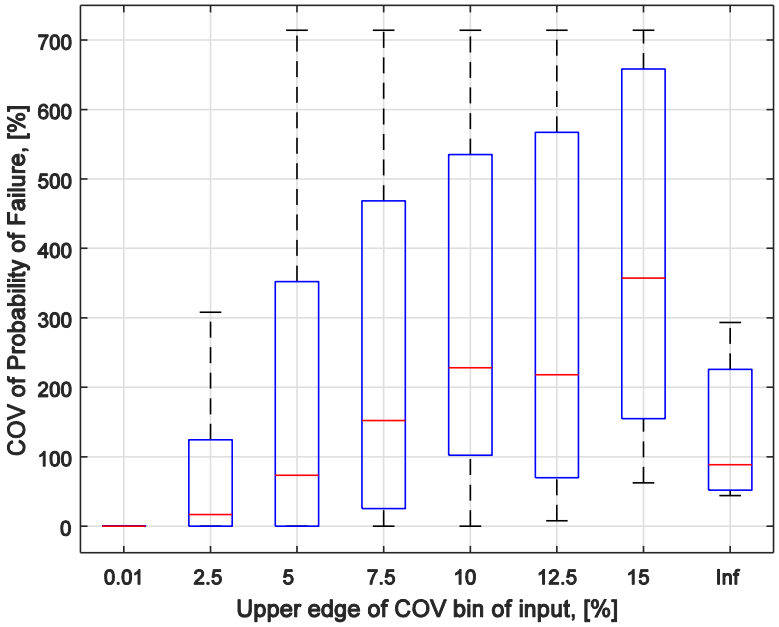

Figure 12.6. Weather input COV and output Probability of Failure COV.

The red line in the plot represents the mean value of COV_{PF}, the blue bars are the 25^{th} -75^{th} percentiles of the data. The black lines represent 5 and 95 % quantiles. The first bar at 0.01 COV represents a deterministic forecast (+0 hour lead-time forecast from ECMWF forecast file) when all 51 ensemble members are equal. The fact that it has 0 output COV_{PF} means that there is no additional uncertainty added while simulating in SIMO or post-processing the responses after simulation. This result is also a good indication of robustness of the method merely because it produces consistent results.

A clear trend of increasing COV_{PF} is visible when the input COV is increased. This is expected as the spread in forecasted met-ocean conditions should imply a spread in Probabilities of Failure. It has to be noted that even a small increase of input COV of eg. 5% can lead to 75% increase in mean COV_{PF}. The increase is induced only by increasing the weather forecast uncertainty without increasing the severity of the input met-ocean conditions (no explicit increase in wave heights or wind speed). For the sake of completeness, the input COV bin of (15, ∞] is added to the plot, but is not deemed representative, because there is not enough data to get reliable estimates of COV_{PF} mainly due to SIMO numerical instabilities above 15% of output uncertainty.

The 5-95% of output COV_{PF} quantiles vary from 0 to 700%. This can be explained by the fact that the analysis is performed taking the full ranges of wave heights and other met-ocean parameters. Therefore one bar at eg. 5% COV_{input} represents the effect of 5% weather forecast COV taking into consideration all the met-ocean conditions shown in Figure 8.1. Also it is possible that combination of 7 met-ocean parameters can result in a very high Probability of Failure even when the met-ocean conditions are not very severe.

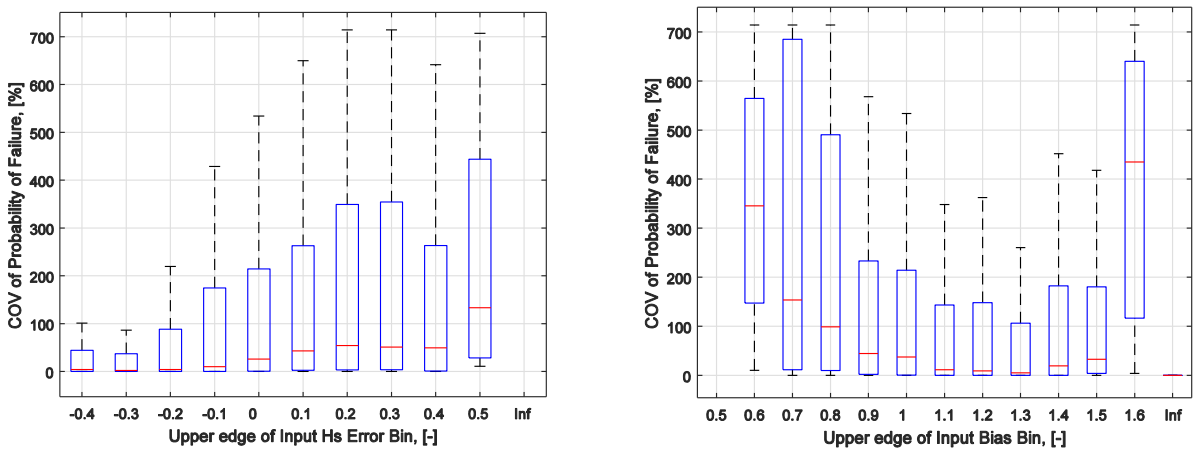

Figure 12.7. Uncertainty of Probabilities of Failure and forecast Hs Error (left) and Bias (right).

Figure 12.7 above show the effect of significant wave height prediction error (left). It is visible that when the model is underpredicting the significant wave height (negative values on x axis, left plot), the output probabilities of failure are quite stable. When it comes to forecasts over-predicting the significant wave height (positive values on x axis, left plot), the change in COV_{PF} becomes

significant – there is an increase in mean COV_{PF} together with wider confidence bounds. When COV_{PF} is analysed in terms of bias of forecasted significant wave height a clear bathtub curve is visible (right plot, Figure 12.7). And it is easy to see that when the forecast has a bias there is an increase in output COV_{PF} both in terms of mean and confidence bounds. Also, when the bias is low (1-1.2) the output uncertainty COV_{PF} is lower and more stable.

It is clearly evident from this analysis that there is a need to reduce the weather forecast uncertainty as much as possible in order to achieve lower and more stable predictions of Probabilities of Failure. This can be achieved by using calibrated weather forecasts, ECMWF weather forecast downscaling, including bathymetric effects etc. On the operational scale, using multiple weather forecast suppliers or more reliable forecasters could be also beneficial.

12.2 Weather forecast uncertainty and its effects on Critical Responses

This section focuses on the effects of weather forecast uncertainty on individual Critical Responses. The basis for this analysis is the same as it was in the previous section. Although, in this section individual Critical Responses are analyzed separately in order to investigate which responses are most affected by increasing weather forecast uncertainty. The Critical Responses are analyzed in terms of maximum values, since that was the focus of most (11/13) limit states. Therefore the figures in this section will show the COV of the maximum value of any given Critical Response.

The following Figure 12.8-Figure 12.9 show a few selected Critical Responses (see more in Appendix D). The selected responses are picked in such a way, that it represents 4 different types of response (load, acceleration, motion and velocity). These 4 types cover all the Critical Responses that were investigated.

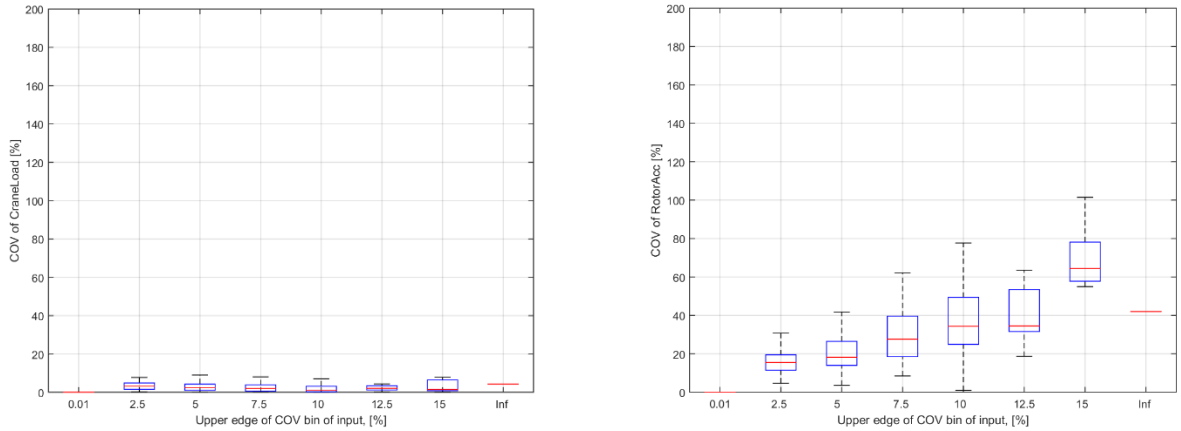

Figure 12.8. Weather input COV and output COV for few selected Critical Responses.

As it was for the case of Probability of Failure, a 0.01 COV_{Input} bar is used to determine whether there is additional uncertainty appearing during the simulation and post-processing phases. The figures are presented on the same Y axis scale for ease of comparison.

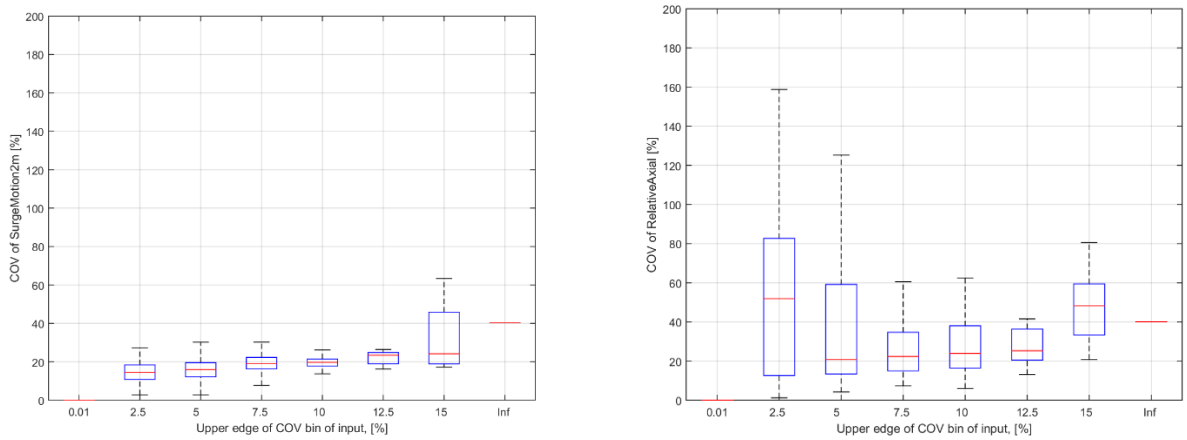

Figure 12.9. Weather input COV and output COV for few selected Critical Responses.

It is safe to say that the simulation/post-processing methodologies are robust and produce consistent results. It is clearly visible that all the Critical Responses are affected by increased weather forecast uncertainty, although the extent of the effect varies from response to response.

There are some inconsistencies in the figures and most of them can be explained by the fact that all the simulations from the test period of summer 2014 were used in this analysis and every bar in the plots represents a full dataset of multi-parameter met-ocean condition forecasts. This implies that some of those combinations are very severe and can result in a big increase of magnitude of the Critical Responses. In order to avoid these types of problems, a dedicated analysis for individual weather forecast parameters should be done. Although it is possible to isolate each met-ocean parameter and run simulations with increasing uncertainty this type of analysis would be very time consuming and beyond the scope of this report.

Crane Load seems to be relative stable and unaffected by increased weather forecast uncertainty, as is the Lift Wire tension (see Appendix D), change in $COV_{CraneLoad}$ and $COV_{LiftWire}$ is < 10%. Rotor acceleration (both linear and angular) are highly affected by increased weather forecast uncertainty. The uncertainty in Rotor Surge and Sway motions are also affected by COV_{input}, although the effect is limited to 15-40% increase in COV_{Surge} and COV_{Sway} depending on the motion. Uncertainty in rotor Tilt angle motions are affected more than that of Yaw angle motions. This is easily explained by the nature of the motion – Yaw motion being rotation on horizontal plane mostly due to misalignment of wind and waves whereas Tilt motion is rotation in a vertical plane primarily induced by water elevation changes. The uncertainties in Relative Radial and Axial velocities of the lifted rotor are also highly affected by the increase of COV_{input}.

In general it can be concluded that weather forecast uncertainty, represented here as COV_{input}, is a very important parameter and efforts should be made in order to reduce it.

13 Summary, conclusions and discussion

The main focus of the report was to document the methodology developed under the DECOFF project and demonstrate if the new methodology performs better than the standard method for estimating weather windows for offshore operations from (DNV, 2011).

A general introduction is given in sections 1-3 covering the uncertainties involved and how the uncertainties should be handled within DECOFF. Also, a description of possible limit states and ways of including them into the analysis is presented.

Main focus of section 5 was to describe the new methodology used to determine the weather windows for offshore operations and test it on a short term weather forecast. The procedure for obtaining the probabilities of failure of offshore operations was successfully tested on a 3 day weather forecast. A weather window was obtained and in general the total Failure Probability of the Operation (PF_{OP}) was following the evolution of the met-ocean conditions (increasing PF_{OP} when met-ocean condition became more severe). At this point it was regarded as sufficient "proof of concept" to move forward to a more detailed study of DECOFF model performance and benchmarking it against the standard methods.

Section 7 focused on "reverse-engineering" the met-ocean condition limits for the Hywind Rotor Lift Operation. This was necessary because the initial limitations of the operation were only given in terms of installation equipment loads/accelerations/motions etc., but standard method proposed in (DNV, 2011) uses met-ocean conditions as operation limiting parameters. The analysis revealed that the operation is highly sensitive to wave period ($T_p \leq 5s$). Also, due to the fact that the operation itself is highly complex - a floating crane installing a wind turbine rotor on a floating foundation – the maximum allowable met-ocean conditions obtained from the analysis were relatively low ($H_s \leq 1.5m$ and $W_s \leq 7m/s$). This implied that a limited number of weather windows during late spring-summer of 2014 would be available for installation.

In section 9 the standard methodology for determining weather windows for offshore operations is applied to Hywind Rotor Lift Operation using the reverse-engineered met-ocean limits. Standard tabulated *alpha-factors* were used in order to take into account the uncertainty inherent in the weather forecasts. There are multiple *alpha-factors* presented in (DNV, 2011) and all the relevant ones were investigated. Also (DNV, 2011) allows to compute site-specific alpha factors for significant wave heights using historical measurement and forecast data from the installation location. FINO3 site was chosen as the installation site therefore it was possible to use the measurements from met mast together with the ECMWF weather forecasts to obtain the site-specific *alpha-factors.* Since the operation was determined to be highly sensitive to wave periods, it was important to take into consideration the uncertainty of wave period forecasts. (DNV, 2011) does not provide a way to determine *alpha-factors* for wave periods therefore the methodology used to obtain site specific *alpha-factors* for H_s was extended and used for forecasted wave peak period. The results from the analysis using the standard method was used as a baseline case later in benchmarking the DECOFF methodology.

Section 10 focused on determining weather windows during the test period of *late spring-summer 2014* for Hywind Rotor Lift Operation using the DECOFF methodology. ECMWF weather forecasts were used together with measurements at FINO3 location. Measurement information was used in order to determine whether there is an influence of the uncertainty of the weather forecast and, if possible, try to quantify it. Weather windows were obtained using the DECOFF methodology for both cases and compared with the standard method in section 11.

As a general conclusion after comparing DECOFF methodology with the standard methods for weather windows estimation can be stated that **the DECOFF method is performing better or at the least as good as the method described in (DNV, 2011)**. Also it can be stated that weather forecast uncertainty plays a central role in the number and duration of estimated weather windows. This claim is based on the fact that when a "deterministic" case of measurements at FINO3 site is used as input to DECOFF for the same period of *late spring-summer 2014* significantly more and longer weather windows are obtained in comparison to ECMWF forecasts. It can be also stated that there is potential for even better DECOFF model performance if weather forecast quality is improved (reduced uncertainty).

Since a significant effect of weather forecast uncertainty was observed while benchmarking the DECOFF methodology against the one of (DNV, 2011) a more detailed analysis of the effects of weather forecast uncertainty was done and presented in section 12. The uncertainty in output Probabilities of Failure was investigated in terms of input (weather forecast) uncertainty, represented as Coefficient of Variation, bias and forecast error. In all cases there was an increase in the uncertainty of output Probabilities of Failure when the uncertainty of the input was increased (both on average and in extremes of output uncertainty). This analysis serves as good basis for further development of techniques that reduce the weather forecasting uncertainty (calibrated weather forecasts, downscaling etc.).

Also, individual physical responses of installation vessel/equipment were analyzed in terms of weather forecast uncertainty. The results suggest that uncertainties in weather forecast are translated into uncertainty in most of the responses that were relevant as operation limiting parameters. Therefore it is safe to state that uncertainty in input weather forecast is translated into uncertainty of output Probabilities of Failure through the uncertainty of simulated critical responses. This information could be later on used to update the DECOFF model with structural reliability techniques for obtaining Probabilities of Failed Operations and reducing the number of simulations necessary to achieve reliable results.

14 Future work

Possible future work would include but should not be limited to:

- Updating the model with Structural Reliability techniques in order to reduce the demand on a lot of simulations necessary to obtained reliable results;
- Splitting the limit states in Serviceability and Ultimate;
- Including Costs of Failure to produce a “Risk-Based” aspect allowing to evaluate different weather windows in terms of expected Risk rather than just Probability of Failure.
- Improving the accuracy of weather forecasts;
- Extending the methodology to more general Offshore Operations (Oil and Gas, Wind turbine installation on monopoles/jackets etc.);
- ….

Bibliography

Albert, A. & Zhang, L., 2010. A novel definition of the multivariate coefficient of variation. *Biometrical Journal,* 52(5), pp. 667-675.

Clauss, G., Lehman, E. & Ostergaard, C., 1994. *Offshore Structures. Volume II. Strength and Safety for Structural Design.* 1 ed. London: Springer-Verlag.

DNV JIP, 2007. *Technical Report, Marinoe Operation Rules, Revised Alpha Factor - Joint Industry Project,* Oslo: DNV.

DNV, 2004. *DNV-RP-H102. Marine Operations During Removal Of Offshore Installations,* s.l.: DNV.

DNV, 2011. *DNV-OS-H101. Marine Operations, General,* s.l.: DNV.

EN 1990, 2002. *EN 1990. Eurocode - Basis for structural design,* Brussels: European Committee for Standartization.

IEC, 2014. *IEC 61400-1. Wind Turbines - Part 1: Design requirements,* s.l.: IEC.

ISO, 1998. *General Principles on Reliability of Structures,* Genewa: ISO.

JCSS, 2002. *Probabilistic Model Code,* Copenhagen: JCSS Publications.

Lindley, D., 1976. *Introduction to Probability and Statistics from a Bayesian Viewpoint, Vol. 1+2.* Cambridge : Cambridge University Press.

Vatne, S. R., 2013. *Operating phases of test case operations,* Tondheim: MARINTEK.

Vatne, S. R., 2015. *Operation_phases_extendedNew.xls.* Tondheim: MARINTEK.

Vatne, S. R. & Helian, Ø., 2014. *DECOFF rotor lift test case. Project memo,* Tondheim: MARINTEK.

Wilcken, S., 2012. *Alpha factors for the calculation of forecasted operational limits for marine operations in the Barents sea,* Stavanger: University of Stavanger.

Wist, H. T., 2003. *Statistical properties of successive ocean wave perameters,* Trondheim: NTNU.

Appendix A. Response plots for Alpha-Factor weather limit estimation

Rotational Rotor Acceleration limit state

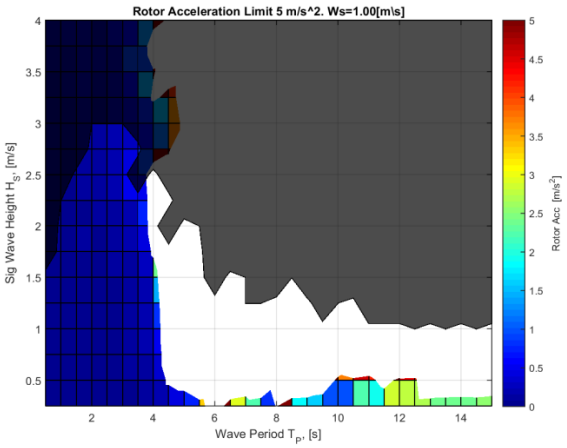

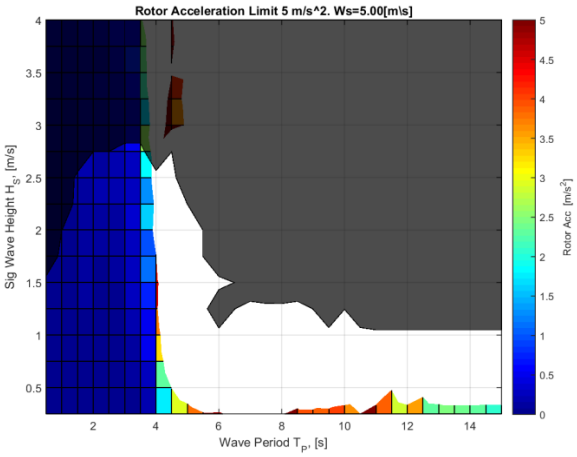

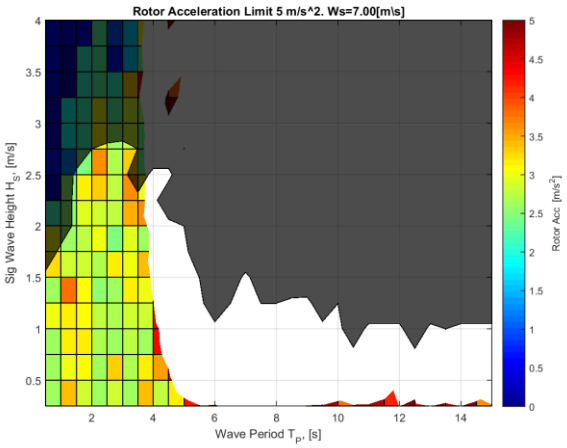

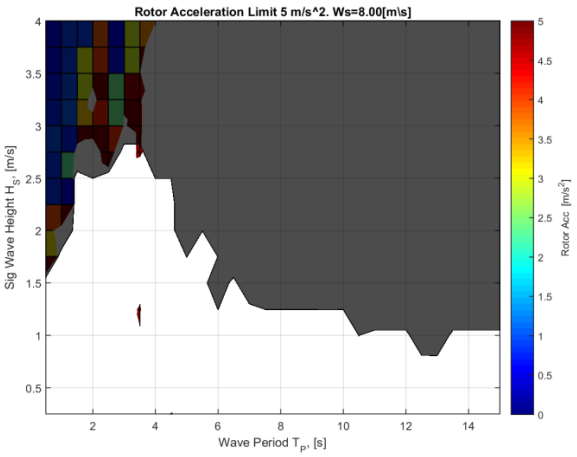

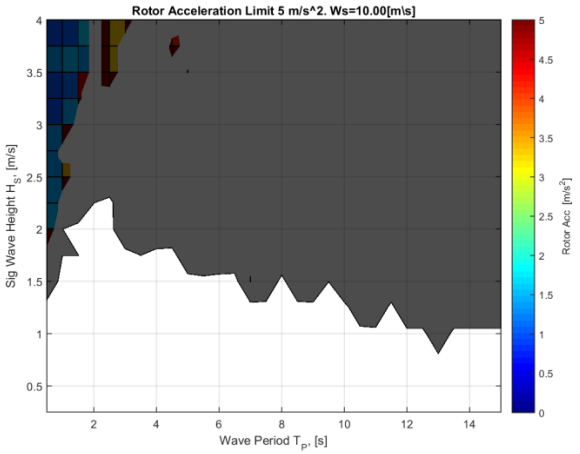

Rotor Sway Motion limit state

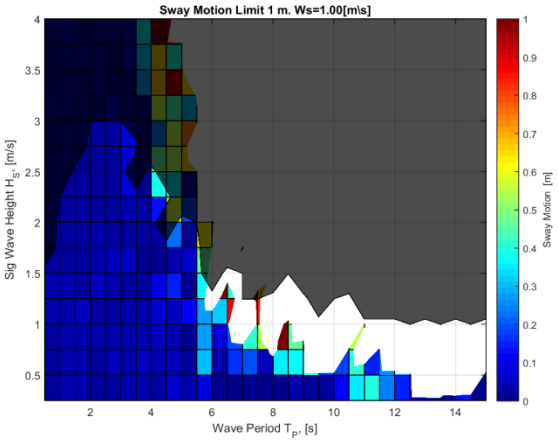

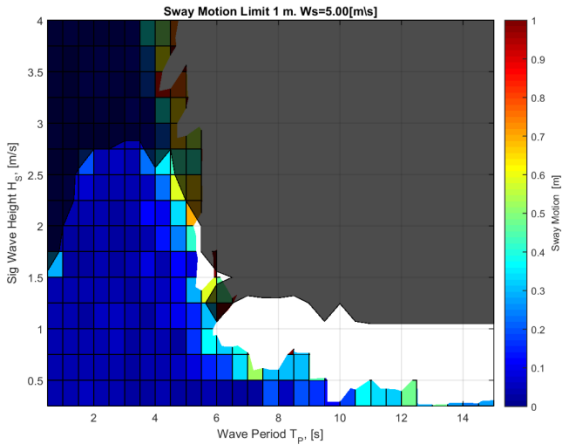

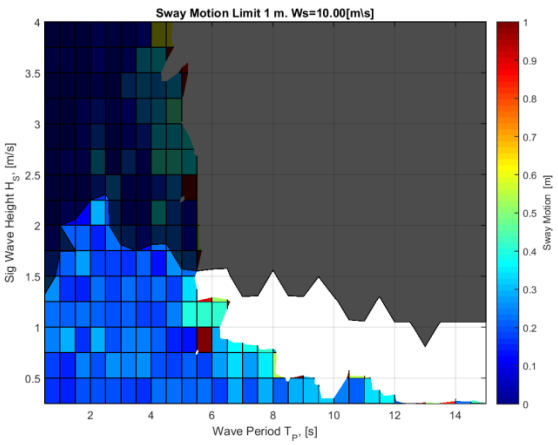

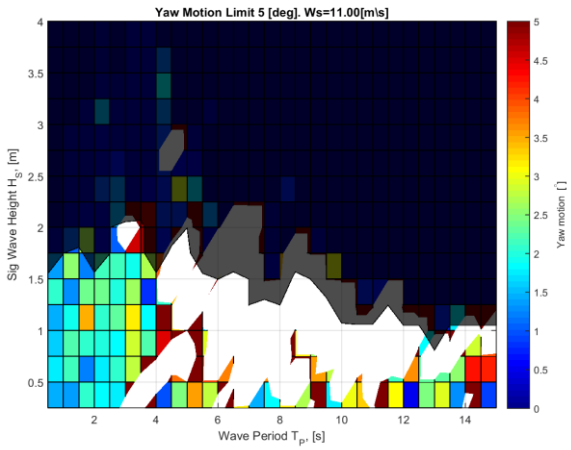

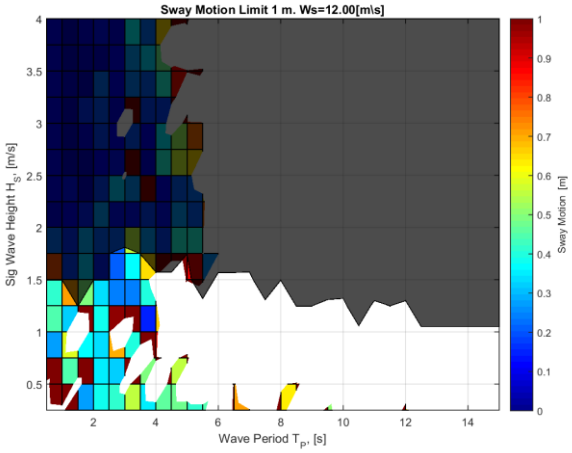

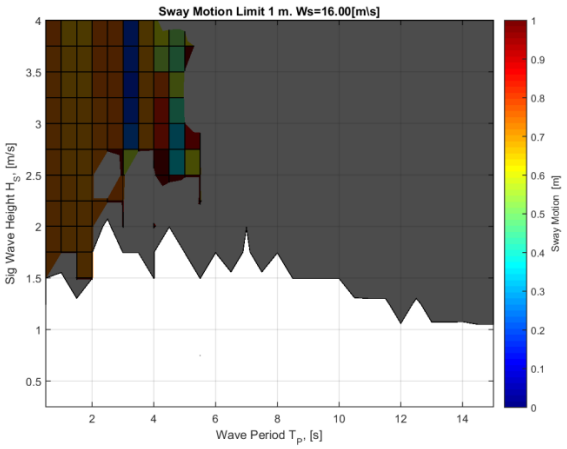

Rotor Yaw Angle limit state

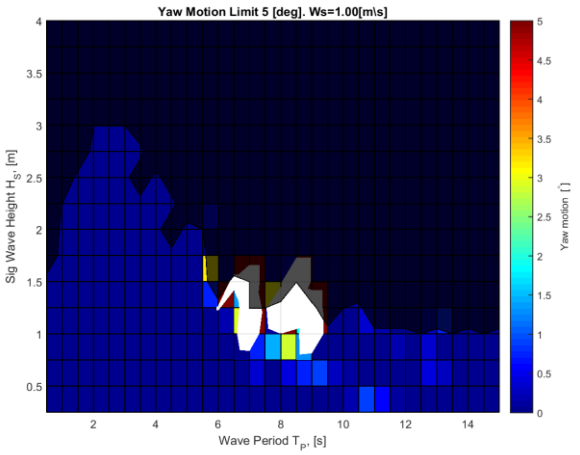

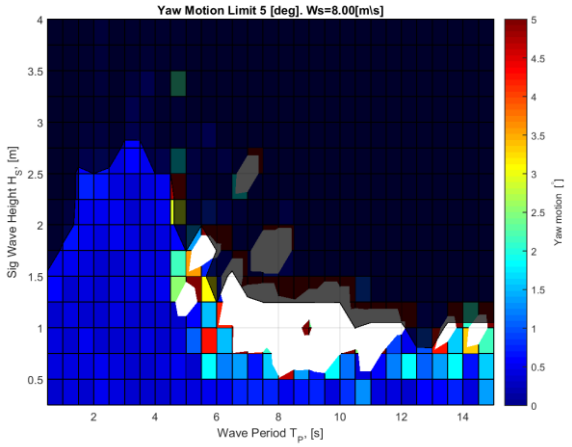

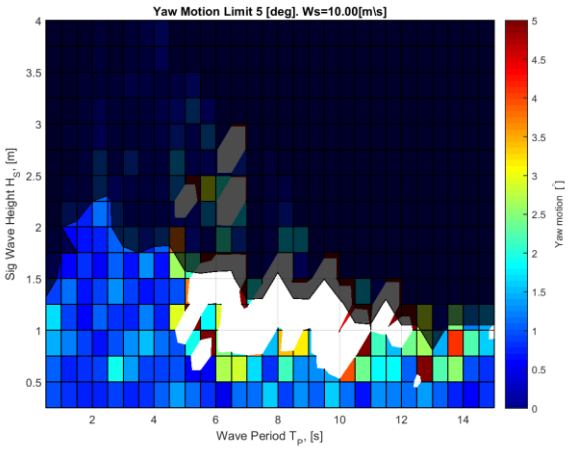

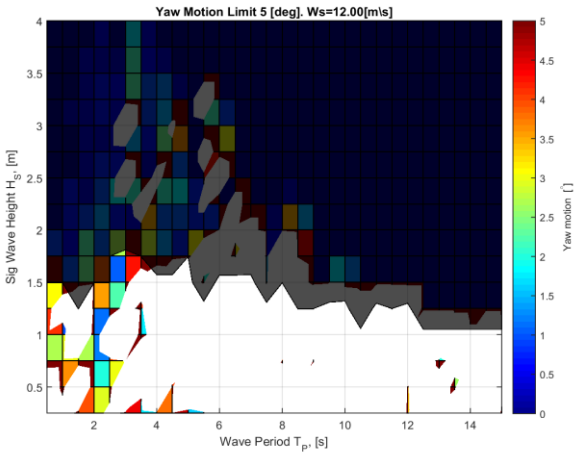

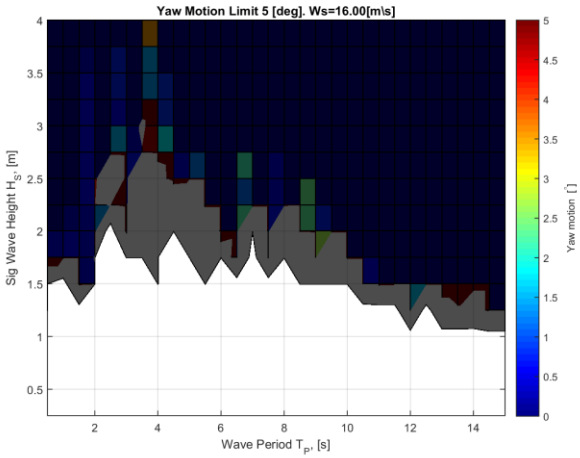

Rotor Tilt angle limit state

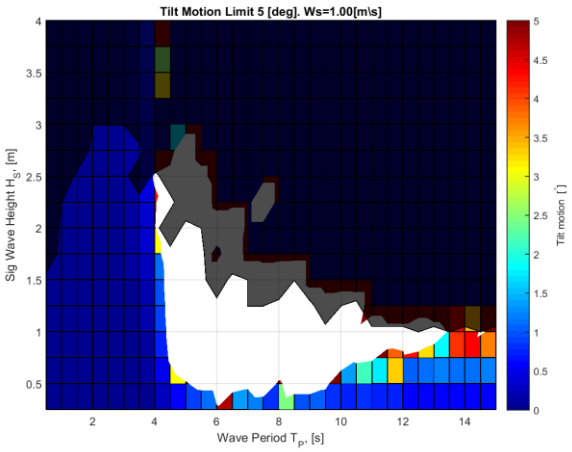

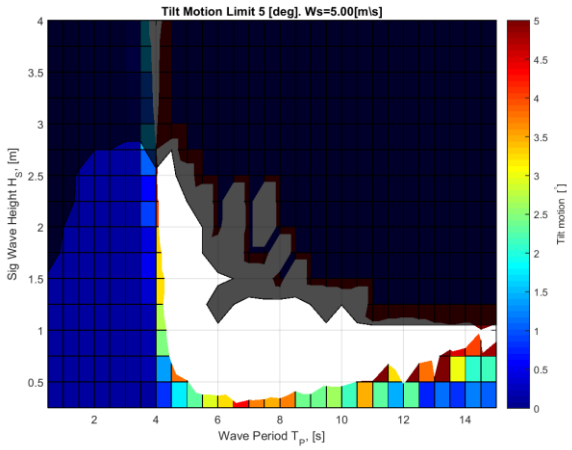

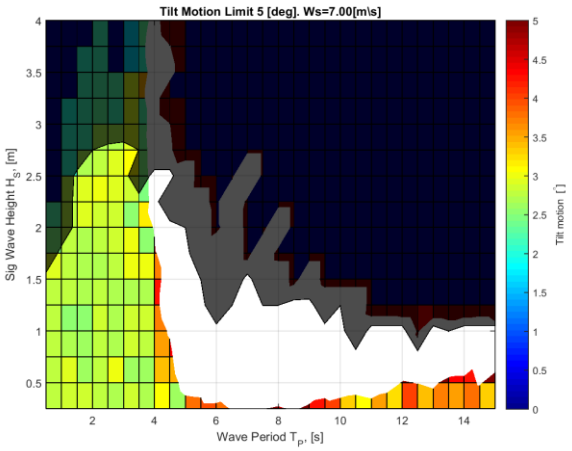

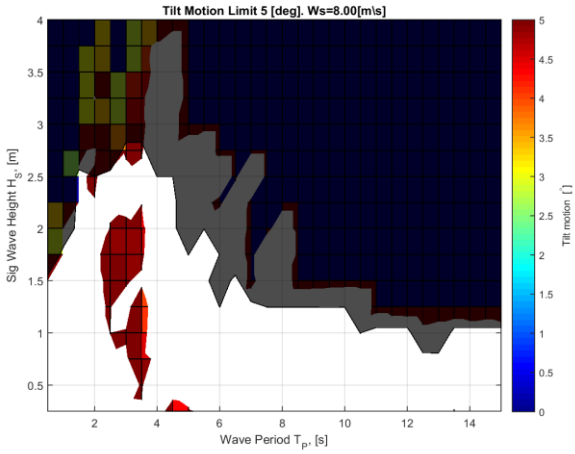

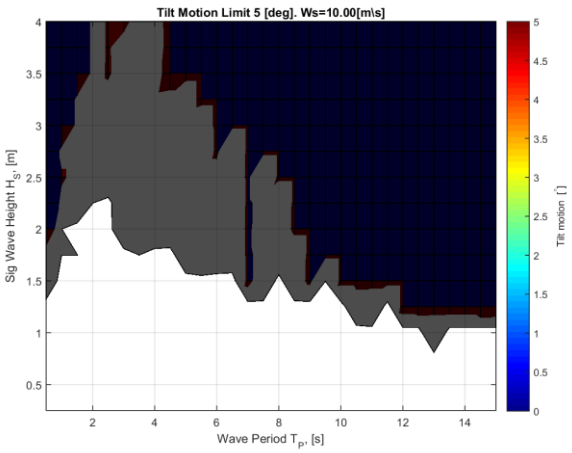

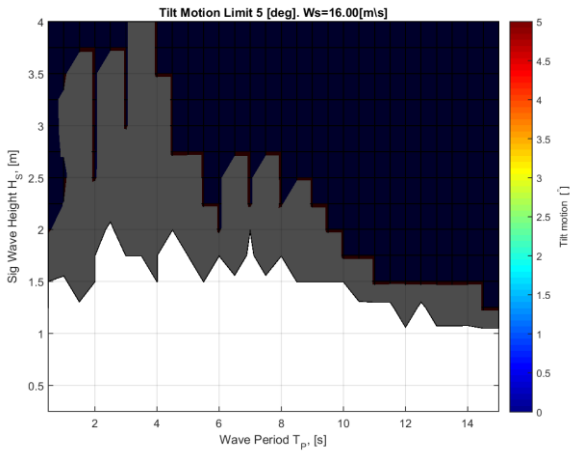

Relative Yaw Angle limit state

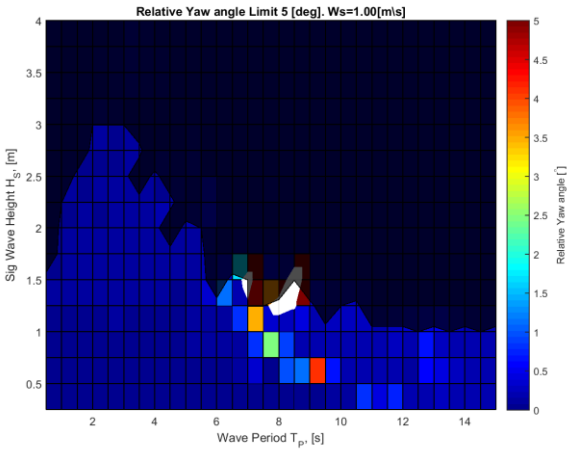

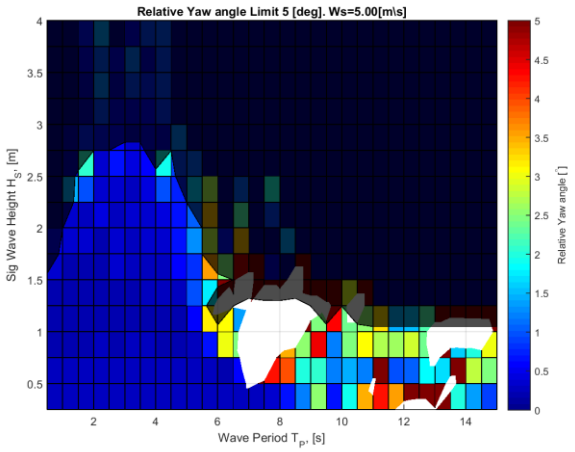

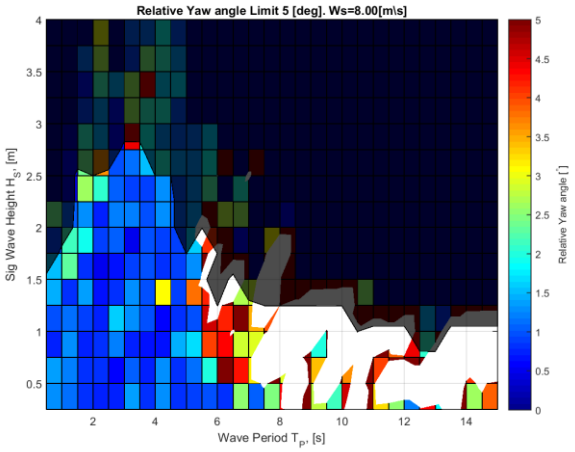

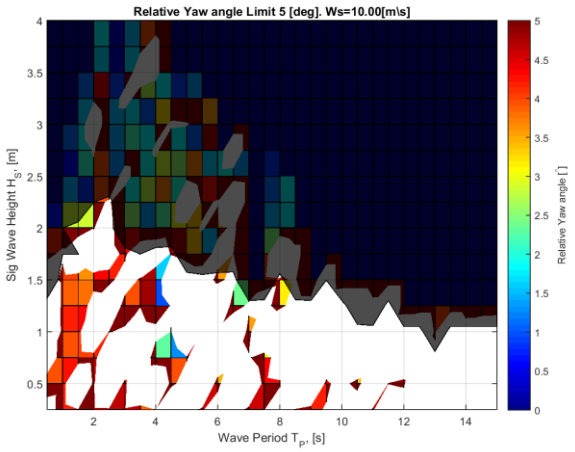

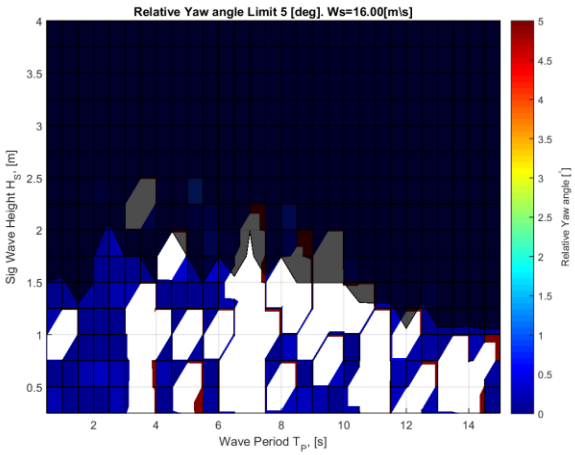

Relative Tilt Angle limit state

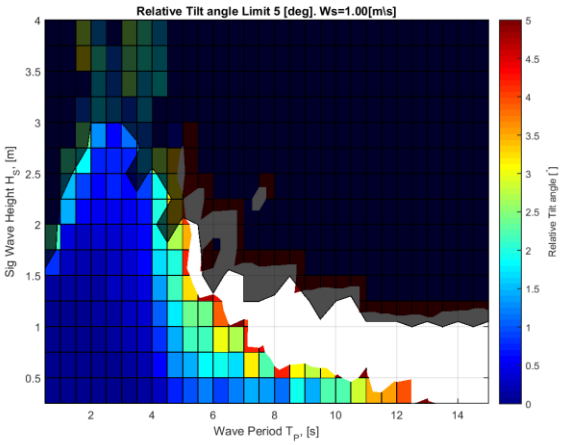

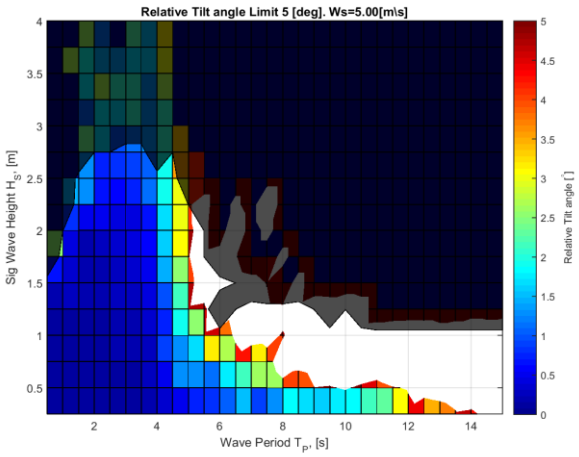

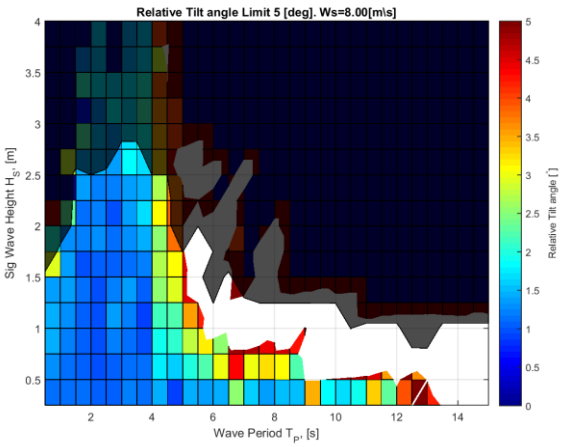

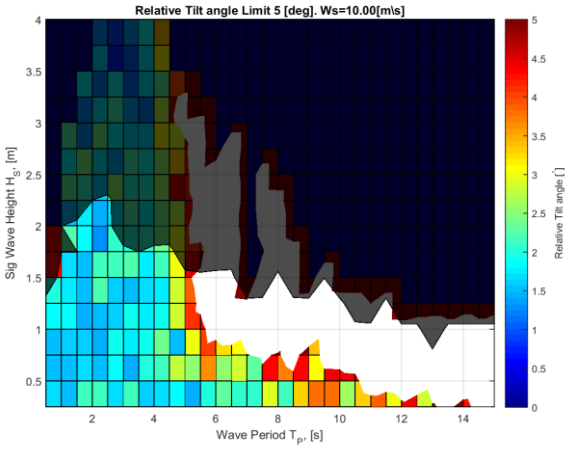

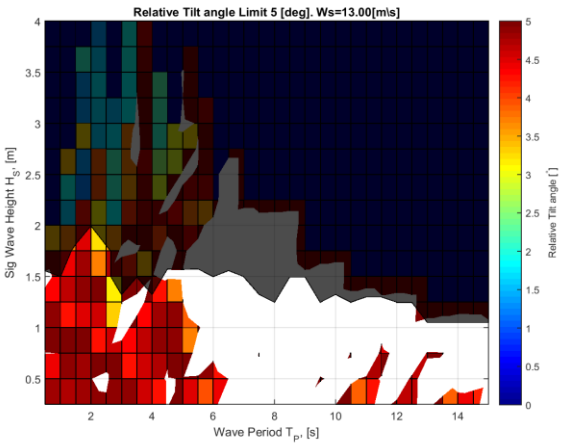

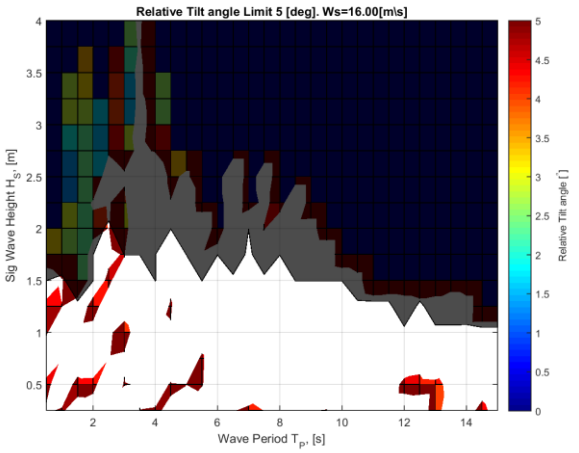

Rotor Radial Velocity limit state

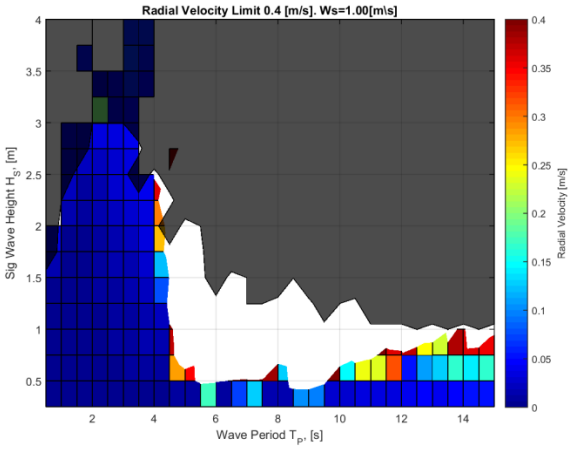

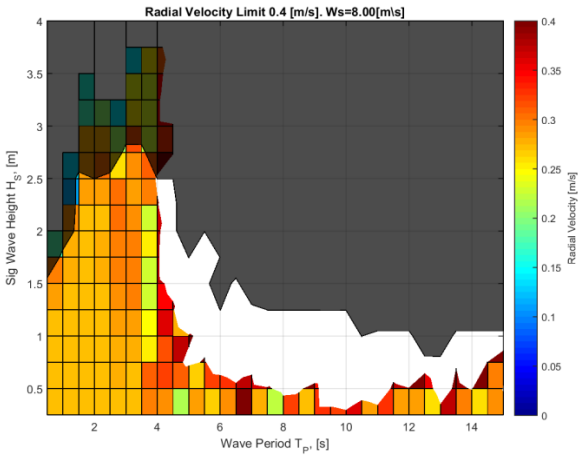

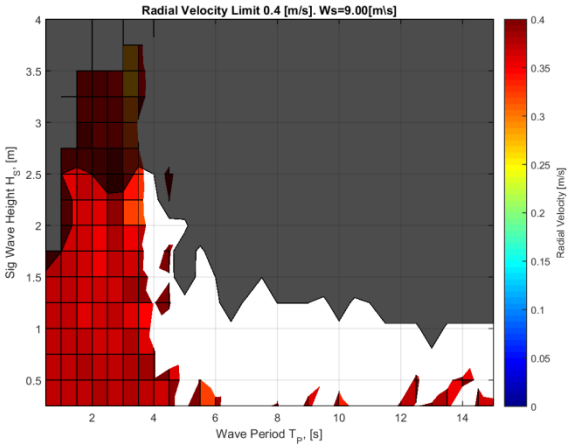

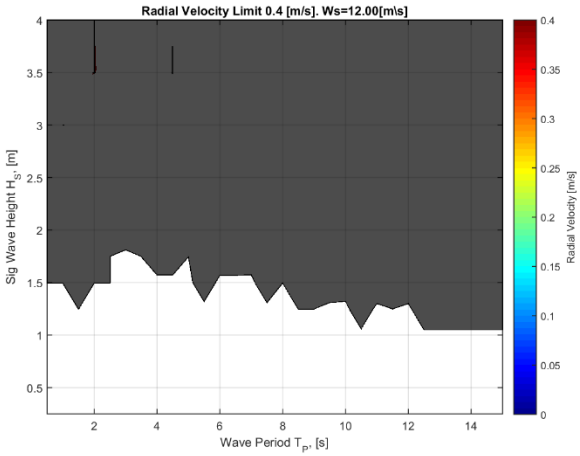

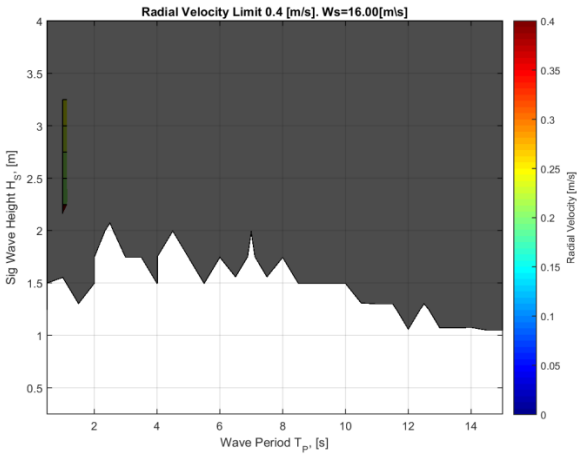

Rotor Axial Velocity limit state

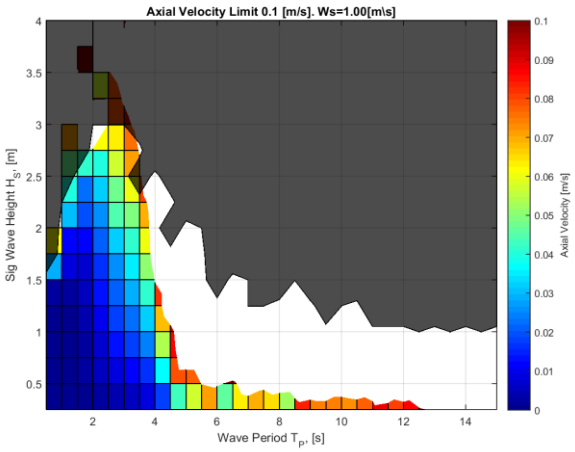

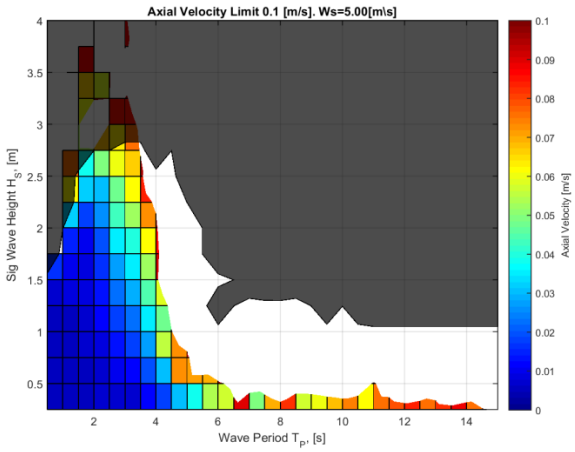

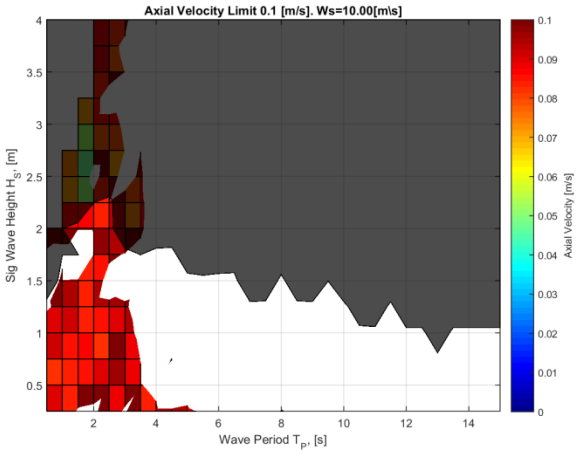

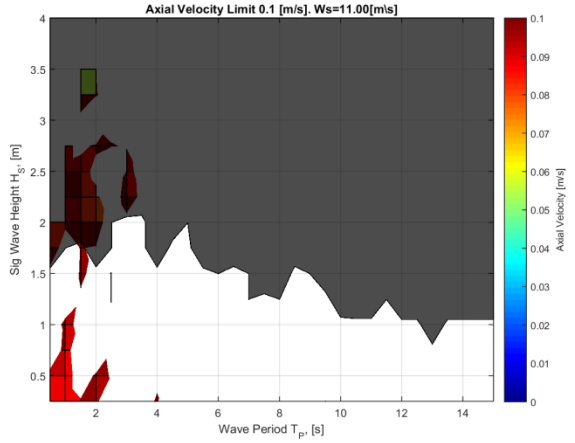

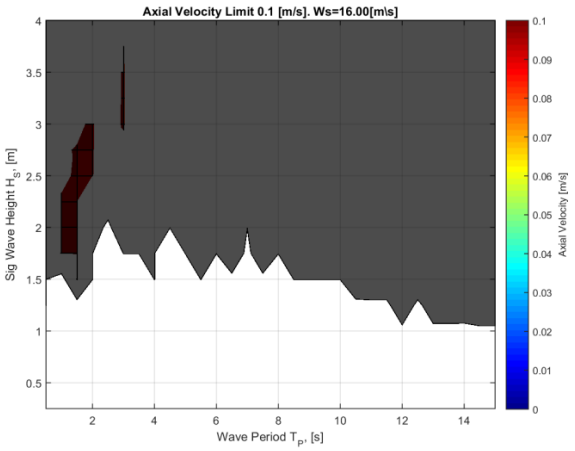

Appendix B. Weather Windows obtained by DECOFF method with ECMWF forecasts

AirGap Tower Limit state

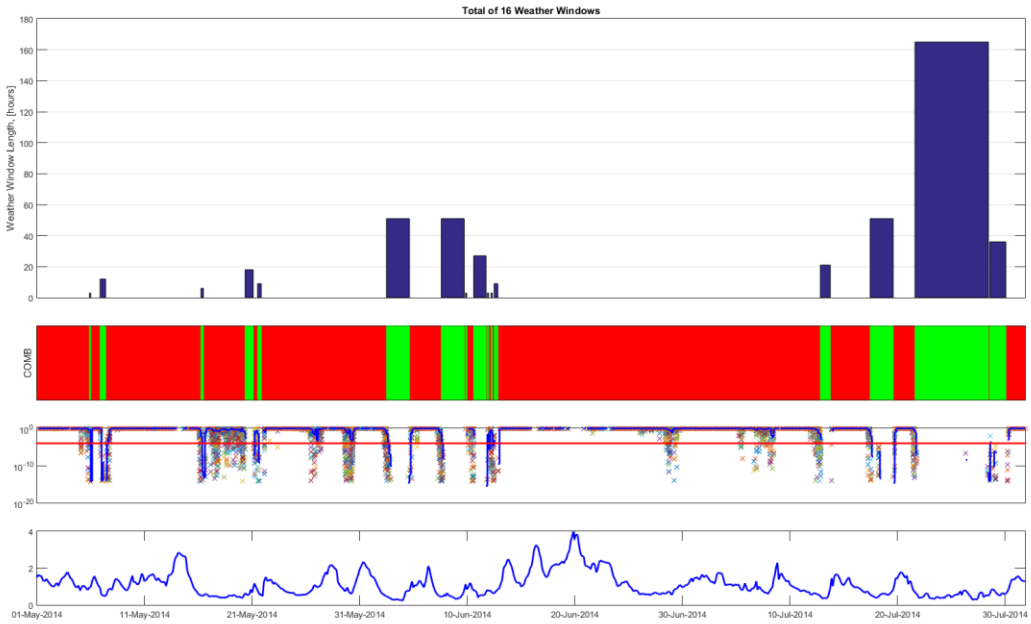

Axial Velocity limit state

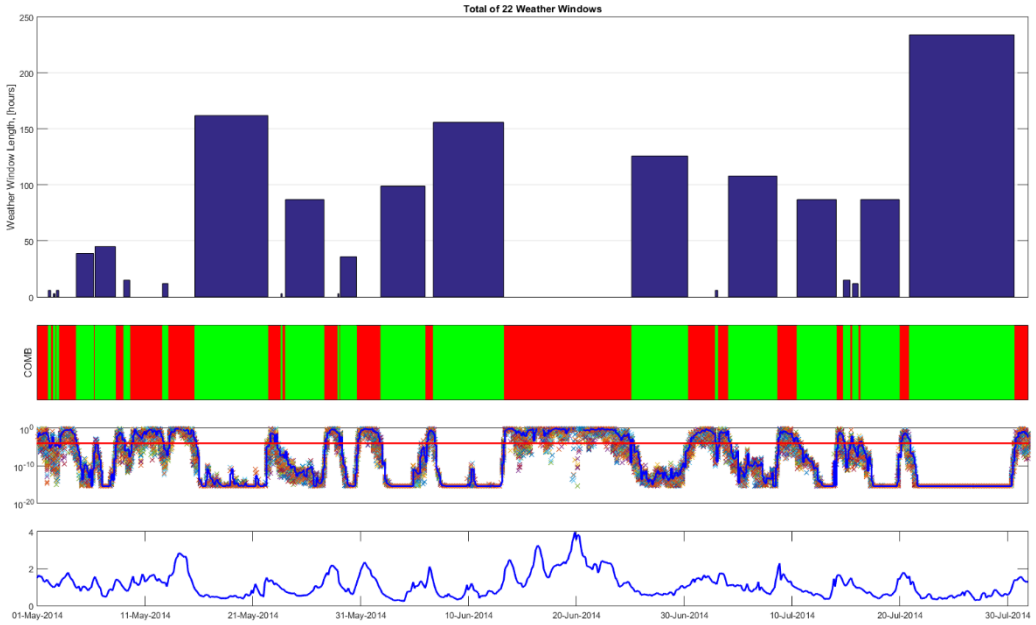

Crane load limit state

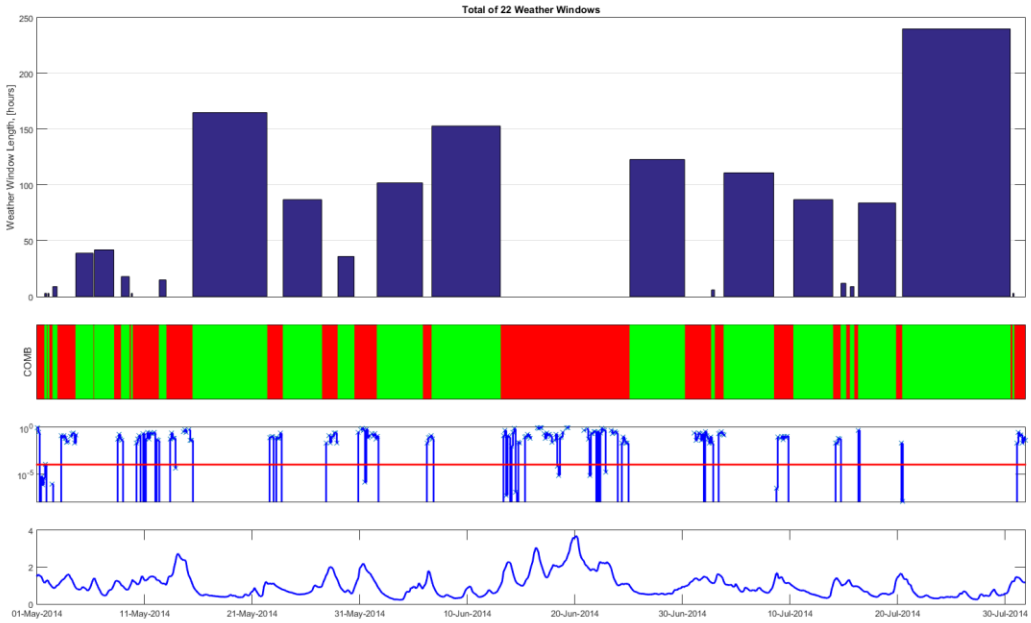

Lift Wire limit state

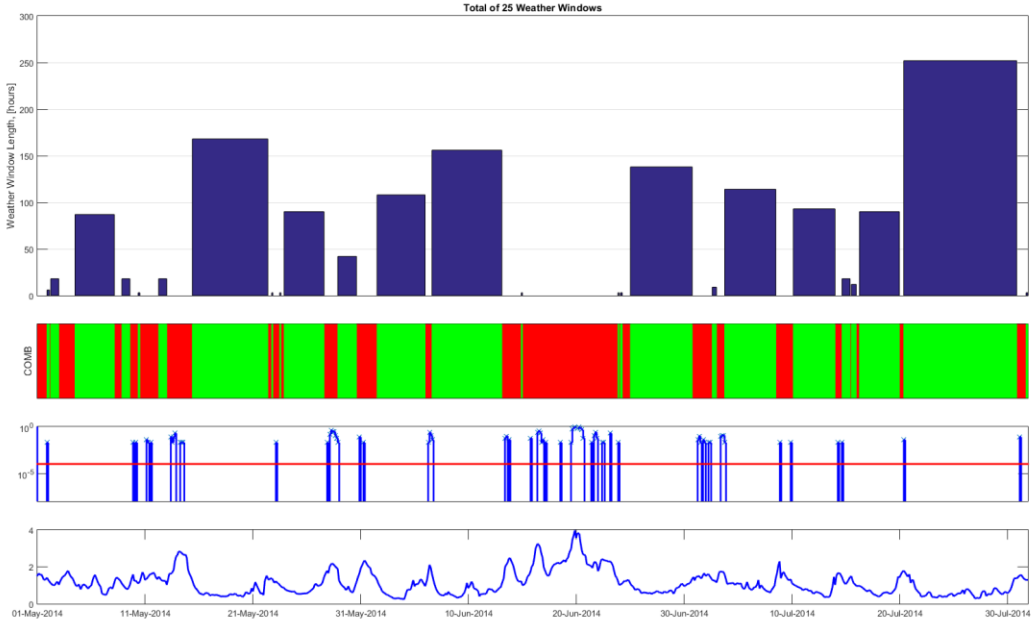

Radial Velocity limit state

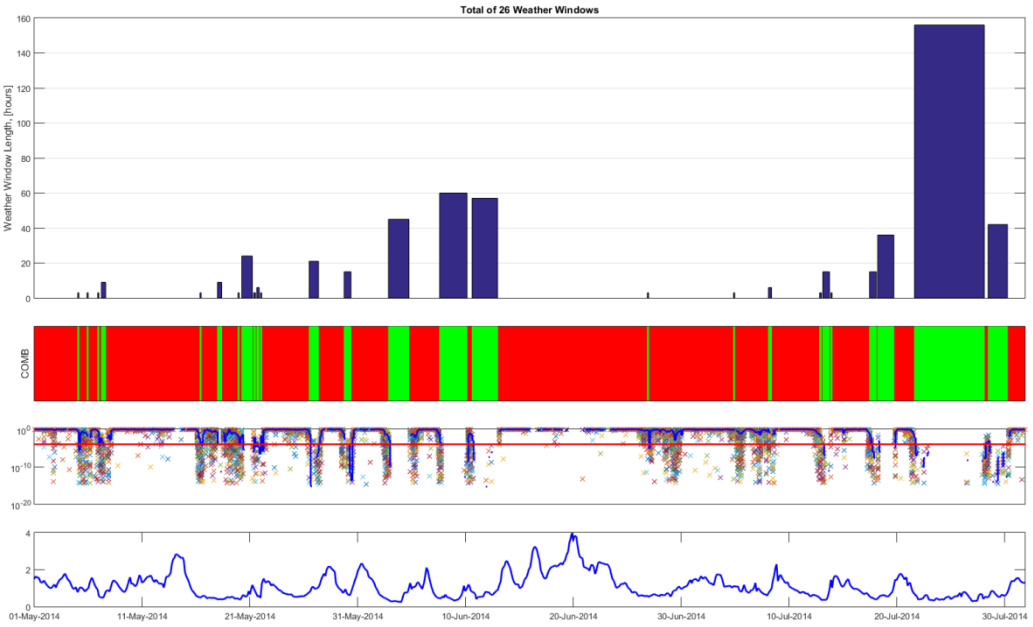

Relative tilt angle limit state

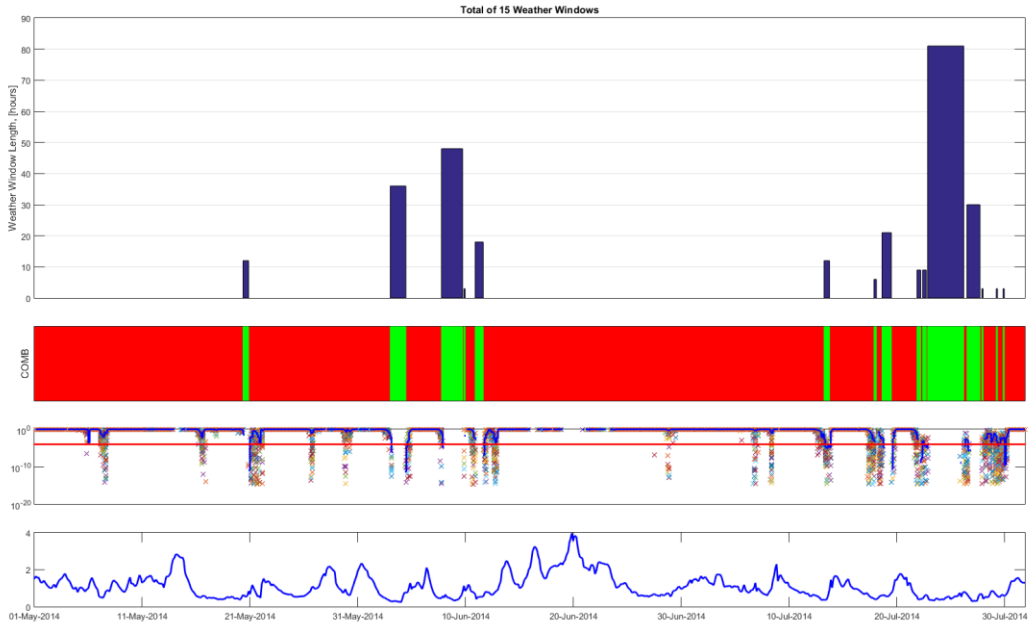

Relative Yaw angle limit state

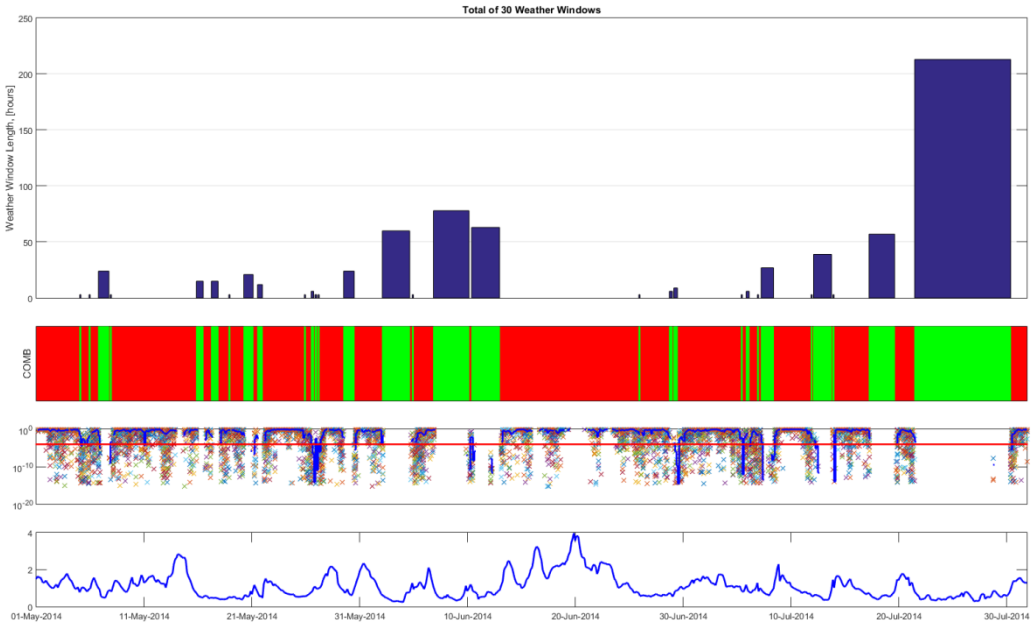

Rotor Acceleration limit state

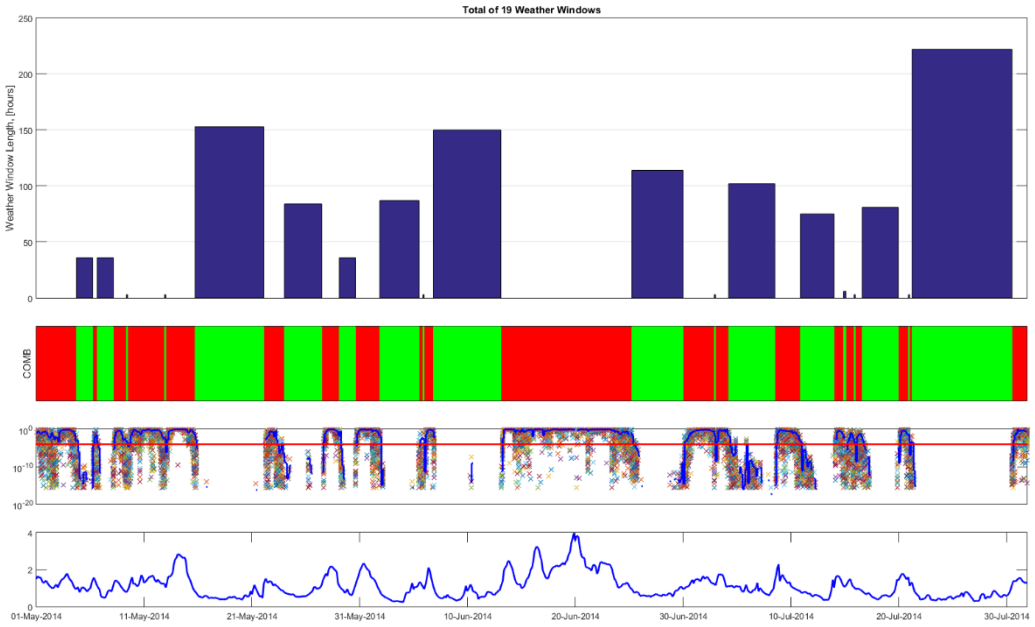

Angular rotor acceleration limit state

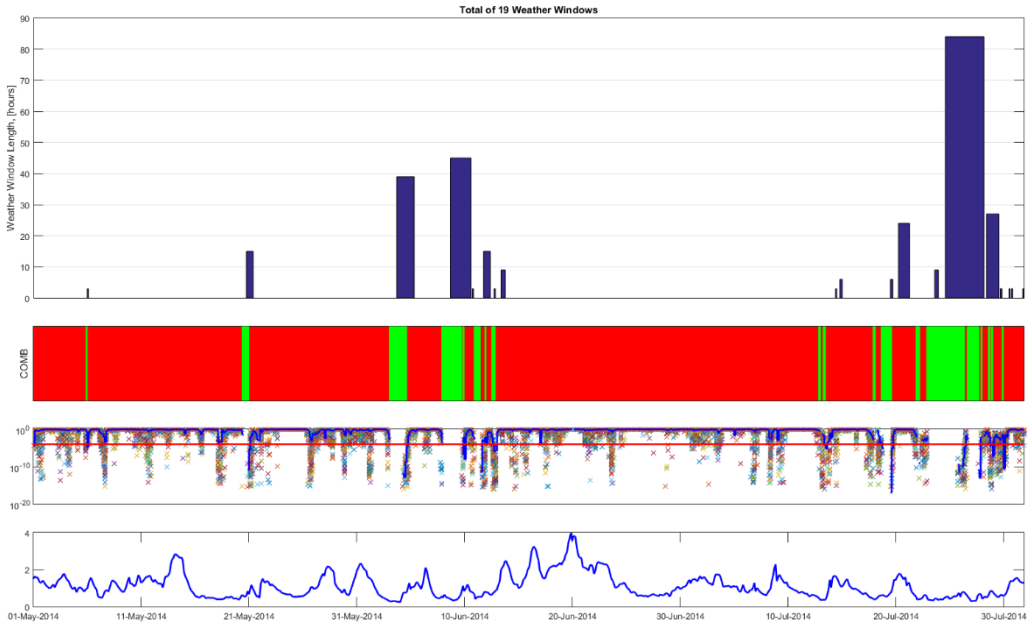

Sway motion limit state

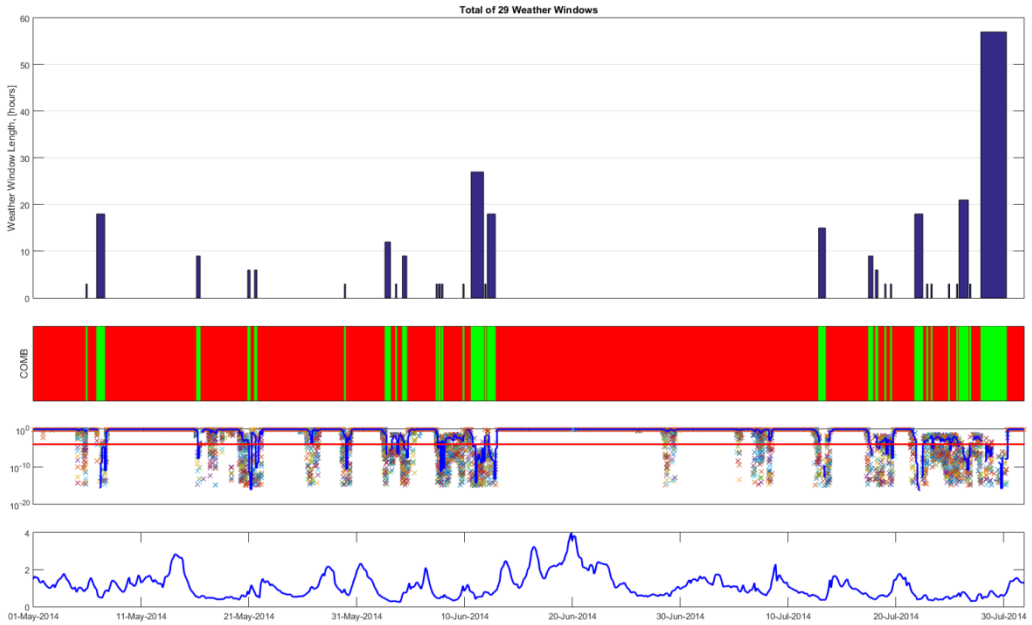

Surge motion limit state

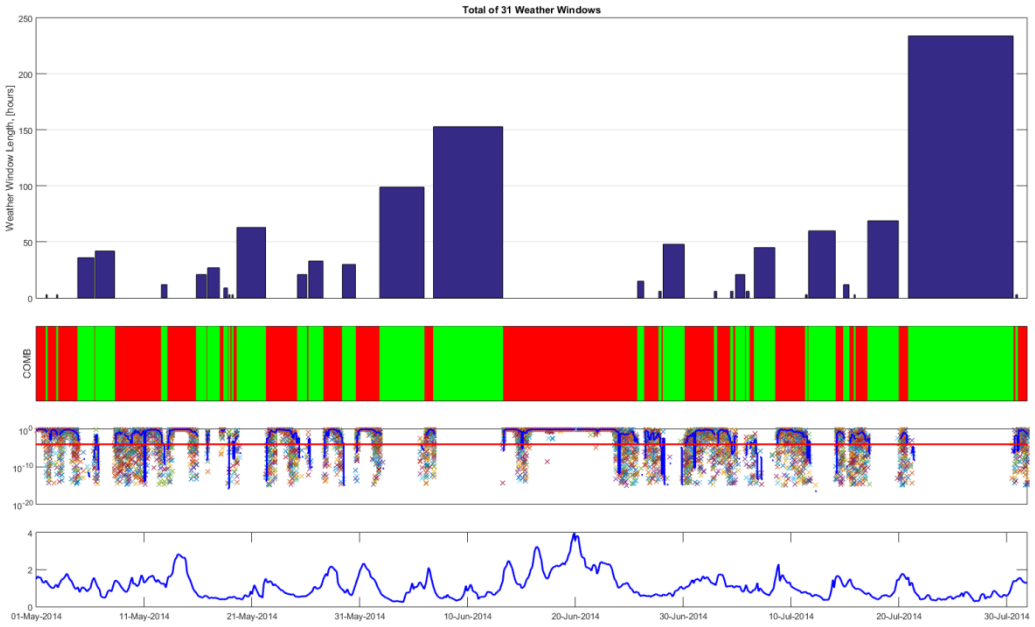

Tilt angle limit state

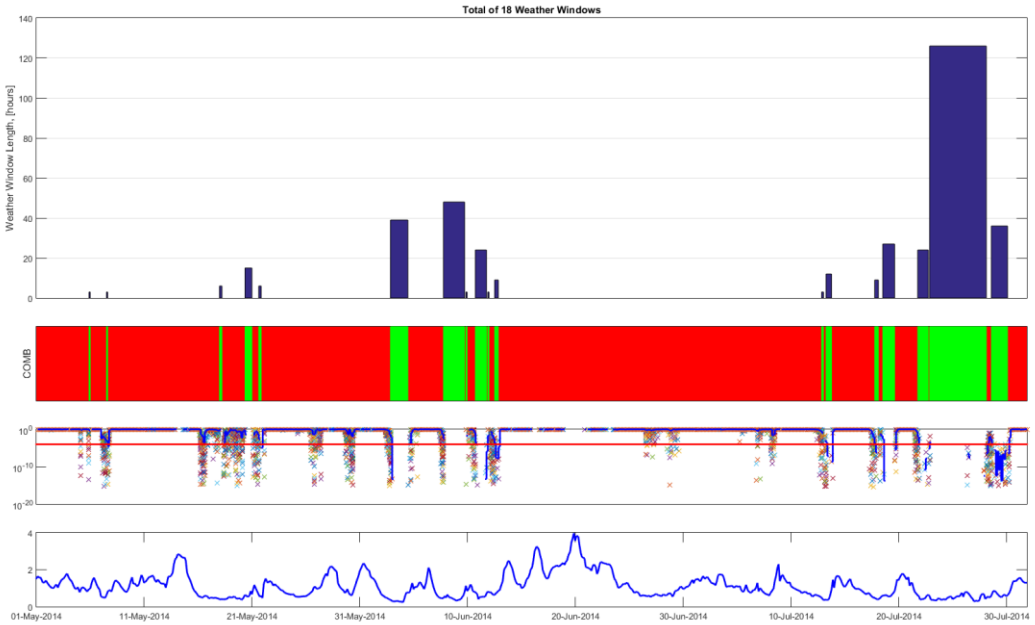

Yaw angle limit state

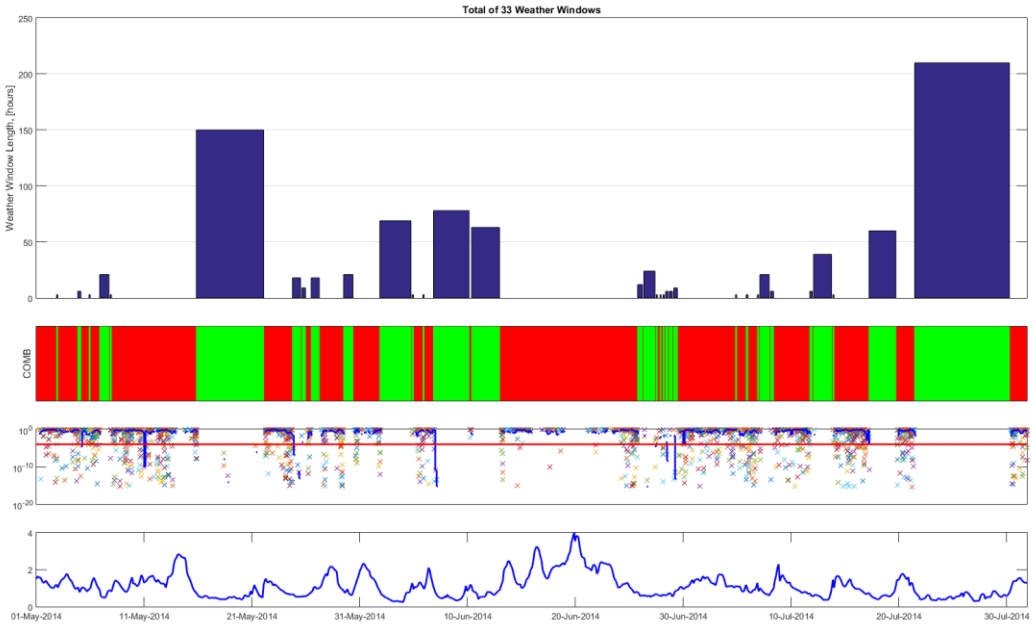

Appendix C. Weather Windows Obtained by DECOFF method with measurements at FINO3.

Airgap Tower Limit state

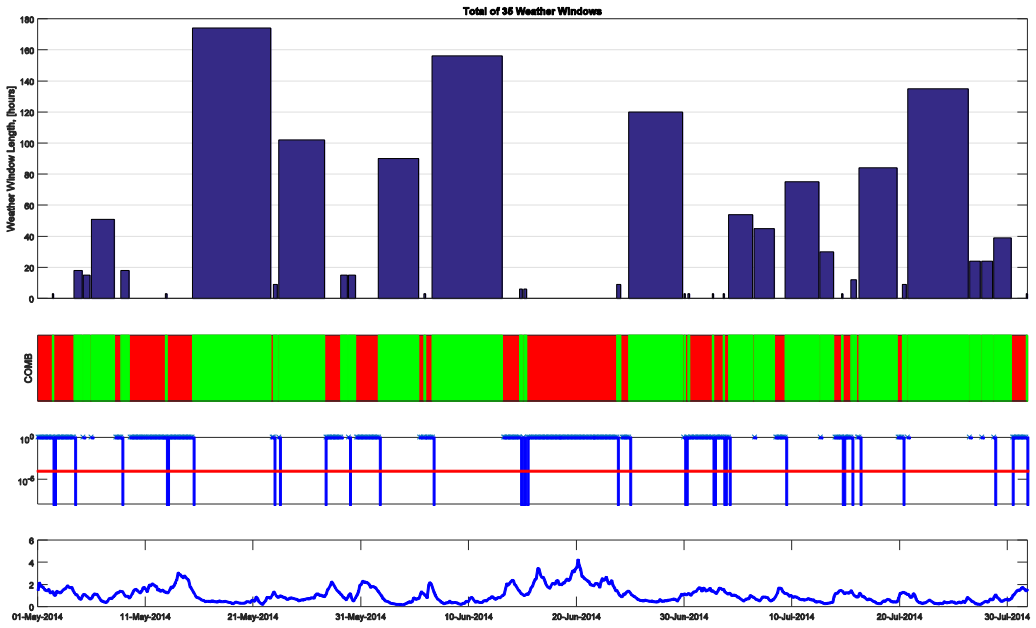

Axial Velocity Limit state

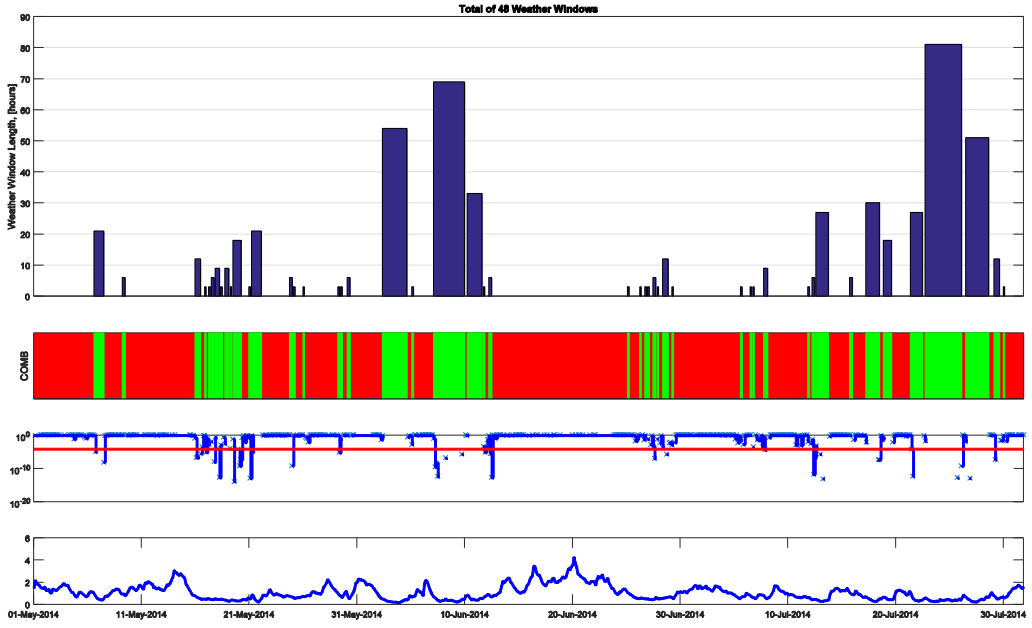

Crane Load Limit state

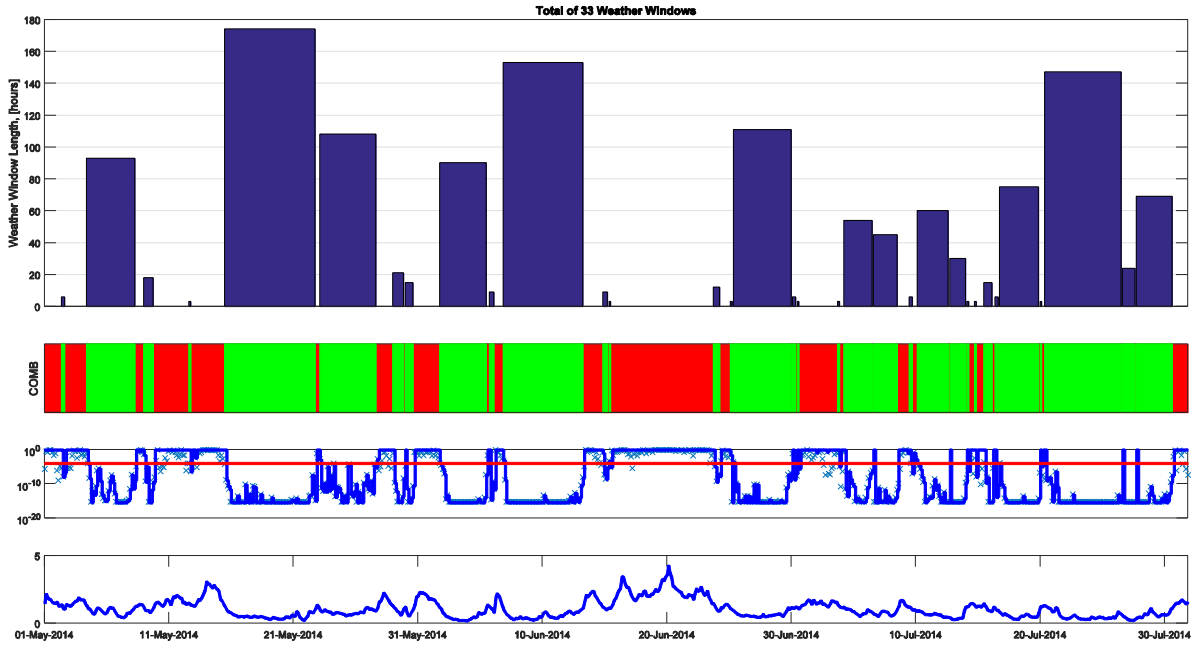

Lift Wire Limit state

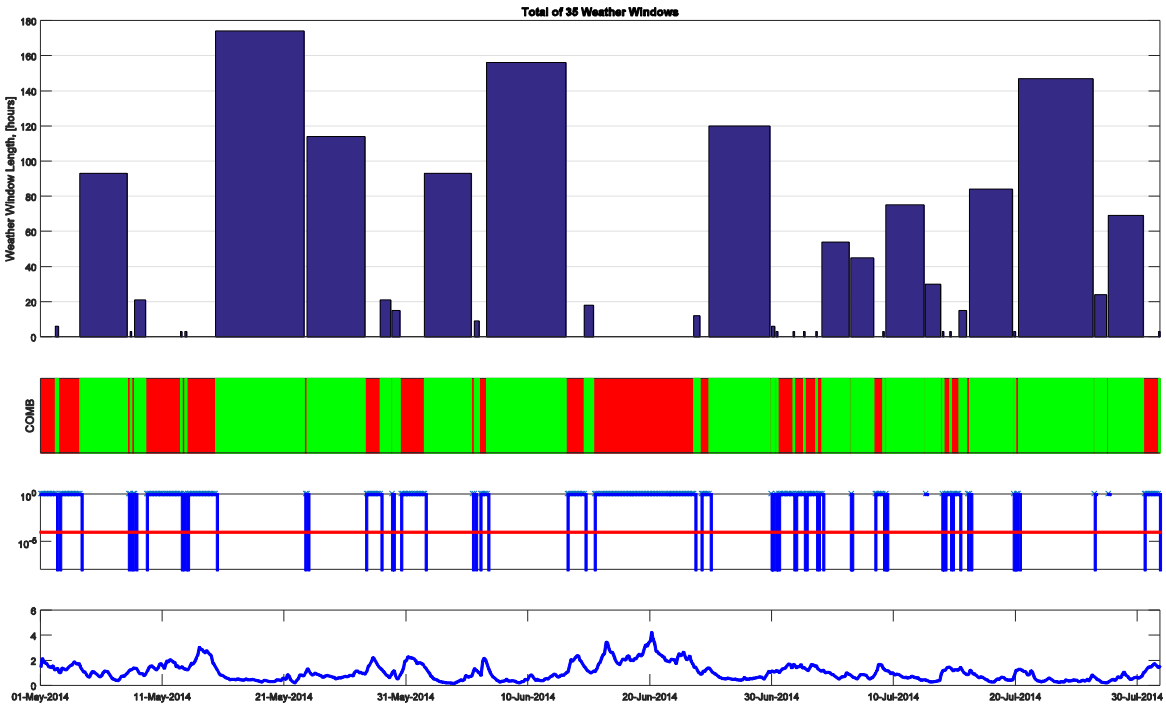

Radial Velocity Limit state

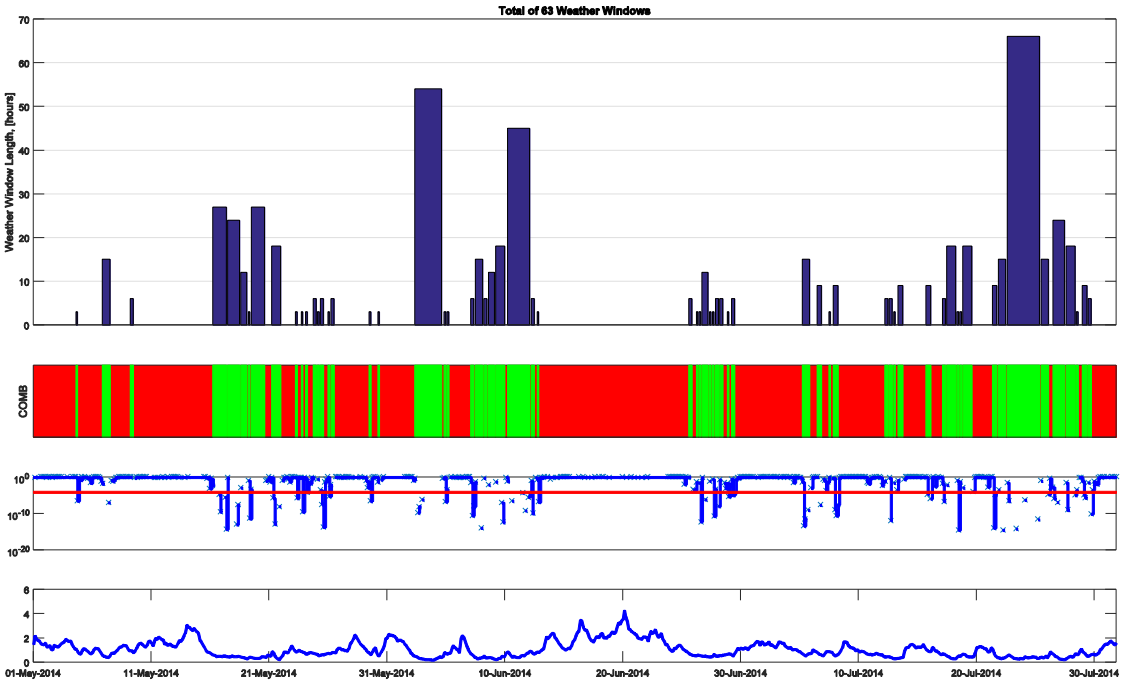

Relative Tilt Angle Limit state

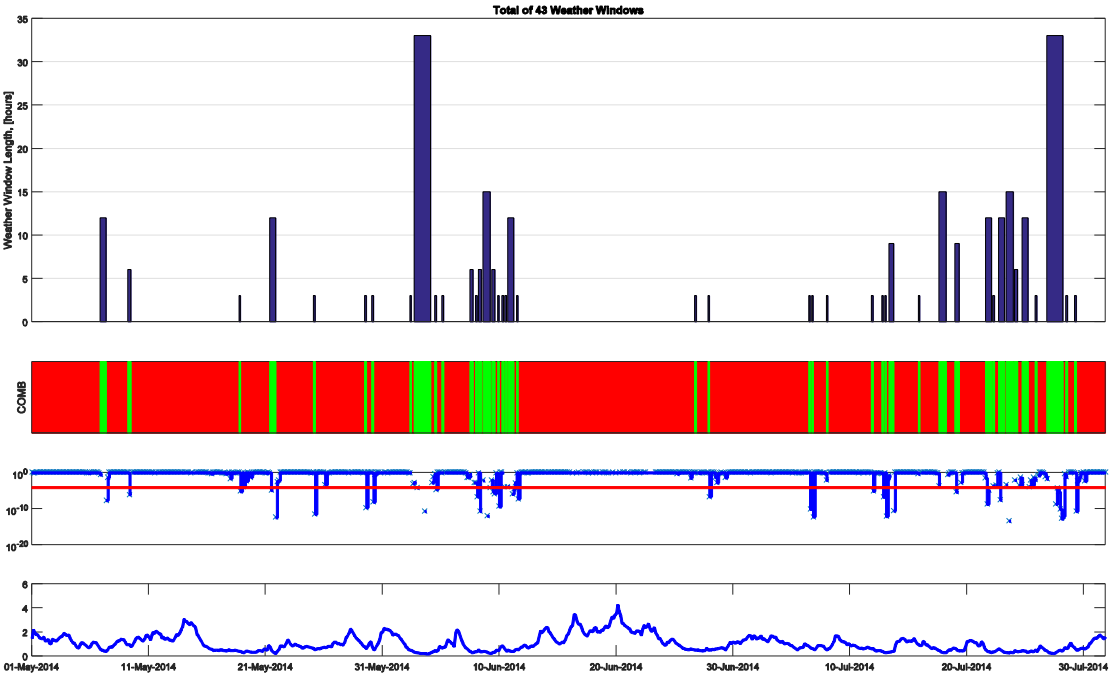

Relative Yaw Angle Limit state

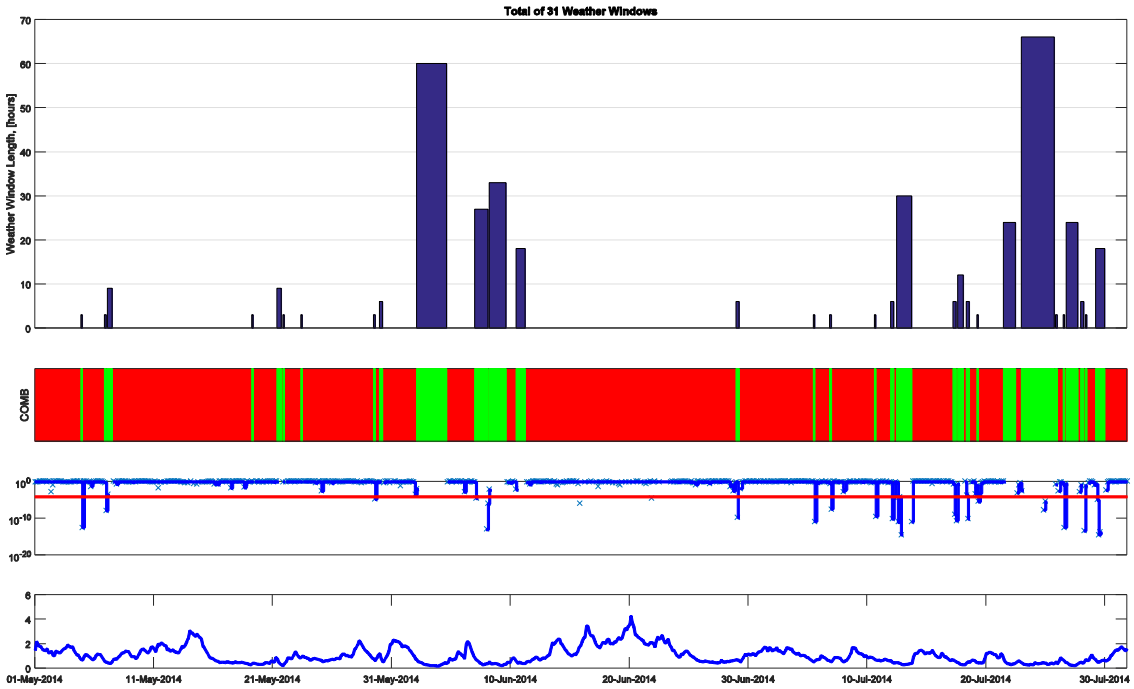

Rotor Acceleration Limit state

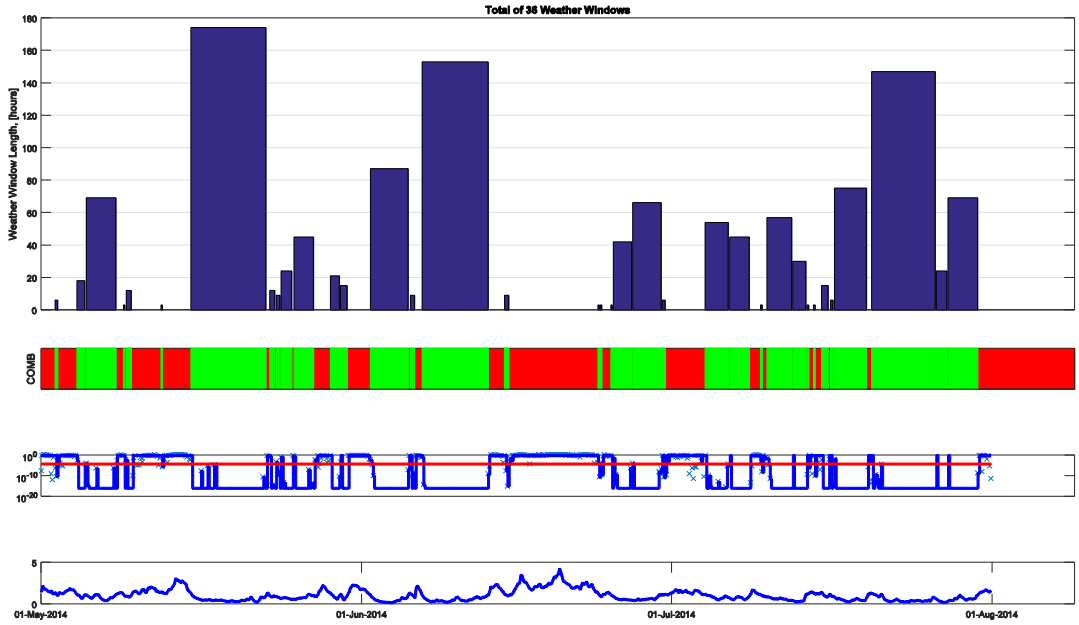

Angular Rotor Acceleration Limit state

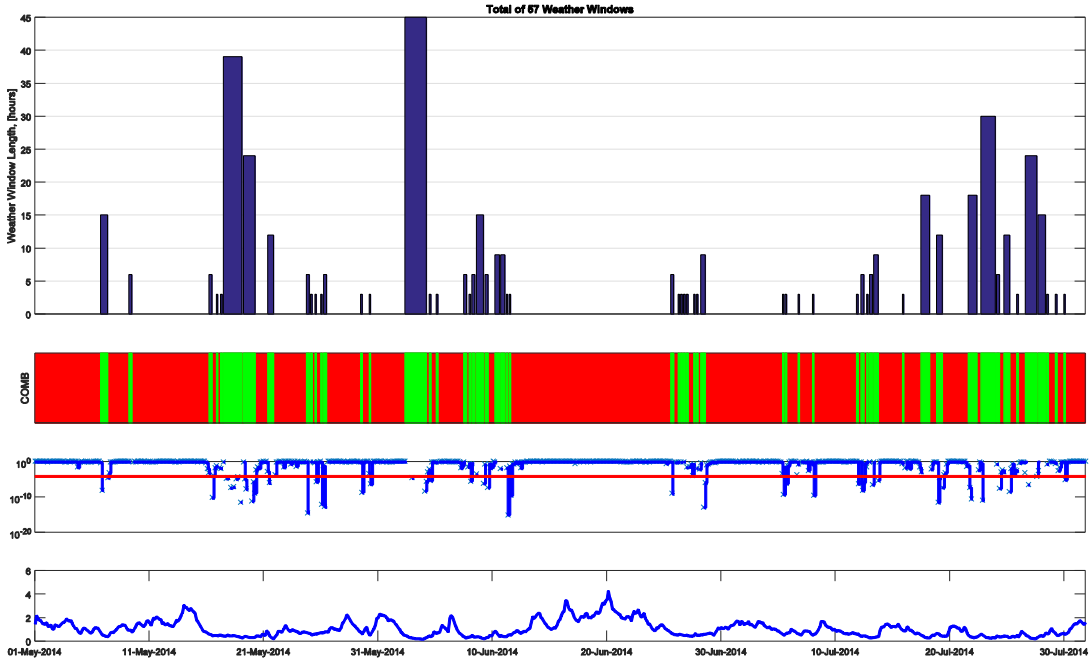

Sure Motion Limit state

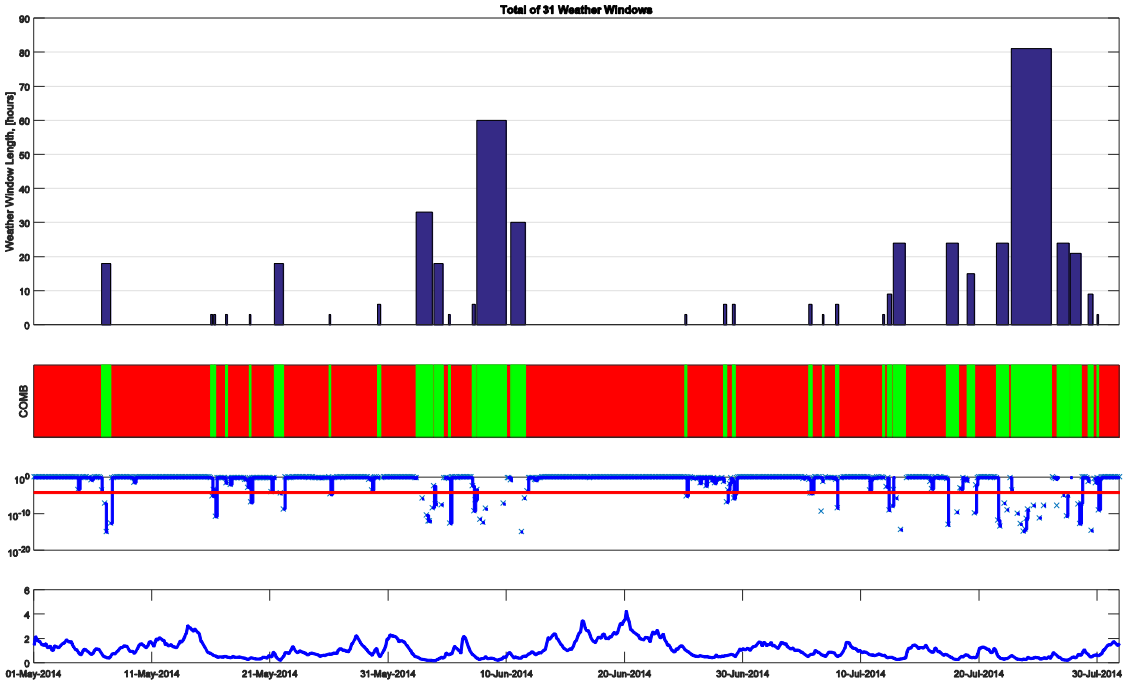

Sway Motion Limit State

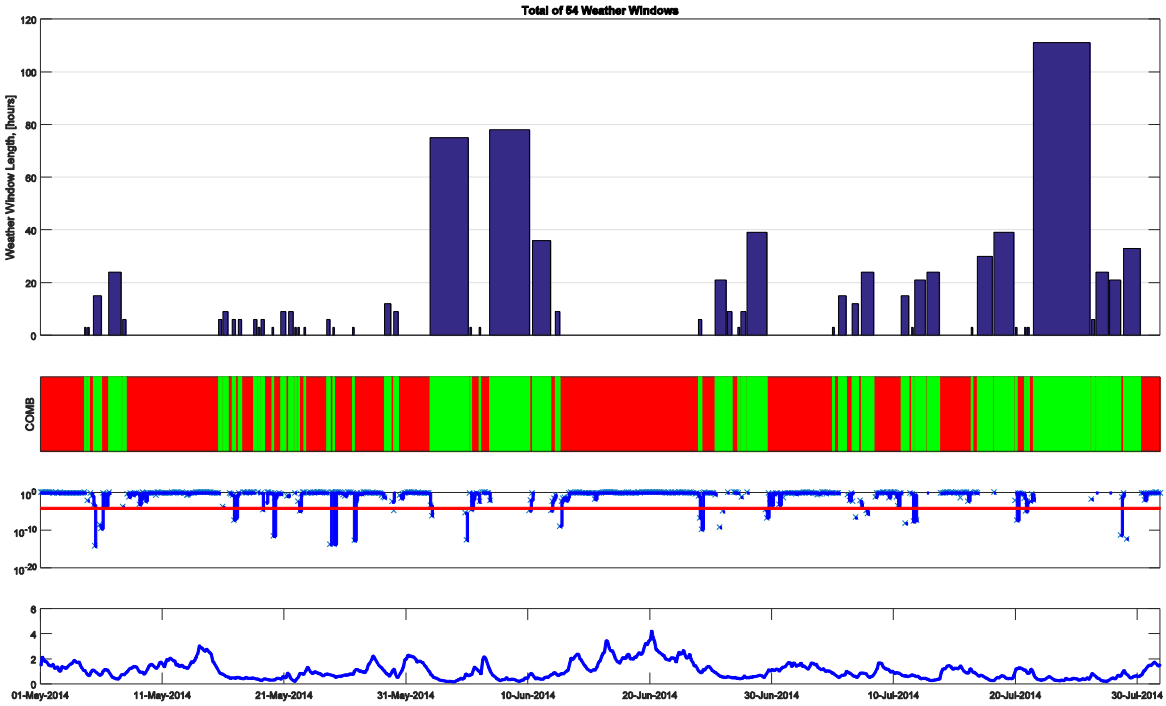

Tilt Motion Limit state

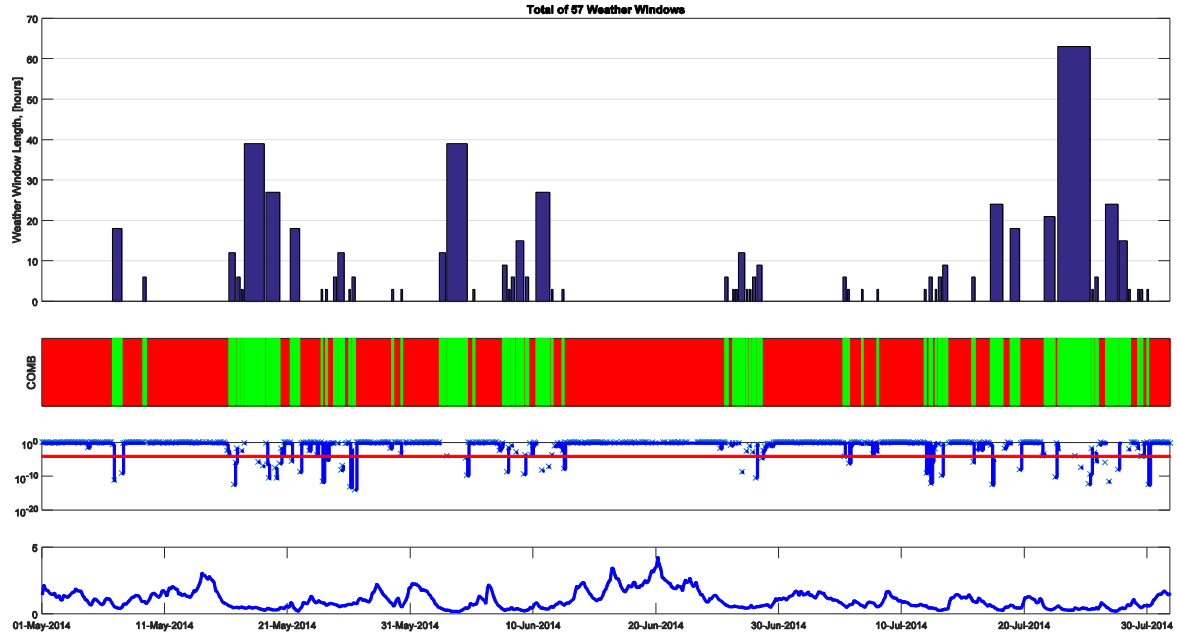

Yaw Motion Limit state

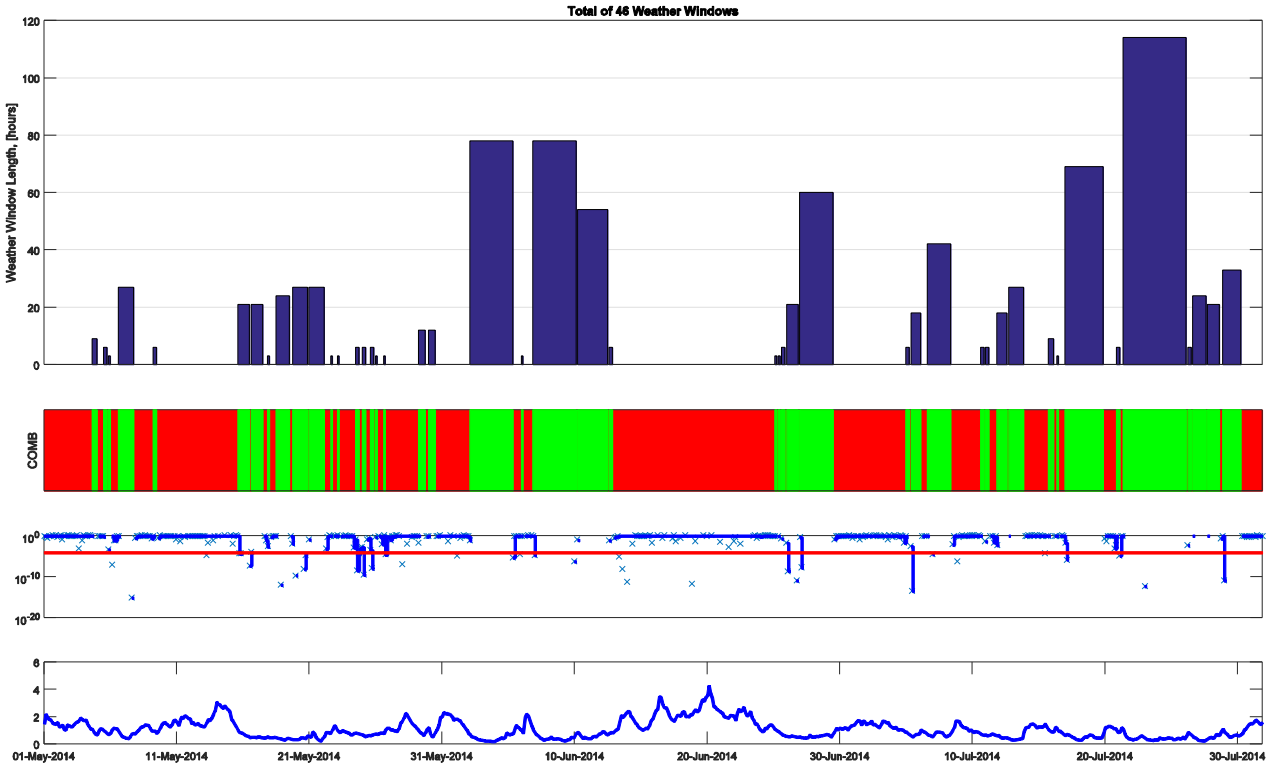

Appendix D. Effects of weather uncertainty on Critical Limit State Responses

Crane Load Limit State

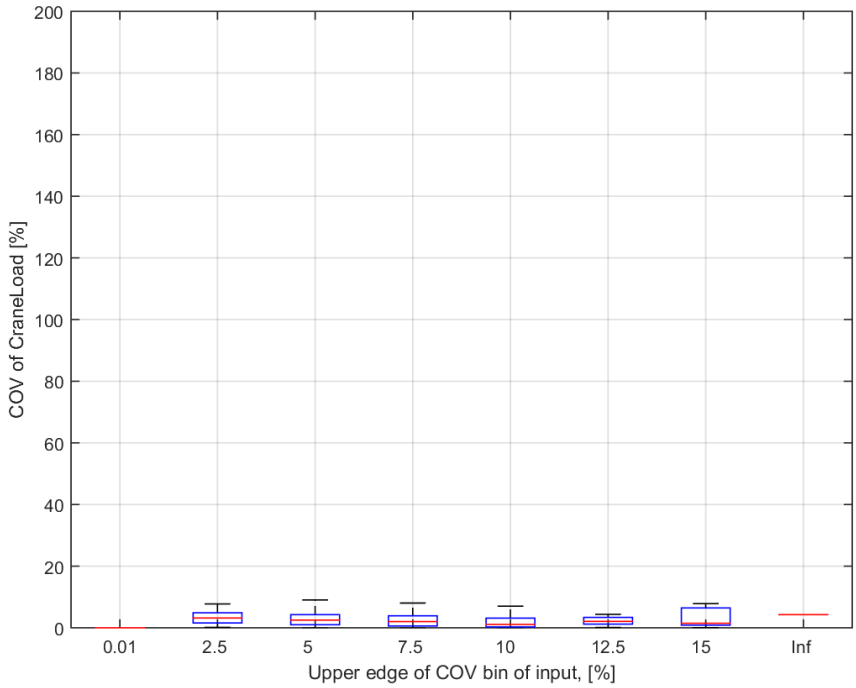

LiftWire Limit State

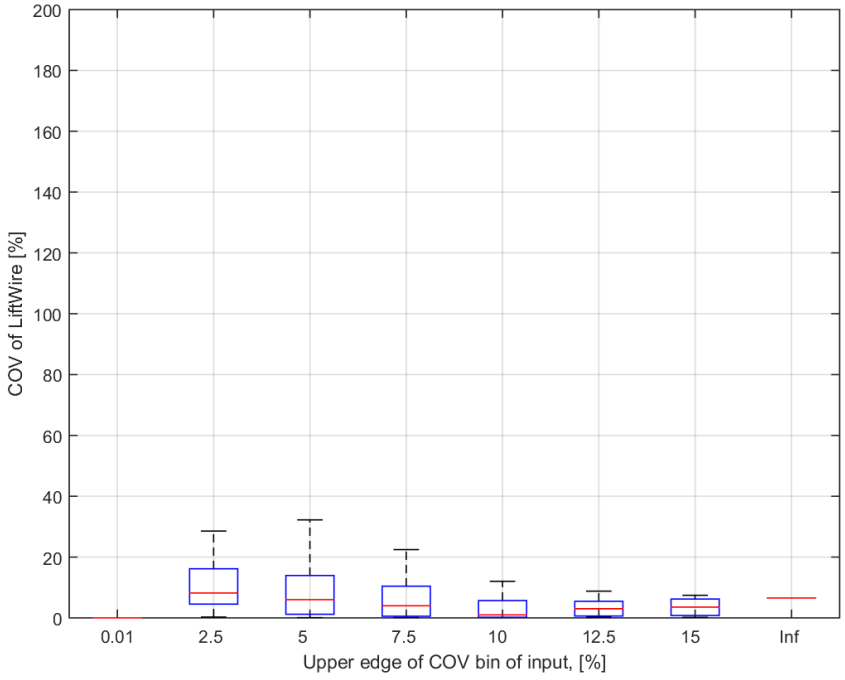

Rotor Acceleration Limit State

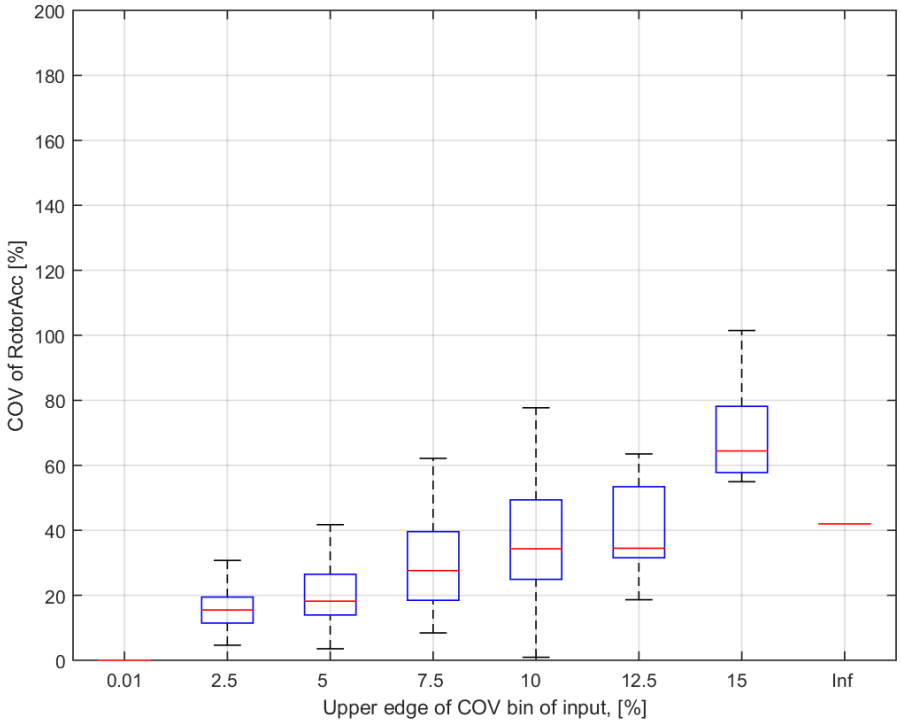

Rotor Angular Acceleration Limit State

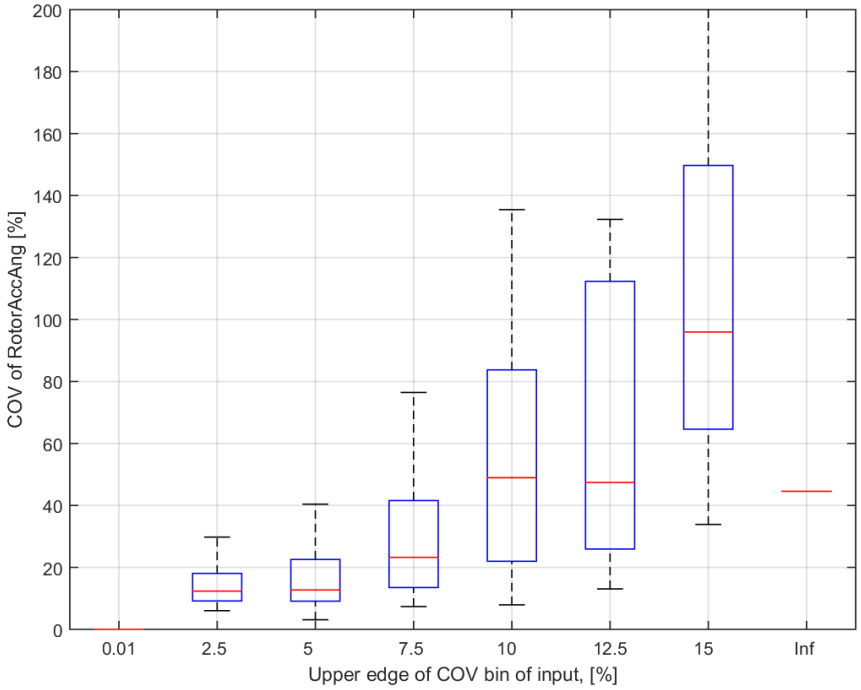

Surge Motion Limit State

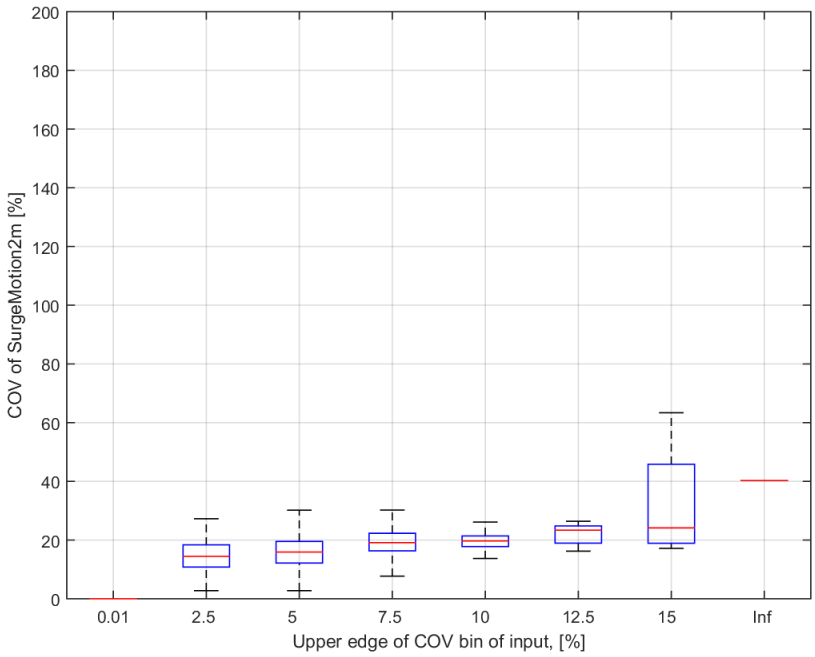

Sway Motion Limit State

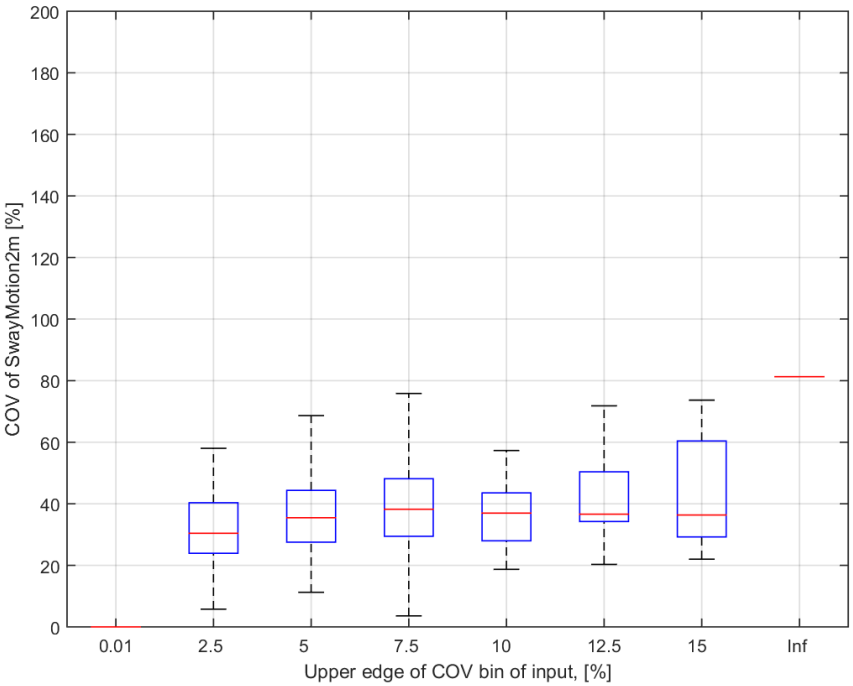

Tilt Angle Limit state

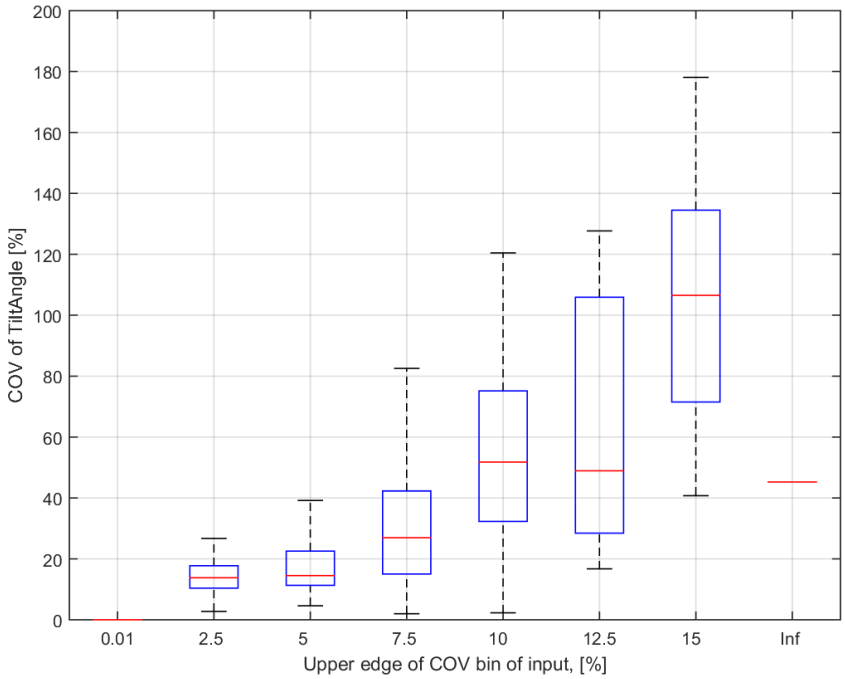

Yaw Angle Limit State

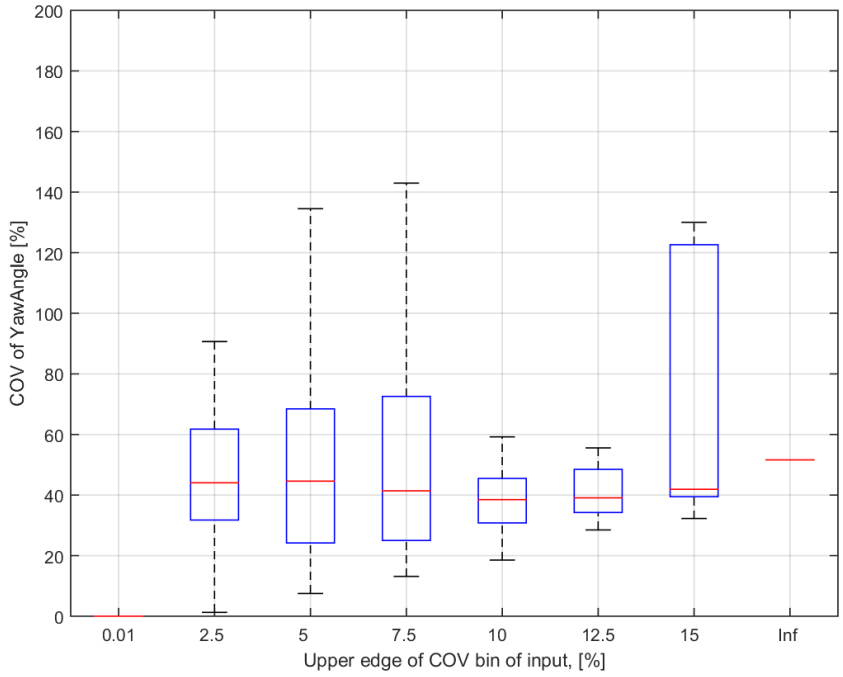

Relative Tilt Angle Limit State

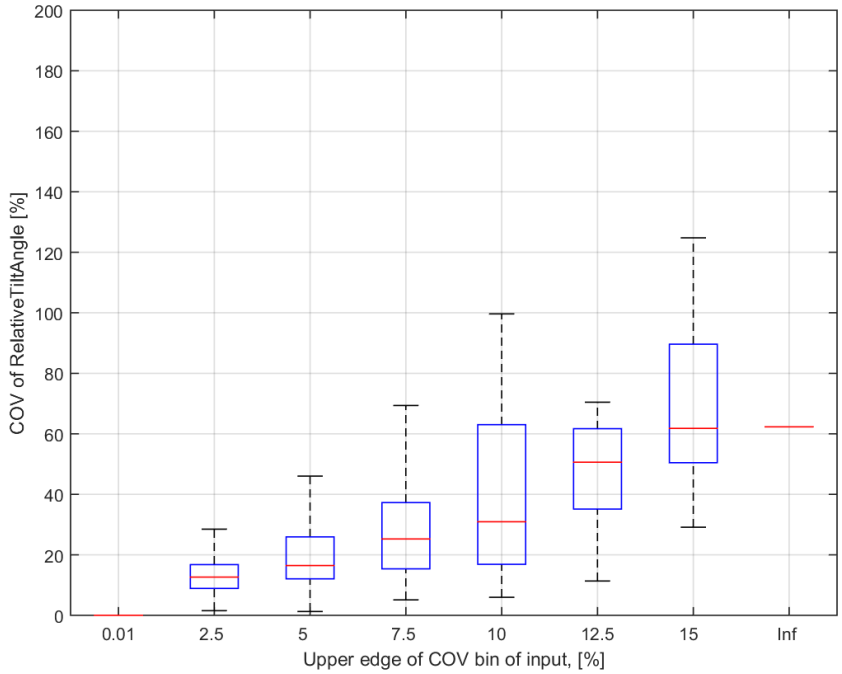

Relative Yaw Angle Limit State

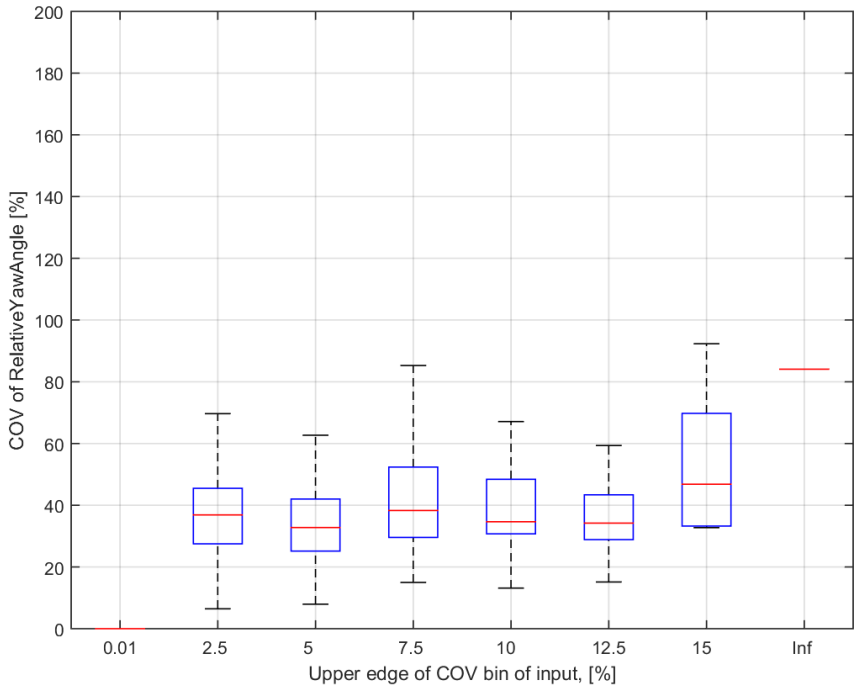

Relative Radial Velocity Limit State

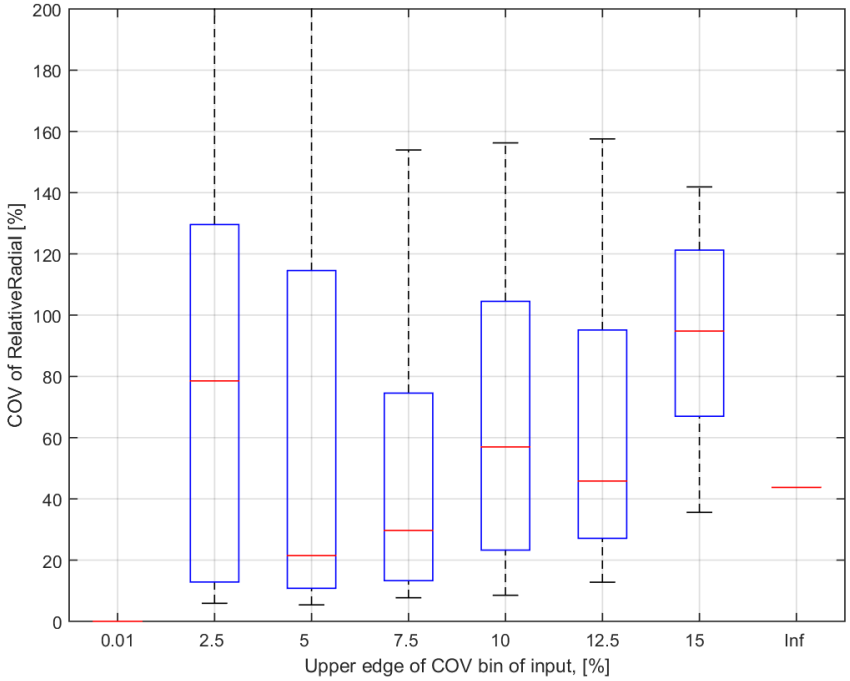

Relative Axial Velocity Limit State

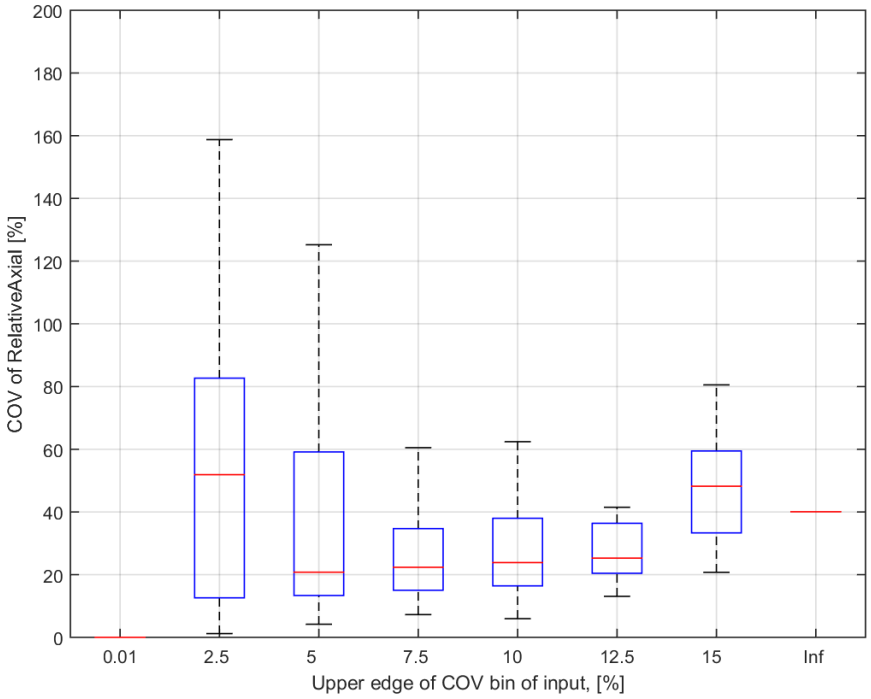

Airgap Tower Limit State